Back cover

UiO : University of Oslo

Marion Masitsa Malenge
Combination of anti-CD37 radioimmunotherapy with anti-CD20 immunotherapy and small molecule inhibitors to improve therapy of non-Hodgkin lymphoma

This thesis presents preclinical studies evaluating the effect of combining radioimmunotherapy (RIT) with immunotherapy and small molecule inhibitors with the aim of improving therapeutic outcomes in non-Hodgkin lymphoma (NHL). RIT uses monoclonal antibodies (mAb) paired with radionuclides to selectively deliver cytotoxic radiation to tumour cells. The radioimmunoconjugates (RIC) Betalutin® and Humalutin consisting of murine and chimeric mAbs respectively were used. These mAbs are linked to the chelator DOTA that chelates the β-emitting radionuclide lutetium-177. The RICs bind to CD37 proteins expressed on NHL cell surfaces and irradiate the cells inducing DNA-damage and subsequent cell death. Betalutin® was evaluated in combination with rituximab, a CD20-targeting immunotherapy that activates immune cells to attack and decimate the tumour cells. The combination resulted in synergistic effects in rituximab-sensitive and rituximab-resistant NHL animal models. The combination of Humalutin and Olaparib, a small molecule inhibitor that inhibits the PARP enzyme whose function is to repair DNA single strand breaks was explored. The combination resulted in synergistic effects in NHL cells.
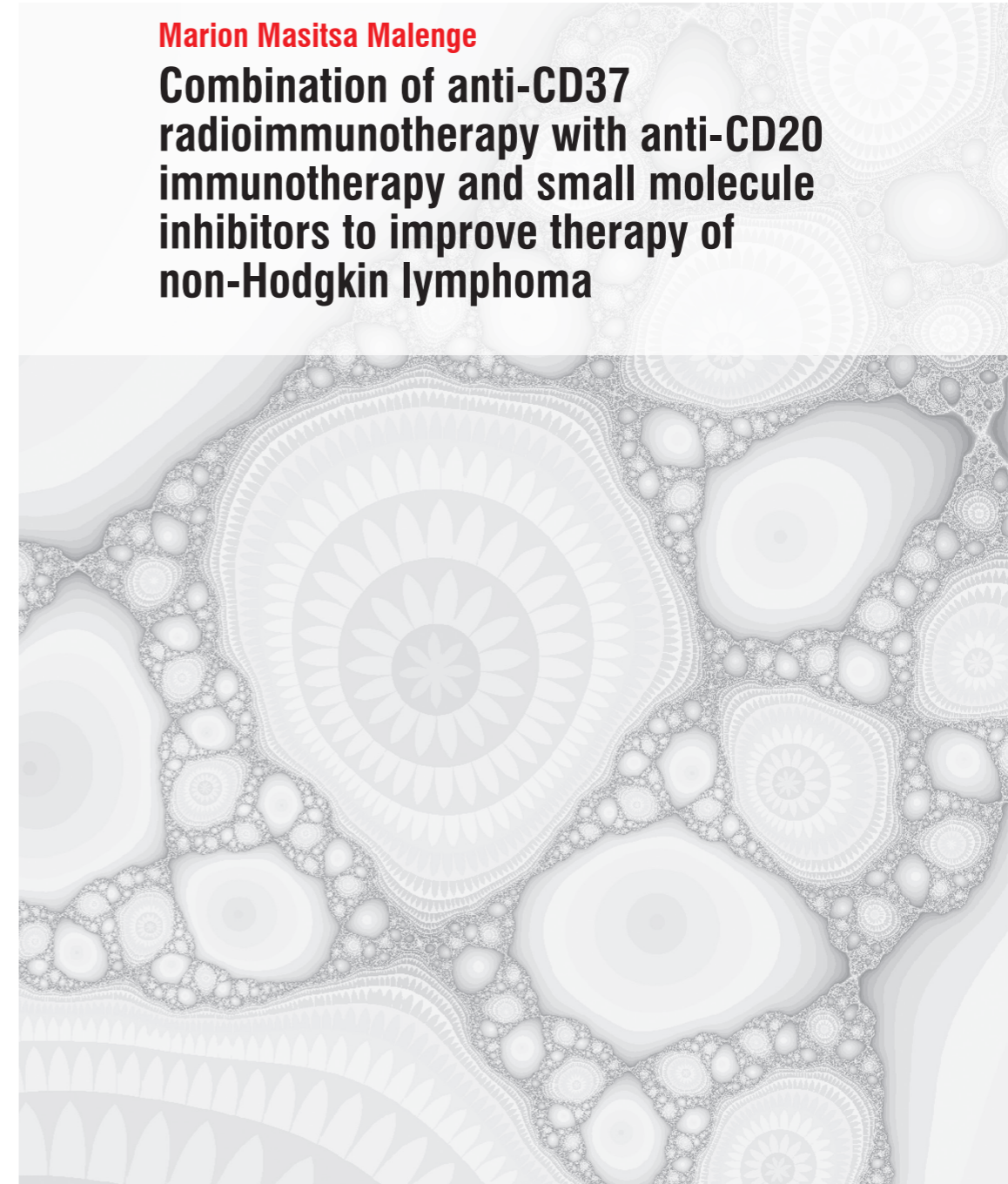
Dissertation for the Degree of PhD 2020
Institute of Clinical Medicine
Faculty of Medicine

2020

Spine

Marion Masitsa Malenge

Combination of anti-CD37 radioimmunotherapy with anti-CD20 immunotherapy and small molecule inhibitors to improve therapy of non-Hodgkin lymphoma

2020

Front cover

UiO : University of Oslo

Marion Masitsa Malenge

Combination of anti-CD37 radioimmunotherapy with anti-CD20 immunotherapy and small molecule inhibitors to improve therapy of non-Hodgkin lymphoma

Faculty of Medicine

2020

Combination of anti-CD37 radioimmunotherapy with anti-CD20 immunotherapy and small molecule inhibitors to improve therapy of non-Hodgkin lymphoma

Marion Masitsa Malenge

Thesis for the Degree of Philosophiae Doctor

Institute of Clinical Medicine

Faculty of Medicine

University of Oslo

Nordic Nanovector ASA

The Norwegian Radium Hospital

Oslo University Hospital

Table of Contents

Acknowledgement

I take this opportunity to express my deepest appreciation to my main supervisor Ada Repetto for the constant teaching, guidance, encouragement and provision. Your concerned input towards my professional and personal well-being has played a big role towards the completion of this thesis and I am forever grateful.

To my supervisors Jostein Dahle, Trond Stokke and Anne Hansen Ree, I am grateful that you sacrificed your time to tirelessly offer me your guidance and support. Your knowledgeable contribution towards my research has been the pillars to which my foundations stand. Thank you.

A big thank you to my current and former R&D colleagues: Adam, Helen, Helene, Katrine, Roman, Sebastian, Véronique, Laura, Ajna, Tatiana, Vilde, Tina, Sara and Elisa. It would be impossible to have submitted this thesis without the hours you all put in with technical and intellectual help. A special gratitude to Astri, for the wonderful collaboration and supportive office conversations.

Thank you to all collaborating co-authors for your knowledgeable contributions towards all the manuscripts. Thank you so much Roy for your genius and invaluable input. I have learnt so much from you and look forward to learning even more.

Mum and dad, I truly appreciate the support you offered me. Thank you for every prayer and every blessing you proclaimed upon me. That you spared no expense to ensure that I received an education that has led me to this point in life is an honour and even words cannot express my gratitude. *Nyasaye avagasize ligali muno no vulamu vonene ligali na avakumbelizi no vuyanzi bwibwe zimbega tsiosi.*

Thank you, my dear sisters for encouraging me, for always offering a listening ear and a shoulder to lean on through this journey.

Ken-Vidar, my best friend and life partner, I cannot thank you enough for always being there for me. You literally 'took one for the team' just to ensure that my head was always above water. Thank you for the warm dinners, the clean laundry and home, for the office pick-ups and drop-offs, and for all the kind things you have done to ensure that this journey was bearable and lovingly comfortable.

To the Ananiassens', the Isaksens' and my dear friend Cathy, you guys have been very supportive and I appreciate each and every one of you. Thank you.

In this journey, I have crossed paths with dozens of fantastic people who have imparted a lot of knowledge to me. To all of you, it was my pleasure interacting with you and thank you.

Declaration of interests

The affiliations of the authors that contributes towards the publications included in this thesis: Marion M. Malenge, Astri F. Maaland, Ada Repetto-Llamazares, Jostein Dahle, Helen Heyerdahl and Adam O'Shea are employees of Nordic Nanovector ASA. Sebastian Patzke was employed at Nordic Nanovector at the time of his contribution towards the publications. Ada Repetto-Llamazares, Jostein Dahle, Helen Heyerdahl, Adam O'Shea, Trond Stokke and Roy Larsen are shareholders in Nordic Nanovector. Jostein Dahle is a member of the executive leadership team at Nordic Nanovector ASA.
There is no conflict of interest to disclose for Anne Hansen Ree, Peter Ceuppens, Brian Middleton and Bergthora Eiriksdottir.

Glossary

^{177}Lu	Lutetium-177
^{177}Lu-chHH1-DOTA	Humalutin
^{177}Lu-HH1-DOTA	Betalutin®
ABC	Activated B-cell like
ADCC	Antigen dependent cytotoxicity
ADP	Adenosine di-phosphate
AML	Acute myeloid leukaemia
ATM	Ataxia-telangiectasia mutated
BCL	B-cell lymphoma
BCR	B-cell receptor
BH	BCL2 homology domain
BL	Burkitt lymphoma
CD	Cluster of differentiation
CDC	Complement dependent cytotoxicity
CDR	Complementarity-determining region
CI	Combination index
CLL	Chronic lymphocytic leukaemia
CTL	Cytotoxic T-cells
DLBCL	Diffuse large B-cell lymphoma
DMSO	Dimethyl sulfoxide
DNA	Deoxyribonucleic acid
DSB	Double strand break
EBR	External beam radiation
FBS	Fetal bovine serum
FDA	U.S Food and Drug Administration
FL	Follicular lymphoma
GC	Germinal center
GCB	Germinal centre B-cell like
HAMA	Human anti-mouse antibody
Ig	Immunoglobulin
i.p	Intraperitoneal
IRF	Immunoreactive fraction
i.v	Intravenous
mAb	Monoclonal antibody
MAC	Membrane attack complex
MCL	Mantle cell lymphoma
MHC	Major histocompatibility complex
NHL	Non-Hodgkin lymphoma
NK	Natural killer

PARP	Poly (ADP-ribose) polymerase
PBS	Phosphate-buffered saline
RBE	Relative biological effectiveness
RCP	Radiochemical purity
RIT	Radioimmunotherapy
RNA	Ribonucleic acid
ROS	Reactive oxygen species
s.c	Subcutaneous
SLL	Small lymphocytic lymphoma
SMI	Small molecule inhibitor
SSB	Single-strand break
WHO	World Health Organisation

List of publications

Paper 1

Combination of ^{177}Lu-lilotomab with rituximab significantly improves the therapeutic outcome in pre-clinical models of non-Hodgkin's lymphoma.

Ada H. V. Repetto-Llamazares, **Marion M. Malenge**, Adam O'Shea, Bergthora Eiriksdottir, Trond Stokke, Roy H. Larsen and Jostein Dahle.

Eur J Haematol. 2018 Oct;101(4):522-531. doi: 10.1111/ejh.13139. Epub 2018 Aug 31.

Paper 2

^{177}Lu-lilotomab satetraxetan has the potential to counteract resistance to rituximab in non-Hodgkin lymphoma.

Marion M. Malenge, Sebastian Patzke, Anne Hansen Ree, Trond Stokke, Peter Ceuppens, Brian Middleton, Jostein Dahle and Ada H. V. Repetto-Llamazares.

Manuscript accepted for publication in Journal of Nuclear Medicine (January 2020)

Paper 3

Anti-CD37 radioimmunotherapy with ^{177}Lu-NNV003 synergises with the PARP inhibitor olaparib in treatment of non-Hodgkin lymphoma *in vitro*.

Marion M. Malenge, Astri F. Maaland, Anne Hansen Ree, Trond Stokke, Arne Kolstad, Brian Middleton, Sebastian Patzke, Helen Heyerdahl, Jostein Dahle and Ada H. V. Repetto-Llamazares

Manuscript

1 Introduction

The global burden of non-Hodgkin lymphoma (NHL) is projected to significantly increase in the coming years due to the increase in the aging populations particularly in western economies (1). Currently, the main therapeutic strategy for NHL is chemoimmunotherapy regimens, combining cytotoxic chemotherapy with anti-CD20 monoclonal antibodies (mAbs); rituximab or obinutuzumab. Although these combination regimens result in high response rates and increased progression free survival (2, 3), there are patient subsets that have refractory disease or relapse after initial response to treatment (4). Various biological mechanisms are speculated to attribute to the lack of response to rituximab treatment. These include the shedding off of CD20/ rituximab complexes (5), the pre-mature internalisation of CD20/ rituximab complexes which limits the engagement of effector cells (6) and the deletion mutations on the CD20 gene (7, 8). This highlights the need to consider variant treatment strategies for patients with refractory/ relapsed disease.

Herein, focus is put on investigating the therapeutic potential of combining radioimmunotherapy (RIT) with FDA approved targeted treatments with the aim of improving therapeutic outcomes in NHL.

Lymphocytes are characteristically radiosensitive, and RIT has been shown to be clinically efficacious against lymphoma, resulting in overall progression free survival of patients with rituximab refractory or relapsed indolent and transformed NHL (9, 10). RIT delivers continuous low dose radiation to tumour sites targeted through use of mAbs tagged with therapeutic radionuclides, thus resulting in radiation mediated biological effects.

In this thesis two different next-generation radio immunotherapeutics: ^{177}Lu-lilotomab satetraxetan (Betalutin®) and its' chimeric version ^{177}Lu-NNV003 (Humalutin) were assessed. Both Betalutin and Humalutin contain CD37 targeting mAbs conjugated to the beta emitting radionuclide, Lutetium-177.

Pre-clinical studies aimed at evaluating the therapeutic outcome of combining Betalutin with anti-CD20 mAbs rituximab and obinutuzumab are presented. First, the effect of Betalutin treatment on the modulation of surface CD20 in rituximab sensitive and

resistant cells was studied using flow cytometry and antibody dependent cellular cytotoxicity (ADCC) assay. Here, Betalutin was shown to facilitate the increased CD20/ anti-CD20 mAb binding therefore increasing ADCC induction by rituximab and obinutuzumab. To further validate the *in vitro* findings, the anti-tumour efficacy of combining Betalutin with rituximab or obinutuzumab was investigated in NHL xenografted nude mice. The combination of Betalutin with rituximab presented significant anti-tumour effect which was greater than the sum of the effects resulting from the individual drug agents, implying synergism.

Using a different approach, the *in vitro* effects of combining Humalutin with the poly (ADP-ribose) polymerase (PARP) inhibitor; olaparib or with the B-cell lymphoma 2 (Bcl-2) inhibitor; venetoclax were evaluated using a fixed ratio cytotoxicity assay by ray design in DLBCL and MCL cells. In combining Humalutin with olaparib to inhibit the repair of the radiation-induced DNA damage, it was hypothesised that an accumulation of single and double strand DNA breaks would occur and this could subsequently result in programmed cell death also known as apoptosis. Here, synergistic effects of the combinations were observed in a significant number of cell lines.
Additionally, the effect of combining Humalutin with venetoclax which inhibits anti-apoptotic proteins in cells was evaluated and synergistic effects were also observed in some cell lines.

The data presented in this thesis if successfully translated in the clinic shows promise for the clinical evaluation of the combination treatments as they may confer significant therapeutic benefit to subsets of NHL patients, particularly those with refractory and relapsed disease.

2 Background

Cancer is a disease that develops through multiple steps of tumorigenesis where genetic alterations transform normal cells to malignant phenotypes with the capacity to invade other body tissues. Cancer prevalence and mortality is rapidly increasing worldwide, paralleled by changing profiles of common cancer types. The World Health Organization (WHO) reported an estimated 9.6 million cancer-related deaths in 2018. Lymphoma was the neoplasm with the seventh highest incidence (11, 12).

Lymphoma is a group of heterogenous neoplasms that originate from cells of the immune system called lymphocytes, residing in lymphoid and haematopoietic tissues (12, 13). Lymphoma is classified into four entities: Hodgkin lymphoma, NHL, multiple myeloma and immunoproliferative diseases (12, 14). This classification is based on morphological, immunophenotypic, genetic, lineage of cell origin and clinical features (12, 14). The scope of this thesis is NHL.

2.1 Non-Hodgkin Lymphoma

NHL represents 90 % of all forms of lymphoma and ranks as the eleventh most common cancer worldwide (1, 14). Globally, an estimated 509 590 new cases of NHL and 248 724 NHL related deaths were reported in 2018 (1). Incidence rates of NHL reveals a gender and age disparity with predominance in males and the aging population (1). WHO has classified and assigned diagnostic designations to more than 60 NHL subtypes, 85 % of which derive from B-lymphocytes (B-cells) while the remainder are natural killer (NK) and T cell derived (14). Depending on disease ferocity and response to treatments, the subtypes are designated 'indolent' and 'aggressive'. Further classification of NHL is based on morphological, immunophenotypic, genetic, lineage of cell origin and clinical characteristics (14).

The genesis of NHL is reliant on the error prone B-cell development process. This process is characterised by functional rearrangement of V(D)J gene segments of immunoglobulin (Ig) chains encoding the B-cell receptor (BCR). This occurs through a series of recombination reactions mediated by recombination activating genes (RAG) 1

and 2. Aberrant recombination can create genetic mutations that result B-cell lymphomagenesis (15, 16).

Activation of naïve B-cells in secondary lymphoid organs is mediated by changes in gene expression that give rise to the germinal center (GC) within the B-cell follicles of these organs. GC reactions are characterized by clonal expansion and somatic hypermutation (SHM) of Ig genes in the dark zone of the GC along with elevated levels of *BCL6*, a transcriptional repressor that negatively regulates genes involved in control of the cell cycle, cell death, terminal B-cell differentiation and DNA damage response (17). In the light zone, B-cells undergo affinity maturation of the Ig receptors by being re-challenged with antigen through interaction with T-cells and follicular dendritic cells and are conferred distinct effector function through class switch recombination (CSR) at the Ig H locus. Cell with low affinity are selected to undergo apoptosis. These genetic modifications are essential for development of normal immune responses but can also be a source of DNA damage initiating lymphoma pathogenesis (16, 18). NHL subtypes are associated with different stages of B-cell differentiation and function within the GC as illustrated in Figure 1 and reviewed in (18-20). Some of the NHL subtypes are highlighted below.
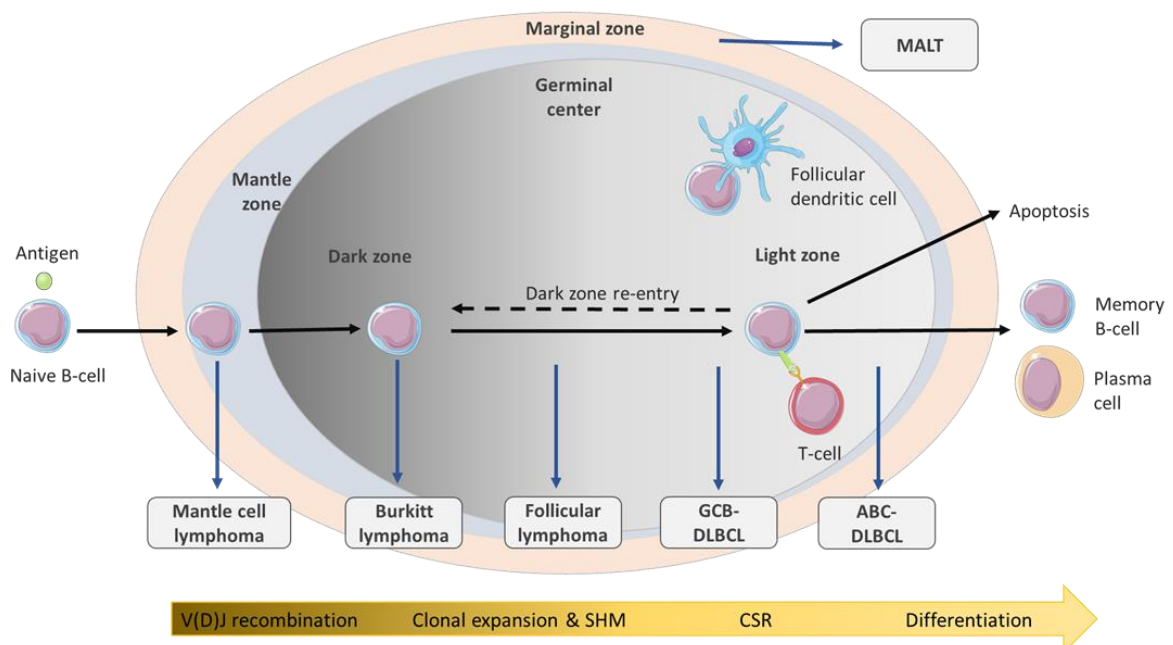

Figure 1. Germinal centre reaction in B-cell development associated with the origin of different NHL subtypes. This figure is inspired by a figure in reference (18) and the illustrations used here were obtained from Servier Medical Art (smart.servier.com)

Diffuse large B-cell lymphoma (DLBCL): This is the most common form of NHL constituting up to 40 % of global incidence. It presents as an aggressive malignancy that involves organs other than the lymph nodes (21). It occurs as 2 different molecular subtypes: activated B-cell like (ABC) and germinal centre B-cell like (GCB), which are characterised by their addiction to different biological signalling pathways and clinical presentations (22).

The ABC subtype is associated with a worse prognostic outcome than the GCB type. The genetic lesions characteristic of DLBCL are *BCL2* translocation; t(14;18)(q32;q21), in the GCB subtype and *BCL6* translocation; t(3;22)(q27;q11), in the ABC subtype. Both are accompanied by rearrangement of the proto-oncogene *MYC* (23).

MYC functions as a regulator of DNA replication, cell proliferation and apoptosis and its dysregulation is associated with aggressive lymphomas (24).

Follicular lymphoma (FL): This is an indolent form of NHL and the second most common form of lymphoma in western countries, accounting for 10-20 % of all lymphomas. It derives from GC B-cells and usually initiates in the lymph nodes and extra nodal involvement is sometimes observed (25, 26). Chromosomal translocation: t(14;18) (q32; q21), is a hallmark of FL which results in overexpression of the BCL2 pro-survival proteins (27). FL can transform into a more aggressive DLBCL form due to recurrent genetic lesions (26, 28).

Burkitt lymphoma (BL): This is an aggressive malignancy derived from GC B-cells. A common characteristic among its' endemic, sporadic and HIV associated forms is the deregulation of *MYC* by translocation t(8;14) (q24; q32) resulting in genomic instability (29, 30). Endemic (African) BL is ecologically associated with *Plasmodium falciparum* malaria. It mainly affects African children of ages 4-7, accounting for 30-50 % of childhood cancers. Sporadic (non-endemic) BL affects mainly non-Africans representing 1-2 % of global NHL. Immunodeficiency associated BL accounts for 30-40 % of NHL in HIV/AIDS patients (30).

Mantle cell lymphoma (MCL): An aggressive malignancy with poor prognosis, MCL accounts for 3-10 % of NHL cases and involves the bone marrow, lymph nodes, spleen, and gastrointestinal system (31). MCL originates from CD5+ mantle-zone B cells and is characterised by overexpression of cyclin D1 (CCND1) as a result of a t(11;14)

(q13;q32) translocation, subsequently deregulating the cell cycle. Mutations in the tumour suppressor gene ataxia telangiectasia mutated (*ATM*), involved in DNA repair are also frequent (32-34).

High-grade B-cell lymphoma: Also known as double hit lymphoma, this is a highly aggressive form with poor prognosis and increased risk of central nervous system involvement. It occurs in less than 10 % of all DLBCL cases and is thought to be a consequent of low-grade FL transformation. It is characterised by changes in *MYC* and *BCL2* or *BCL6* genes with all three genes affected in triple hit lymphoma (35).

2.1.1 Etiology of NHL

Etiology of NHL is variant across the subtypes. While genetic mutations are the main risk factors influencing incidence of NHL, chronic infections (36), environmental and occupational exposures (37) and socio-economic lifestyle changes (38) remains a major risk.

Congenital and acquired immune suppression in the form of immunodeficiency disorders (39), autoimmune diseases (40) and immunosuppressive therapeutics such as chemotherapy, radiotherapy (41) and those administered during organ transplantation (42) attribute to deficient immune surveillance, predisposing patients to BL, DLBCL and marginal zone lymphoma (MZL)(38-42).

Infections caused by Epstein Barr virus (EBV) (29), human immunodeficiency virus (HIV) (39) and hepatitis C virus (43) are associated with BL, DLBCL, FL and MZL (36). Chronic bacterial infections by *Helicobacter pylori, Chlamydia psittaci, Borrelia burgdorferi* and *campylobacter* are mainly associated with the indolent MZL of the mucosa associated lymphoid tissue (MALT) type (44).

High body mass index, cigarette smoking, alcohol consumption and recreational sun exposure are increasingly associated particularly with DLBCL and FL (36, 38). Occupational exposures to organic and inorganic solvents such as herbicides, pesticides, dyes and paints are a predisposition for the t(14:18) chromosomal translocation, associated with DLBCL and FL (36-38).

Although not explicitly termed as hereditary, inherited genetic defects in immune function pose a modest risk associated with NHL. In addition, shared environmental determinants are associated with patterns of familial risk susceptibility for NHL (45, 46).

2.1.2 Treatment of NHL

Patients with NHL are eligible for different types of treatment regimens depending on the stage and localisation of the disease, histology, clinical presentation of the disease, disease ferocity, the patients age and comorbidities as well as whether the cancer is newly diagnosed or recurring. The National Comprehensive Cancer Network (NCCN) and the European Society for Medical Oncology (ESMO) provide guidelines with recommendations for the diagnosis and treatment of the NHL subtypes (47-51).

The standard mode of treatment for both indolent and aggressive NHL, is systemic chemotherapy with cyclophosphamide, doxorubicin, vincristine and prednisolone in combination with rituximab (R-CHOP), delivered in 6 or 8 cycles of treatment (2, 3, 52). Despite the clinical efficacy of R-CHOP, a significant proportion of NHL patients becomes resistant to this treatment or experience disease relapse. Subsequently, combination of obinutuzumab with CHOP (2, 3) or with bendamustine (53) has been employed to improve the therapeutic outcome in previously untreated patients with NHL and patients with relapsed/ refractory disease.

Rituximab and obinutuzumab are CD20 targeting mAbs, FDA approved as therapeutics for the treatment of relapsed/refractory NHL. They function by initiating direct cell death, ADCC, antibody dependent cellular phagocytosis (ADCP) and complement dependent cytotoxicity (CDC) (54, 55). Currently, single agent immunotherapy with these mAbs is used as maintenance therapy after initial chemoimmunotherapy. These mAbs have a low toxicity profile coupled with good overall response rates when compared to chemotherapy (3, 56).

Other immune modulation treatment modalities are available in lower course lines of treatment, when fore-line modalities have been unsuccessfully explored as shown in the example given in Figure 2.
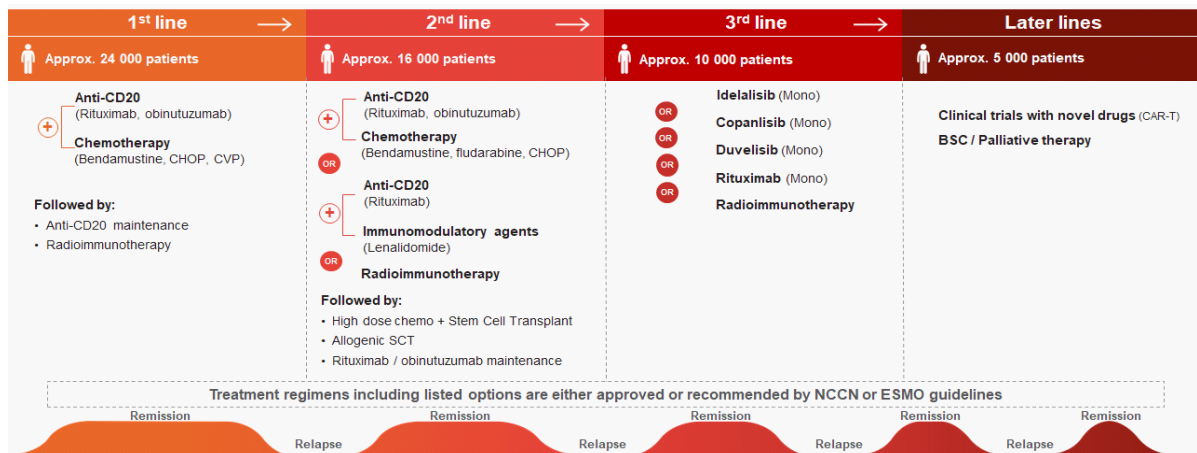
.

Figure 2. FL profile and currently available therapeutic approaches at the onset of the disease diagnosis and progression. First line treatments are prescribed on the onset of the disease and subsequent treatment lines are used depending on the remission-relapse cycles characterisation and on the patients' response and tolerance.

Systemic chemotherapy with either alkylating agents, corticosteroids, platinum drugs, purine analogues, anti-metabolites, anthracyclines or vinca alkaloids are used either as adjuvant or neoadjuvant treatments. These therapeutics function by cytotoxic inhibition of various biological mechanisms such as DNA replication and transcription, cell division and differentiation, all of which result in cell death (57).

Chemotherapeutics indiscriminately affect metabolically active cells, malignant and healthy cells alike. This results in multiple long-term and short-term treatment related side effects such as cytopenia, alopecia, vital organ toxicity, infertility and secondary malignancies. These effects are dependent on the dose, type and duration of the chemotherapy.

External beam radiation (EBR) therapy with high-energy ionising radiation is used to decimate and inhibit growth of cancer cells through induction of DNA damage whilst largely sparing normal tissue (58). Involved field EBR therapy as a single modality is the primary treatment for early stage indolent lymphomas. In multimodality therapy, EBR therapy is given as consolidation therapy after chemoimmunotherapy in patients with localised aggressive NHL subtypes (59). The risk associated with EBR therapy is the possible occurrence of secondary soft tissue tumours as a result of irradiation of normal tissue (60).

Radioimmunotherapy (RIT) using antibodies or antibody fragments conjugated to radionuclides by selective chemistries has been shown to deliver radiation payloads selectively to the antibody targets sparing normal tissue (9, 61, 62). The specificity and selectivity of RIT presents a significantly low non-haematological toxicity profile in comparison to chemotherapy and EBR therapy (9). Zevalin (^{90}Y-ibritumomab tiuxetan) and Bexxar (^{131}I-tositumomab) are currently the two radioimmunotherapeutics approved for the treatment of chemotherapy refractory/ relapsed FL and DLBCL, both targeting CD20 (9, 63). The use of Bexxar is however currently discontinued.

Clinical trials investigating the benefits of RIT in combination with other interventions have been documented. The combination of Zevalin and rituximab has been shown to result in a high number of complete responses in patients with NHL (NCT00387023). Additionally, combination of chemotherapy, rituximab and Zevalin has been shown to improve progression free survival in patients with relapsed FL (NCT00732498).
NHL patients in remission or with relapsed/refractory disease may receive autologous haematopoietic stem cell transplantation after treatment with high-dose chemotherapy or radiation therapy (57).

The 'watch and wait' strategy is utilised in patients with asymptomatic indolent NHL. For non-progressive lymphomas with low tumour burden, active surveillance is implemented to closely monitor disease symptoms. This is done to minimise treatment related risks to patients of good overall health (64).

2.2 Tumour immunology

The immune system is a biological defence system comprising of special organs, cells and chemical cues that identify and neutralise pathogens to maintain a status quo of a pathogen-free internal environment. It is classified into two main components: innate and adaptive immune system (65).

Innate immunity comprising of basophils, eosinophils, neutrophils, dendritic, macrophages, mast and natural killer (NK) cells is the first in line defence against antigens and does not require prior stimulation from the antigens for activation.

During growth, tumour cells undergo stromal remodelling which results in the production of pro-inflammatory chemokines by the cells and a loss of major histocompatibility complex (MHC) class I molecules; ligands for inhibitory receptors on NK cells that influence self-tolerance of NK cells. The NK cells are recruited to the tumour sites and assess the tumour cells for MHC class I molecules. If none are detected, the NK cells initiate an active immune response by commencing the production of interferon-γ (IFN-γ), in turn inducing persistent production of chemokines by the tumour cells. This results in the recruitment of tumour infiltrating macrophages that induce production of interlukin-2 (IL-2), subsequently stimulating NK cells to produce more IFN-γ through a process of positive feedback mechanisms. As a result, signalling pathways that enhance antiproliferative, pro-apoptotic and angiostatic mechanisms are activated to eliminate the tumour cells (66, 67).

Adaptive immunity on the other hand is antigen-specific as it requires activation through antigen contact. It exhibits immunological memory to prior antigen exposure and has the capacity to recognise self from non-self-antigens due to self-tolerance developed during maturation of B and T lymphocytes. Humoral immunity, one of two arms of adaptive immunity, is responsible for antibody production in response to antigens and is carried out by B-lymphocytes. The antibodies produced are either soluble or cell membrane-bound and differ in their biological features, structure, target specificity and distribution. Based on the amino acid sequence in the constant region of the antibody heavy chain, they are classified into five immunoglobulin (Ig) isotypes: IgA, IgD, IgE, IgG and IgM, collectively these together with a signal transduction protein; CD79a (Igα) and CD79b (Igβ), make up the B-cell receptor (BCR) complex. The BCR is fundamental in the development, function and survival of B-lymphocytes, including subtypes of NHL (65, 68). BCR recognise antigens and trigger antigen specific antibody responses. Antibodies have effector functions that can neutralise antigens through activation of natural killer cells, the classical complement pathway and phagocytosis.

Developing concurrently to humoral immunity is the largely T-lymphocyte driven cell-mediated immunity. This is not characterised by antibodies but acts synergistically with humoral immunity in response to antigens through cytokine release. MHC antigen presenting cells such as dendritic cells recruited to tumour sites by innate immune responses present tumour peptide antigens to CD4+ T helper cells.

Activated CD4+ cells secrete IL-2, TNF-α, and IFN-γ that promote activation of CD8+ cytotoxic T-cells (CTL) that secrete cytotoxic effector proteins. In this way, CTL are the custodians of immune surveillance, able to identify and respond to tumour-specific and tumour-associated antigens therein eliminating tumour cells (68).

2.3 Targeted therapies

Cancer research and therapy has evolved over the years, resulting in the development of a variety of targeted treatment modalities that exploit molecular vulnerabilities in cancer cells with limited toxicity in normal cells. Targeted therapies interact with specific cancer-associated molecular targets to inhibit tumour proliferation and survival. Various targeted therapeutics have been approved by FDA or are under clinical or pre-clinical investigations for cancer treatment. Majority of these are small molecule inhibitors targeting signal transduction pathways, chimeric antigen receptor T-cells (CAR-T), immunotherapeutic mAb and by extension radiolabelled mAb all targeting cell surface receptors indicated for B-cell malignancies (69) (Table 1).

2.3.1 Immunotherapy

The use of antibodies as immunotherapeutics to enhance or restore the ability of immune cells to recognize and eliminate tumour cells through targeting a variety of antigens has been shown to be clinically beneficial for many patients with lymphoid malignancies (70-72). The efficacy of immunotherapy is largely dependent on the characteristics of its' target antigen.

An ideal target antigen should be readily accessible, disease-specific, highly expressed on malignant cells at all stages of disease progression, should have high specificity for the antibody with limited shedding off to the bloodstream or internalisation after antibody engagement (70, 73). However, antigen/ antibody complex internalisation may be beneficial particularly when the targeting mAb is conjugated to a cytotoxic agent (74).

Table 1. Overview of some of the different target therapeutics in clinical and pre-clinical use for the treatment of B-cell malignancies (75).

Drug category	Therapeutic	Target	Indication
Immunotherapy			
mAb	Alemtuzumab (Lemtrada)	CD52	CLL/SLL
	Dacetuzumab	CD40	NHL
	Lucatumumab	CD40	CLL/SLL
	Obinutuzumab (Gazyva®)	CD20	FL, CLL
	Ofatumumab (Arzerra)	CD20	FL
	Rituximab (Rituxan®)	CD20	NHL, CLL, MZL
	Ublituximab (TG-1101)	CD20	NHL
Drug conjugated mAb	Camidanlumab tesirine (ADC-301)	CD25	DLBCL
	Polatuzumab vedotin (DCDS4501A)	CD79b	DLBCL, FL
Radionuclide conjugated mAb	^{90}Y-ibritumomab tiuxetan (Zevalin®)	CD20	NHL
	^{131}I-tositumomab (Bexxar®)	CD20	DLBCL, FL
	^{177}Lu-lilotomab satetraxetan (Betalutin®)	CD37	DLBCL, FL
CAR-T	Axicabtagene ciloleucel (Yescarta)	CD19	DLBCL
	Tisagenlecleucel (Kymriah)	CD19	ALL, DLBCL
Bispecific mAb	AFM13	CD30/CD16A	DLBCL
	Blinatumomab (Blincyto)	CD19/CD3	DLBCL
	DART	CD19/CD3	DLBCL
	Mosunetuzumab (BTCT4465A)	CD19/CD3	CLL/SLL, iNHL
Immune checkpoint inhibitors	Atezolizumab (Tecentriq)	PD-L1	FL, DLCBL
	Ipilimumab (Yervoy)	CTLA-4	NHL, FL
	Nivolumab (Opdivo)	PD-1	DLBCL, FL
	Pembrolizumab (Keytruda)	PD-1	DLBCL
	Pidilizumab (MEDI4736)	PD-1	DLBCL
	Urelumab	CD137	CLL/SLL
Small molecule inhibitors			
BCR Inhibitors	Acalabrutinib (Calquence)	BTK	CLL/SLL
	Ibrutinib (Imbruvica)	BTK	CLL, MCL
	Buparlisib (BKM120)	PI3K	DLBCL
	Copanlisib (Aliqopa™)	PI3K γ	DLBCL, FL
	Idelalisib (Zydelig)	PI3K δ	CLL/SLL, FL
Bcl-2 Inhibitor	Venetoclax (Venclexta™)	Bcl-2 proteins	DLBCL, CLL/SLL
HDAC Inhibitors	Mocetinostat (MGCD0103)	Class I & IV	DLBCL, FL
	Panobinostat (Farydak)	Class I, II & IV	DLBCL
	Vorinostat (Zolinza)	Class I & II	FL
mTOR inhibitors	Everolimus (Afinitor)	mTORC1	CLL/SLL, DLBCL
	Temsirolimus (Torisel)	mTOR	DLBCL, MCL
PARP inhibitor	Olaparib	PARP 1 & PARP 2	MCL

ALCL (Anaplastic large cell lymphoma), ALL (Acute Lymphocytic Leukaemia), CLL/SLL (Chronic Lymphocytic Leukaemia/Small Lymphocytic Leukaemia), DLBCL (Diffuse Large B-cell Lymphoma), FL (Follicular Lymphoma), iNHL (indolent NHL), MCL (Mantle Cell Lymphoma), MZL (Marginal Zone Lymphoma).

Therapeutic monoclonal antibodies

Antibodies are ~150 kDa Y-shaped IgG composed of two pairs of light and heavy polypeptide chains linked by disulphide bonds (Figure 3). They are made up of two variable light chains (V_L) and two variable heavy chains (V_H), two constant light chains (C_L), and six constant heavy chains (C_H). Complementarity determining regions (CDR) in the hypervariable regions of the variable region determine the antigen-binding characteristics of the antibody.

The antigen-binding region (Fab) consists of the V_L, V_H, C_L and C_H1 domains while the fragment crystallisable (Fc) region which interacts with cell surface receptors consists of the C_H2 and the C_H3 domains. The Fc region determines the isotype and mediates effector functions associated with antigen binding including CDC and ADCC (76, 77).
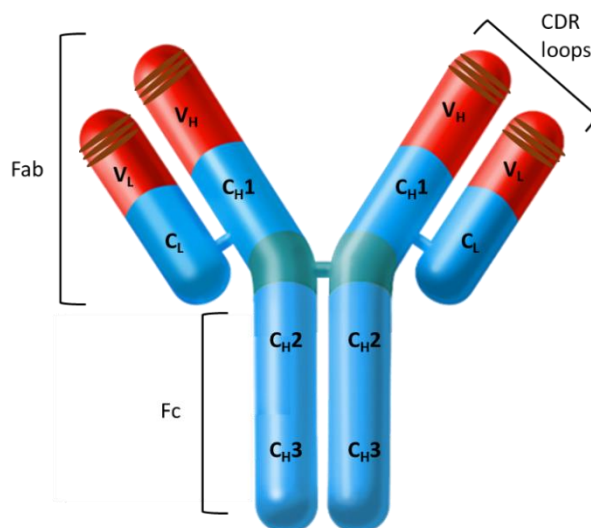
Figure 3. Schematic showing the structure of an IgG antibody

Monoclonal antibodies are developed for the treatment of a variety of cancer types, immunological disorders and infectious diseases (78). Their use as therapeutics stems from their conception by Kohler and Milstein in 1975 where they developed murine hybridoma cell lines that produced antibodies with predetermined antigen specificity (79).

The first approved therapeutic mAb was Orthoclone OKT3 (muromonab-CD3); a murine IgG2a directed against CD3 expressed on T-lymphocytes.

Its use as an immunosuppressant to prevent transplant organ rejection was limited due to induction of human anti-mouse antibody response (HAMA) (72, 80). In addition to HAMA, murine derived mAb have a short biological half-life, they inadequately recruit the human immune effector function and have limited penetration capability in tumour sites (72, 81). This prompted the search for mAb with relatively low immunogenicity by minimising non-human sequences in the antibody framework. Currently, the use of murine mAbs is limited to RIT with antibodies such as ibritumomab, lilotomab and tositumomab.

Chimeras were produced by fusion of murine Ab variable domains with human Ab constant domains making these chimeric mAbs 70 % human (82). Rituximab (MabThera) recognising CD20 on B-cell lymphoma was the first anti-cancer FDA approved chimeric mAb. Further Ab engineering through CDR grafting made it possible to substitute the hypervariable region of a fully human antibody with the hypervariable loops of the murine antibody of interest, creating a humanised mAb that is 85-90 % human (83).

Trastuzumab (Herceptin), specific for HER2/neu protein, was the first humanised mAb approved for therapy of metastatic breast cancer (84). The evolution of the Ab engineering process, from a fully murine antibody to the humanised antibody as seen in Figure 4 has greatly lowered the risk of inducing immunogenic responses (84).
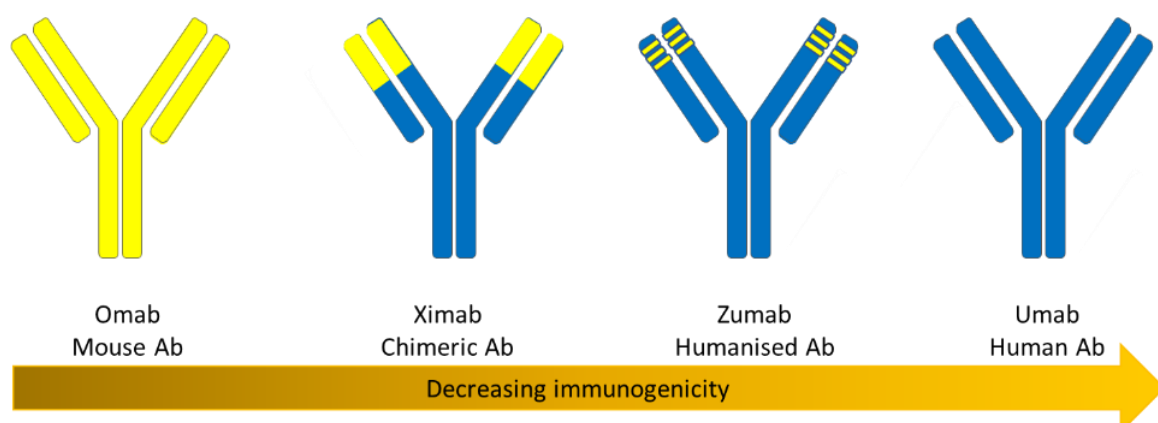

Figure 4. Schematic of the evolution of therapeutic mAbs towards the decrease in immunogenicity. The nomenclature suffixes: omab, ximab, zumab, and umab denote their origin from mouse, chimeric, humanised, and human antibodies respectively (85). Illustrations used in this figure were obtained from Servier Medical Art (smart.servier.com).

Currently, the FDA has approved seven therapeutic mAbs for the treatment of NHL (69) and a multitude of new ones are undergoing clinical investigations for their efficacies and toxicities.

Mechanisms of action of therapeutic mAb

Binding of therapeutic mAbs to target antigens inhibit the function of the bound antigen and activate direct or indirect effector functions that initiate the biological fate of the antigen expressing tumour cells (Figure 5).

Direct mechanisms lead to induction of apoptosis through receptor dimerization, activation of death receptors, and prevented activation of receptors that modulate proliferation and survival, making the tumour cells susceptible to therapy (86). Rituximab and obinutuzumab are examples of mAbs that induce apoptosis in malignant B-cells (54, 55).

The ability of mAb to mediate cellular cytotoxicity can be initiated through indirect effector functions. ADCC is an important indirect effector mechanism in therapeutic mAb. The antibodies bind to the target cell antigens and recruit immune effector cells such as NK cells, monocytes, macrophages and dendritic cells. NK cells express Fc receptors: FcγRIIc and FcγRIIIa, which bind to Fc regions of mAb. Subsequent binding of NK cells releases cytokines and granules containing perforin and granzyme B proteins which digest cell membranes, causing formation of pores and resulting in osmotic lysis of the antibody targeted cell (87).

Macrophages express all classes of Fcγ receptors and like NK cell they bind to Fc regions of tumour-bound antibodies resulting in antibody-dependent cellular phagocytosis (ADCP) which may lead to antigen presentation, initiating an adaptive immune response against tumours (88).

Monoclonal antibodies can activate a complement cascade on the surface of tumour cells, inducing cell death. The classical complement pathway is activated when complement component C1q complex binds to the Fc region of IgG or IgM attached to an antigen. This sequentially activates C1r and C1s proteins which in turn cleave C4 into C4a and C4b and C2 into C2a and C2b, creating a C3 convertase enzyme complex C4aC2b. This

enzyme cleaves C3 into C3a; a modulator of inflammation, and C3b which associates with C4aC2b to form C5 convertase.

C5b, cleaved from C5 by C5 convertase binds to the cell surface and recruits C6-C9 and together they form the membrane attack complex (MAC) which facilitates cell lysis (89).
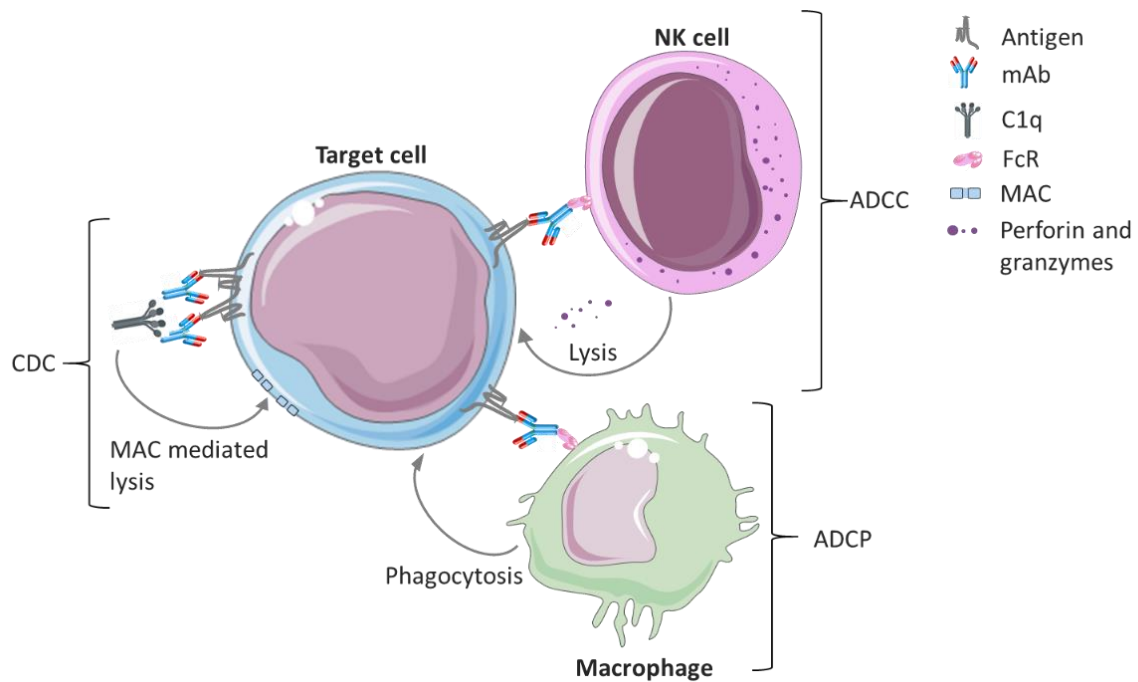
Figure 5. Mechanisms of action of therapeutic mAbs including ADCC and ADCP induced by effector cells, CDC through the membrane attack complex and by inhibition of the receptor dimerization, inducing an apoptotic signal.
Illustrations used in this figure were obtained from Servier Medical Art (smart.servier.com).

Rituximab

Rituximab is a first-generation type I mAb with immune effector function. It is formulated for intravenous (i.v) administration and has a terminal elimination half-life of 22 days after the first cycle of infusion (75).

Rituximab binds to CD20, resulting in the relocalisation of CD20 into lipid rafts, a mechanism that mediates direct cell death through apoptosis (90, 91). Complexing of the relocalised CD20 with rituximab increases C1q binding to Fc subsequently activating CDC activity (91, 92). Rituximab also binds NK cell Fc receptors with high affinity to induce ADCC. However, binding of complement components obstructs rituximab- Fc binding thus decreasing the intensity of ADCC activity (93).

CD20 is a 33–37 kDa non-glycosylated integral membrane phosphoprotein encoded by *MS4A1* gene (94). It contains 297 amino acids spanning the membrane with two extracellular loops and four transmembrane domains and cytoplasmic C- and N-termini (95).

Although absent in stem cells, CD20 is expressed on the surface of B-cells from early pre-B cell stage up until the activated mature B-cell stage where it is lost prior to terminal differentiation into antibody secreting plasma cells. CD20 has no known natural ligand and is thought to function as a calcium ion channel and binds to Src family tyrosine kinases involved in phosphorylation of intracellular proteins (15, 95, 96).

CD20 is non-shedding as cannot be detected in serum. However, exposure to rituximab may result in the decline of CD20 expression, primarily due to shaving off of the CD20/mAb complexes by THP-1 monocytes via Fcγ receptors and the pre-mature internalisation of the same, making it impossible for initiation of effector function. (5, 6, 97, 98) Additionally, exposure to rituximab results in increased expression of complement inhibitory proteins: CD55 and CD59 (99, 100), and rapid exhaustion of complement (101). All together, these events result in the development of rituximab resistance (6, 99, 102, 103).

To increase drug accessibility while maintaining safety and efficacy standards, rituximab biosimilars have been developed and are commercially available.

In an effort to improve patient outcome and as a new treatment strategy to overcome resistance, second and third generation humanised and fully human anti-CD20 mAbs have also been developed such as obinutuzumab, ocaratuzumab, ocrelizumab, ofatumumab and veltuzumab (95).

Obinutuzumab

Obinutuzumab is a recombinant, humanised glycoengineered type II anti-CD20 mAb presenting superior efficacy when compared to type I mAbs (54). It is formulated for i.v administration and has an elimination half-life of 28.4 days (75).

Unlike rituximab, obinutuzumab does not stabilise CD20 in lipid rafts therefore not initiating CDC to an extent similar to type I mAb. However, it induces caspase-independent direct cell death through the reorganisation of the actin cytoskeleton and homotypic adhesion followed by lysosome mediated cell death (104, 105).

Obinutuzumab binds at a different orientation to an overlapping CD20 epitope to that of rituximab (106). At saturating conditions, it binds half as much CD20 as rituximab (55, 104, 106). Afucosylation of the Fc portion of obinutuzumab results in a higher affinity for FcγRIII receptors on immune effector cells, significantly increasing ADCC and ADCP (55, 104). Unlike type I mAbs, obinutuzumab potently induces caspase independent cell death

2.3.2 Radioimmunotherapy

RIT is a powerful tool for the potential eradication of targeted tumour cells while sparing normal cells. It exploits the use of mAb as carriers of radioactivity, to deliver therapeutic doses of radiation that cause lethal DNA damage to tumour cells expressing disease-specific antigens (9).

To optimally exploit the therapeutic abilities of RIT, the biology of the target, the choice of mAb, the choice of radionuclide and the metabolic fate of the antibody/ antigen complex must be taken into consideration (61, 107).

The biology of the target is based on a similar principle as in immunotherapy discussed earlier in section 2.3.1, where identification of the tumour-associated antigen is fundamental.

Antibody characteristics such as size, tissue penetration and clearance rate influence the therapeutic and toxicity profile of RIT. Circulation of chimeric/ humanised antibodies via the neonatal Fc receptor (FcRn) and the molecular weight of the antibodies being above the glomerular filtration limit of the kidneys may result in medium to long biological half-life of antibodies. This imposes a risk for haematological toxicity because of increased radiation dose exposure to the bone marrow. The large molecular weight might also hinder the penetration of the antibody into the tumour (61, 108).

Choosing a radionuclide to use for RIT is dependent on the type of application the therapeutic is intended for i.e. tumour size and heterogeneity, radionuclide distribution and pharmacokinetics. Radionuclide properties primarily determine the extent of dose deposition.
The physical half-life of the radionuclide should match with the tumour uptake kinetics of the antibody in order to optimise radiation dose to the tumour. A short half-life in the

order of days is optimal because a longer half-life is likely to increase absorbed dose not only in the targeted cells, but also in the surrounding tissues. In addition, the radionuclide should emit particulate ionising radiation sufficiently abundant to exert a cytotoxic reaction in tumour cells often mediated by reactive oxygen species (ROS) from radiolysis of intracellular water (109-111).

Radioactive emissions

Emission of particulate and electromagnetic radiation occurs as a result of radioactive decay where an unstable atomic nuclei approaches a more stable neutron to proton ratio by releasing different forms of ionizing radiation, including: alpha (α) particles, beta (β) particles and auger electrons as well as gamma (γ) and X-rays, all having different path lengths (Figure 6).

Radionuclides emitting alpha particles (e.g. ^{211}At, ^{211}Bi, ^{212}Pb, ^{223}Ra, ^{225}Ac and ^{227}Th); identical to a helium nucleus with two protons and two neutrons, are highly potent due to the high linear energy transfer (LET) of 50-230 keV per µm. Alpha particles have low penetration power traversing a short path length covering approximately 50 to 90 µm in tissue (109, 112) making them highly effective at eradicating microscopic and disseminated tumour cells with minimal undesirable irradiation of healthy tissue. When compared to the other radiation emissions, α particles confer a high relative biological effectiveness (RBE) for cell death through irreparable DNA double strand breaks, presenting as apoptosis or necrosis (112). RBE of α-particle therapy is not impeded in tumours under hypoxic conditions (113).

Auger electron emitters (e.g. ^{67}Ga, ^{111}In, ^{125}I and ^{195m}Pt) have intermediate LET of 4–26 keV per µm and similar to α-particles, they have a low penetration power (<1 µm) and are highly cytotoxic when in close proximity to nuclear DNA subsequently minimising cross-fire toxicity (114).

Beta emitters (e.g. ^{90}Y, ^{177}Lu and ^{131}I) release a single negatively charged electron or positron from an unstable atomic nucleus. The particle mass is 1/8000th that of an α particle. This particle has low LET of 0.2 keV per µm and a high penetration power with a tissue path length of between 0.3 to 12 mm. The long range of the particle is desirable

for RIT of tumours with heterogenous antigen expression as it allows for irradiation of proximal tumour cells within striking distance of the β-particles through a process known as crossfire effect. Unlike high LET radiation, low LET radiation is dependent on oxygen to generate ROS and therefore its RBE is decreased in hypoxic tumours (109).

Gamma rays are high energy electromagnetic radiation with no mass or charge and a wavelength of <1nm. γ radiation follows α and β radioactive decay processes and is useful for imaging diagnostic evaluation and dosimetry (115).
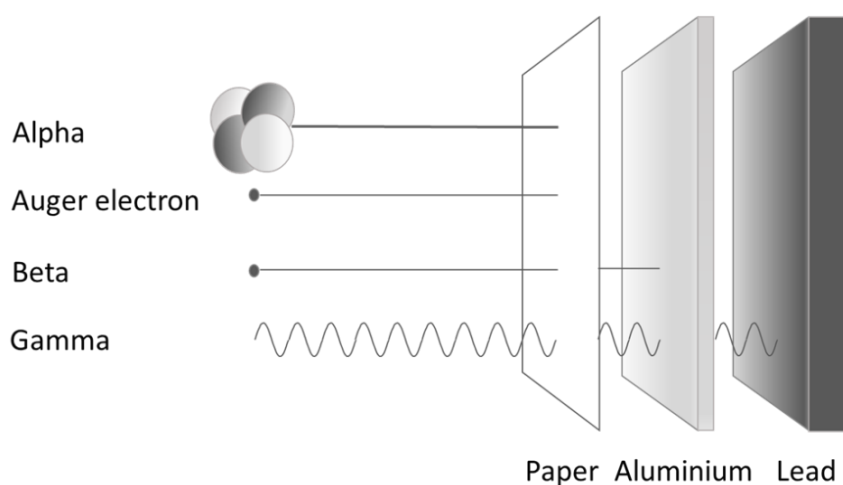
Figure 6. The different types of radiation emissions have different abilities to penetrate matter depending on their mass and energy. α-particles and auger electrons can be stopped by a sheet of paper, while β-particles can be stopped by an aluminium plate and a block of lead can stop penetration of γ rays.

Biological effects of radiation

I. <u>DNA damage</u>

Radiation induced DNA lesions primarily occur as highly genotoxic double strand breaks (DSB) formed by a break in the phosphodiester backbone of both strands of the DNA separated by 10 or less base pairs. Single strand breaks (SSB) and the generation of ROS are secondary radiation induced effects (58, 116). Collectively, these effects increase linearly with the radiation dose and if unrepaired, can result in altered genome structure (58). Accumulation of unrepaired DNA damage in cells resulting in genomic instability

causes the activation of proto-oncogenes and inhibition of tumour suppressor genes that can lead to cancer formation.

In response to DNA damage, cells initiate a protein phosphorylation driven signalling cascade known as the DNA damage response (DDR) entailing activation of DNA repair pathways, cell cycle checkpoint mechanisms and apoptosis depending on the complexity of the DNA lesion (116).

DSB are repaired by two main pathways: i) homologous recombination (HR) pathway which requires the homologous sequence of undamaged sister chromatid during the late S and G2 phases of the cell cycle as a template for DNA repair (117) and ii) non-homologous end-joining (NHEJ) pathway which is an error prone process that recognises and ligates fragmented DNA ends throughout the cell cycle. This process can lead to loss of genetic information (118).

SSB are normally corrected by the base excision repair (BER) pathway which include proteins such as PARP-1, XRCC1, DNA ligase IIIα, and apurinic/apyrimidinic endonuclease (APE1). BER ensures that damaged bases are excised and replaced with newly synthesised DNA. At points of bulky SSB that distort DNA helical structures, the nucleotide excision repair (NER) pathway is activated (119, 120).

II. Cell-cycle arrest

Cell cycle arrest functions interdependently with DNA damage repair and apoptosis. As a result of radiation induced DNA damage, cell cycle checkpoint protein kinases ATM and ATR are activated and recruited to sites of DSB and SSB respectively. ATM/ATR coordinate a cascade of downstream events through phosphorylation of CHK1 and CHK2 protein kinases, resulting in activation phosphorylation of Cdc25A and p53 transcriptional factors which downregulate the activity of cell cycle regulating kinases CDK1 and CDK2. This results in cell cycle arrest in G1 and G2 phase respectively, availing time for DNA repair processes to occur before replication or mitosis takes place (116, 121, 122).

III. Mitotic catastrophe

Radiation-induced DNA damage may cause aberrant mitosis. Hyper amplification of centromeres produces multipolar mitotic spindles resulting in atypical chromosome segregation and cell division with daughter cells containing abnormal nuclear

morphology leading to mitotic catastrophe. Cell death through mitotic catastrophe is delayed by up to six days following irradiation. Compromised DNA repair mechanisms facilitate amplification of chromosomal aberrations over several cycles of cell division forming aneuploid/polyploid colonies (122, 123).

IV.   <u>Apoptosis</u>

An evolutionary conserved process of cell death, apoptosis is characterised by cell morphological changes such as cytoplasm and nucleus condensation, DNA fragmentation and formation of apoptotic bodies which are rapidly phagocytised by macrophages. Unsuccessful DNA repair of radiation induced DNA damage primarily activates the intrinsic apoptotic (mitochondrial) pathway. This pathway results in mitochondrial outer membrane permeabilization (MOMP) by pro-apoptotic Bak, Bax and Bok proteins, facilitating the mitochondrial release of cytochrome c to the cytosol where apoptosome complexes form and subsequently activate caspase 9 which triggers a cascade of caspase activation and eventual cell death (122, 124).

Radiation mediated activation of tumour suppressor gene *p53* causes the activation tumour necrosis factor receptors (TNFR) induces the extrinsic apoptotic (death receptor) pathway, resulting in caspase activation through formation of death-inducing signalling complex (DISC). This executes cell death as well as activate the intrinsic pathway (122, 125).

V.   <u>Necrosis</u>

High dose radiation can induce necrotic cell death. Unlike apoptosis, necrosis does not require a signalling cascade. Cellular organelles swell and dysfunction and cells lose their plasma membrane integrity. Often, necrotic cells initiate an inflammatory response in the surrounding tissue (126).

VI.   <u>Senescence</u>

Senescent cells undergo a stable loss of proliferative capacity while maintaining their viability and metabolic activity. These cells are characteristically enlarged, flat, extensively vacuolized, have condensed chromatin and often multinucleated. They also acquire alterations in gene expression and secrete factors that change the surrounding microenvironment, influencing cell growth or suppression (122, 123).

CD37 targeting RIT

A plethora of clinical studies have demonstrated the efficacy of RIT with Zevalin and Bexxar in NHL, resulting in significantly improved survival and manageable haematological toxicity with exception of patients with bone marrow involvement (127). Currently, RIT targeting CD37 with Betalutin® is under clinical evaluation for its efficacy and toxicity profile in patients with relapsed/ refractory NHL under ClinicalTrials.gov identifiers: NCT01796171, NCT02658968 and NCT03806179.

These studies aim to: Determine the maximum tolerated dose, pharmacokinetics and efficacy of Betalutin in patients with relapsed/refractory FL (NCT01796171) and DLBCL (NCT02658968) as well as characterise the safety, tolerability, pharmacokinetics, pharmacodynamics and preliminary anti-tumour activity of Betalutin in combination with rituximab in relapsed FL (NCT03806179).

Betalutin® consists of the beta (β)-particle emitting radionuclide Lutetium-177 (^{177}Lu), conjugated to CD37 targeting murine mAb lilotomab linked with the bifunctional chelator satetraxetan (p-SCN-Bn-DOTA) (128) (Figure 7).

CD37 is a glycosylated tetraspanin transmembrane protein of molecular weight 40-52 kDa. It is expressed in high density on the surface of pre-B cells all through to mature B-cells and is absent on plasma cells (129). Although the function of CD37 is largely unknown, it is thought to function as a death receptor through mediating signal transductions that initiate cell death (130). Additionally, CD37 is present in endosomes and exosomes suggesting its involvement in intracellular trafficking and antigen presentation (130, 131). CD37 sheds off the surface of B-cells and it is also internalised, prominently so, when compared to CD20 (128, 132, 133).

^{177}Lu has a half -life of 6.7 days and decays to the stable isotope Hafnium-177 (^{177}Hf). The β particles are emitted with energy β(max) of 497 keV and low energy gamma photons of 208 keV (11 %) and 113 keV (6.4 %) are simultaneously emitted. The radiation emissions allow for the development of theranostic agents using ^{177}Lu. The average tissue penetration depth of ^{177}Lu is 0.67mm (134).
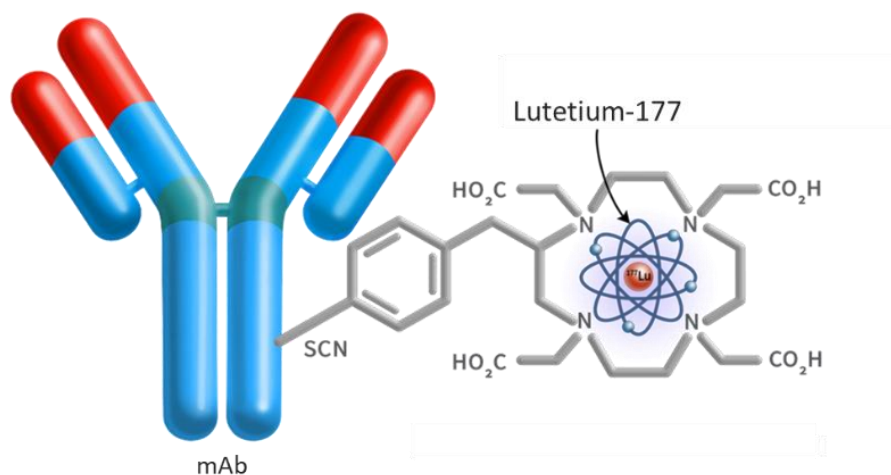
Figure 7. Structure of the radioimmunoconjugates: Betalutin and Humalutin.

Betalutin binding to CD37 and its' internalization initiates targeted radiation-induced DNA damage by producing irreversible DNA strand breaks resulting in cell death. Due to the long tissue penetration path, malignant cells in the vicinity of the target bound cell also receive a dose of the cytotoxic radiation through the crossfire effect process (Figure 8). Betalutin can also modulate the immune system and the tumour microenvironment, initiating an immune response (135).

Pre-clinical and clinical studies evaluating the pharmacokinetics of Betalutin report modest haematological toxicity at maximum tolerated doses, a good biodistribution profile with high tumour to normal organ absorbed dose ratio. Red marrow is the dose-limiting organ for Betalutin treatment and pre-dosing with lilotomab increases the tumour to red marrow absorbed dose ratio. Accordingly, the gamma yield of ^{177}Lu allows for post-therapy imaging of Betalutin (133, 136-141).

Humalutin® on the other hand consists of a chimeric CD37 targeting mAb; NNV003, which has been characterised to function through induction of ADCC and ADCP (142) in addition to radiation induced effects. These additional mechanisms of action indicate that Humalutin may have superior potency in comparison to Betalutin.
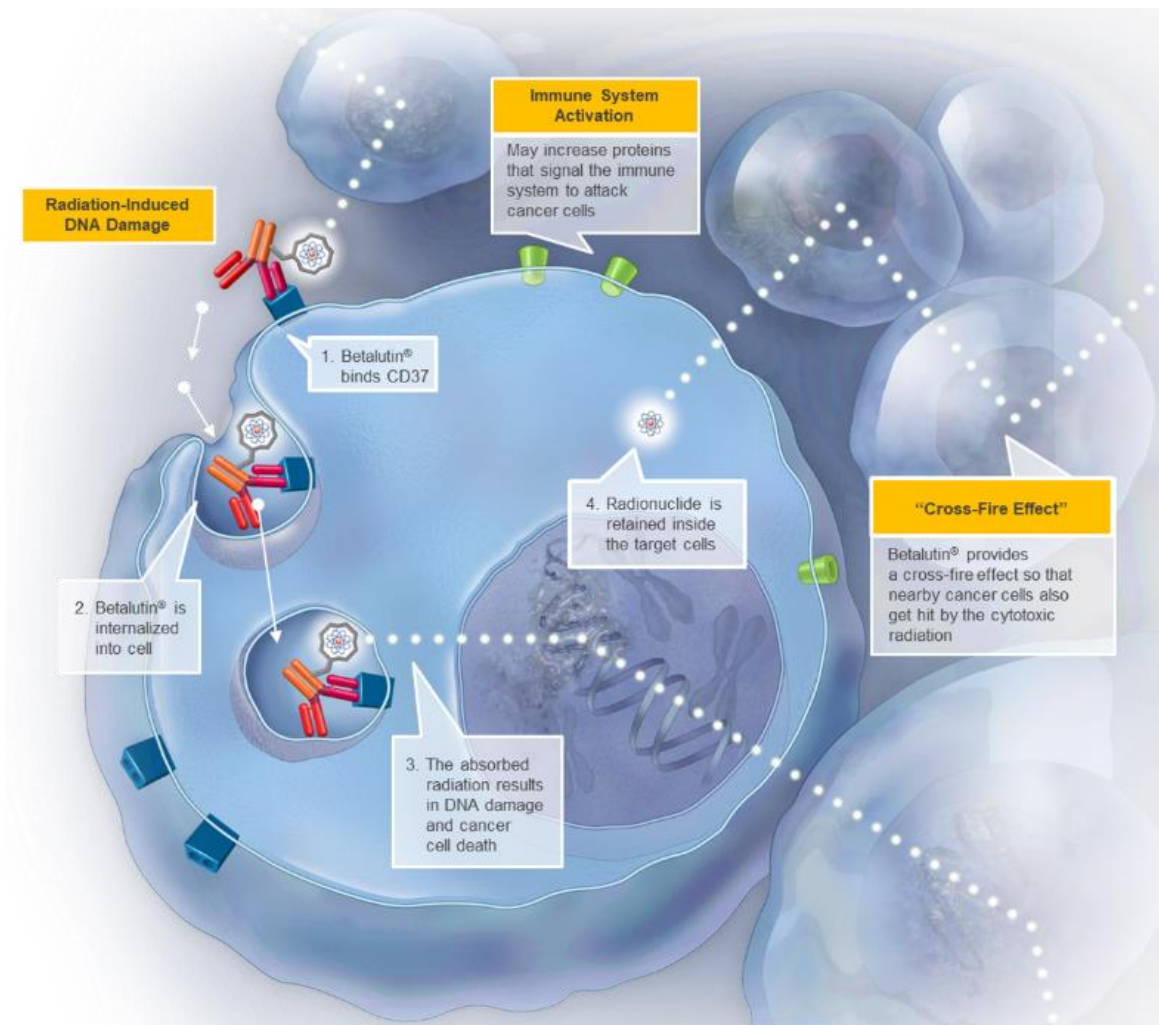
Figure 8. Schematic illustrating the mechanism of action of Betalutin and Humalutin.

2.3.3 Small molecule inhibitors

Multiple molecules in cellular pathways play a vital role in the development and progression of cancer, thereby presenting alternative targets for tumour therapy. Small molecule inhibitors (SMIs) target the different components of these pathways, eliciting changes in the transduction of signal cascades. SMIs, typically ≤ 500 Da in size, easily translocate across cell plasma membranes allowing for rapid interactions with their molecular cell targets.

SMIs have been successfully used as potent and effective therapeutics. The targets for SMIs include transcription- regulating proteins, protein kinases, apoptotic proteins and transport proteins. Regulation of these proteins alters cell signal transduction and primes the cells for decimation (143, 144).

There are limitations associated with SMI therapy. Some SMIs bind to multiple molecular targets, leading to toxicity in patients. Due to biological heterogeneity and molecular evolution, it has been observed that some patients are either non-responsive to SMI therapy or develop resistance (145). Combination therapies are being explored to avert drug resistance and improve therapeutic outcomes in patient sub-groups with refractory/ relapsed disease (144).

In this thesis, the SMIs: olaparib which targets and inhibits PARP and venetoclax which targets and inhibits Bcl-2 have been evaluated when in combination with Humalutin.

PARP inhibitors

DDR mechanisms are activated by DNA lesions, further recruiting signalling molecules that mediate DNA repair. While repair of damaged DNA is fundamental, it is also desirable that malignant cells carrying mutated gene information are decimated. In cancer, several genes involved in DDR among them *ATM*, *BRCA*, *PTEN* and *p53* lose their native function due to loss-of-function mutations (146). Malignant cells inherently display high levels of DNA damage due to loss of DNA repair pathways and accumulation of reactive oxygen species (ROS) resulting from oxidative and replication stress (116). For survival, these cells utilise other compensatory DNA repair strategies to prevent catastrophic DNA damage. Hence, there are many cancer therapeutics designed as stop mechanisms to inhibit functionality of DDR components in malignant cells.

Olaparib is an FDA approved PARP inhibitor for the treatment of BRCA mutated ovarian and breast cancers (147). It is a potent inhibitor of PARP1 and PARP2 isoforms of the PARP enzyme family. PARP1 and PARP2 are correlatively activated in response to DNA damage, catalysing the polymerisation of ADP-ribose (PARylation) to target DNA-associated nuclear proteins. These isoforms induce BER in response to DNA SSB and function as modulators of proteins involved in DNA repair, replication and transcription (119).

Olaparib functions by binding to the catalytic domains of PARP1 and PARP2, inhibiting PARylation. The inhibitor bound PARPs are unable to recruit PARP- dependent DNA repair proteins. Additionally, the inactive PARP enzymes are trapped at the site of SSB

initiating the stalling and collapse of the DNA replication fork which results in cytotoxic DSB of PARP-DNA complexes (148) (Figure 9).

Malignant cells often exhibit upregulated PARP1 activity, making it an attractive target to inhibit. Monotherapy with PARP inhibitors have shown significant therapeutic activity in cancers associated with defects in BRCA1 and BRCA2 genes as a result of synthetic lethality (146, 149). Similarly, MCL harbouring ATM mutations are a viable candidate for PARP inhibition (150, 151). When in combination with radiotherapy, olaparib has been shown to sensitize malignant cells to DNA damage induced by ionizing radiation (152-154).
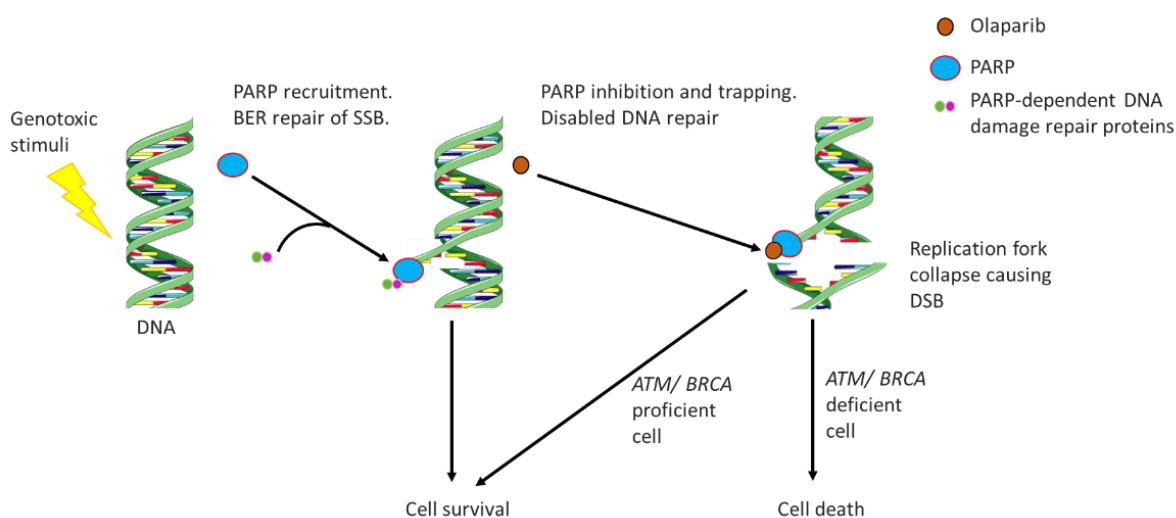
Figure 9. Mechanisms of olaparib action promote cell death by trapping PARP at sites of DNA single strand breaks and subsequently DNA double strand breaks from the collapse of the DNA replication fork. Illustrations used in this figure were obtained from Servier Medical Art (smart.servier.com).

BH3 mimetics

Malignant cells characteristically overexpress pro-survival genes, lose *p53* tumour suppressor gene function and have mutated pro-apoptotic proteins, resulting in the evasion of apoptosis (155). Regulation of apoptosis through the B-cell lymphoma 2 (BCL2) protein family is therefore a therapeutic opportunity for targeted therapy. This protein family is made up of 3 sub-groups, i.e. anti-apoptotic proteins (Bcl-2, Bcl-xl, Bcl-w, Mcl-1 and A1/Bfl-1), pro-apoptotic effector proteins (Bax, Bak and Bok) and pro-

apoptotic BCL2 homology 3-only (BH3) initiator proteins (Bad, Bid, Bik, Bim, Bmf, Hrk, Noxa and Puma) (156).

BH3 mimetics have been developed to inhibit the anti-apoptotic proteins aberrantly expressed in malignant B cells (156, 157).

BH3 initiator proteins activate Bax and BAK proteins directly or indirectly by binding with high affinity to Bcl-2 anti-apoptotic proteins, consequently relieving the effector proteins of inhibition.

Activation of Bax and Bak; which are mitochondrial membrane resident proteins, leads to conformational changes that result in mitochondrial outer membrane permeabilization (MOMP). This facilitates the mitochondrial release of membrane sequestered cytochrome c into the cytosol where it binds Apaf -1 monomers. The APAf-1-cytochrome c assemble to form apoptosome complexes which in turn recruit and activate caspase 9, triggering a cascade of caspase activation and eventual cell death (124, 155, 156) (Figure 10).
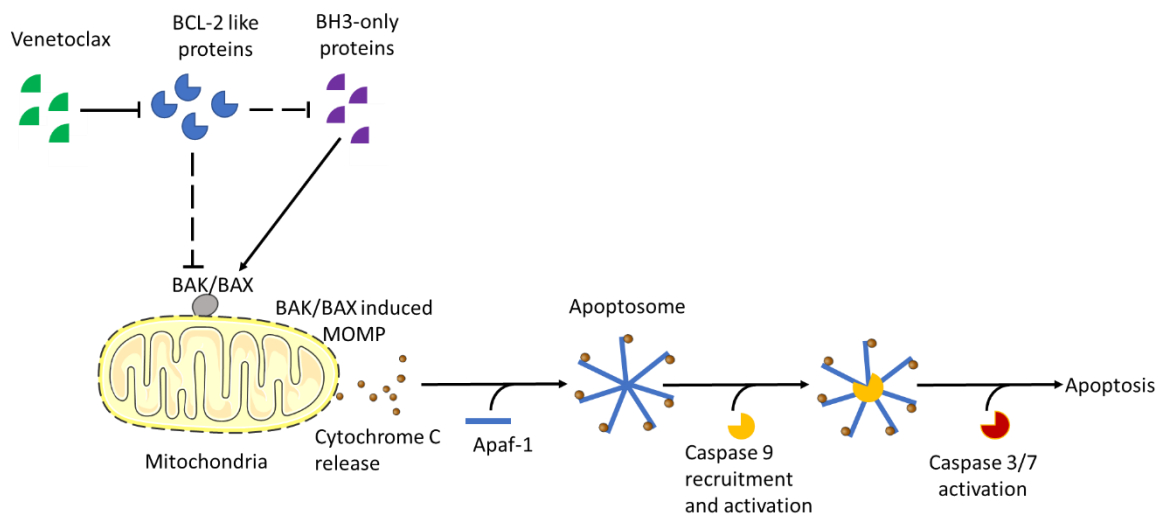
Figure 10. BH3 mimetics bind to and inhibit Bcl-2 anti-apoptotic proteins recurrently overexpressed in malignant cells. Illustrations used in this figure were obtained from Servier Medical Art (smart.servier.com).

Venetoclax (ABT-199) is an FDA approved BH3 mimetic targeting Bcl-2 anti-apoptotic proteins and was developed as a treatment for AML and CLL. The clinical efficacy profile of venetoclax as a monotherapy and in combination with other therapies reveals a significant overall response rate in patients with CLL, DLBCL, FL, MCL and MZL (158-161).

Upregulation of anti-apoptotic proteins, downregulation of pro-apoptotic proteins and acquired mutations in Bcl-2 and BAX proteins may result in acquired resistance to venetoclax monotherapy. To mediate this, strategies such as combination therapies with therapeutics that can deregulate anti-apoptotic proteins are ongoing (162, 163). Venetoclax in combination with RIT has shown synergistic efficacy and improved survival in NHL models (164).

3 Objectives

The overall objective of this thesis was to evaluate the pre-clinical therapeutic efficacy of combining CD37 targeting RIT with CD20 targeting therapeutic mAbs and SMI: olaparib and venetoclax, in NHL.

Combination therapies enable the delivery of potent cytotoxic drugs at lower doses than that of the respective monotherapies, resulting in additive or synergistic therapeutic effects with limited toxicity. Additionally, combination therapy both minimises the risk to develop drug resistance and combats drug resistance.

In this regard, we investigated:

- The effectiveness of Betalutin in increasing rituximab binding to CD20 in both rituximab resistant and rituximab sensitive cells.
- The anti-tumour efficacy of combining Betalutin with rituximab in rituximab sensitive and resistant disease models.
- The *in vitro* combination outcome of Humalutin with olaparib.
- The *in vitro* combination outcome of Humalutin with venetoclax.
- The combination effect of Humalutin with olaparib on gene expression.
- The gene mutations that are determinants of synergistic cytotoxicity induced by the combination of Humalutin and olaparib.

4 Methodology

4.1 Cell lines

Human cancer cell lines are an invaluable tool in cancer research and drug development. They provide a robust disease model to assess tumour pathology and develop new treatment strategies. Cancer cell lines are established from aggressively proliferating, poorly differentiated late stage cancers that have accumulated mutations that enable their indefinite growth. Although many cancer cell lines experience genetic divergence from their primary tumours, lymphoma cell lines coherently restate gene expression profiles identical to their primary tumours and also do not senesce over extended passages (165-167).

As a model system to study the efficacy of combination therapies in NHL, we used BL, DLBCL and MCL cell lines in this thesis. The cell lines were authenticated to validate their identity. In the course of the *in vitro* studies, the cell lines were subcultured up to 30 passages.

In paper I, we used Daudi cells (BL) and Rec-1 cells (MCL) to study the effects of Betalutin on CD20 expression and its therapeutic potential when combined with rituximab. Both cell lines express differing but sufficient quantities of the test targets; CD20 and CD37 (128, 135).

In paper II, we used rituximab resistant BL cell line Raji 2R and the corresponding rituximab sensitive parental cell line Raji, both licensed from Roswell Park Cancer Institute (NY, USA). Rituximab resistance in Raji 2R cells was acquired through cumulative exposure of the cells to escalating concentrations of rituximab in the presence of complement proteins. The CD20 expression density in Raji 2R cells is downregulated by about 90 % compared to that of Raji cells (99). Radioligand binding assays using Betalutin were performed on both Raji and Raji 2R cells and scatchard analysis was used to determine the CD37 expression density in each cell line.

The two cell lines were chosen so as to quantify and comparatively demonstrate the potential of Betalutin in reversing rituximab resistance.

In paper III, DLBCL cell lines: DOHH-2, SU-DHL-4, WSU-DLCL-2 (all of ABC origin) and OCI-LY-10, U-2932 (both of GCB origin) as well as MCL cell lines: Granta-519 and Rec-1 were used to assess the combination effect of Humalutin with olaparib and venetoclax. These cells were chosen due to the unique genetic mutations they harbour which are anticipated to directly or indirectly influence the outcome of the combinations. In all the studies, Ramos cells (BL) were used to validate the immunoreactive fraction (IRF) of the test radioimmunoconjugates (RICs).

4.2 Radioimmunoconjugates

4.2.1 Protein radiolabelling

CD37 targeting murine IgG1; lilotomab, originally developed at the Norwegian Radium hospital and its' chimeric variant; NNV003 conjugated to a bifunctional chelator; 2-(4-isothiocyanatobenzyl)-1,4,7,10 tetraazacycododecane-1,4,7,10-tetraacetic acid (p-SCN-Bn-DOTA/ DOTA/ satetraxetan) were labelled with ^{177}Lu under controlled temperature and pH. The resulting radioimmunoconjugates (RICs) are known as Betalutin and Humalutin respectively.

Before the start of radiolabelling, the pH of the DOTA conjugated mAbs was adjusted to 5.3 ± 0.3 using 0.25 M ammonium acetate buffer and the solution temperature adjusted to 37˚C. An appropriate volume of ^{177}LuCl$_3$ solution (Isotope Technologies Garching, ITG Germany) was added to the DOTA-mAbs making up a specific activity of about 200 MBq and 600MBq per mg of antibody depending on whether the conjugate was required for an *in vitro* or *in vivo* study. The radioconjugate was incubated with gentle shaking at 37˚C for up to 30 minutes after which the reaction was stopped using a formulation buffer. For studies using Betalutin (i.e. papers I, II and combination with obinutuzumab), the formulation buffer was made of phosphate-buffered saline (PBS) containing 7.5 % v/v recombinant albumin (Novozymes Biopharma, Denmark), and 10 mM DTPA (HeylPharma, Germany) pH adjusted to 7.5. For studies using Humalutin (i.e. paper III and the combination with venetoclax), the reaction was stopped by adding PBS containing 20 % Glycerol (Merck, Germany) and 0.3 % Tween20 (VWR, USA).

This solution was used to allow for accurate dispensing of the radioconjugate by the D300e digital drug printer (Tecan, Switzerland). The surfactant and glycerol reduce the fluids' surface tension and enables priming to the dispense heads.

4.2.2 Radiochemical purity

Once the radiolabeling reaction was complete, thin-layer chromatography was used to determine the radiochemical purity (RCP) of the RIC. This was done by mixing the radioconjugate with formulation buffer at a ratio of 1:100 and spotting the mixture on the baseline of an ITLC Tec-Control chromatography strip (Biodex medical systems, NY, USA) as shown in Figure 11.
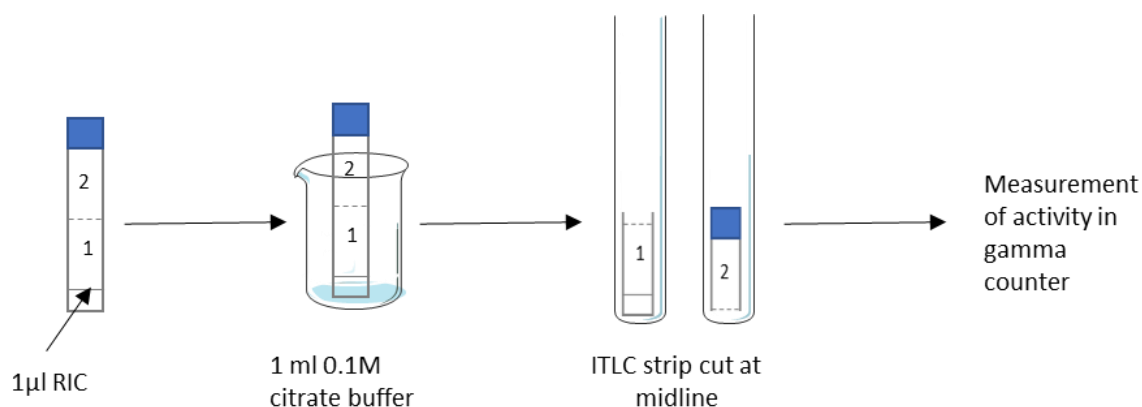
Figure 11. Procedure followed in evaluating the RCP of 177Lu labelled mAbs using 1μl of the RIC placed at the base mark point of an ITLC strip and allowed to develop in citrate buffer. The strip is cut at the mid mark point and the two parts separately measured on a gamma counter.

To allow separation migration of the free radiometal from the RIC, the strip was immediately placed into a vial containing 0.1 M citrate buffer of pH 5 and developed until the solvent front migrated to the front line. The radiolabelled mAb is retained in the base-line and free ^{177}Lu migrates to the front line. The strips were cut at the central line into halves and the radioactivity of each half strip was measured in a gamma counter (2470 Wizard^{2TM}, PerkinElmer, UK).

The RCP is then calculated using equation 1. The conjugation was valid if the RCP was above 95 %. If below 95 %, the radioconjugate was purified using Sephadex G-25 PD-

10 columns (GE Healthcare Life Sciences) and RCP was again measured after purification to verify the 95 % cut-off.

$$RCP\ (\%) = \frac{A}{A + B} \times 100$$

where:

A is activity from the base-line section 1

B is activity from the front-line section 2

4.2.3 Immunoreactive Fraction

The fraction of immunoreactive antibody of the RICs was determined using the Lindmo method where the fraction of radiolabelled mAbs bound to cell antigens in the presence of unlimited antigen excess is determined (168). Validated modifications were made to this method where single-cell suspensions of Ramos cells were prepared to a cell concentration of 75×10^6 cells/ml and 0.2 ml aliquots made in 5 ml glass tubes as illustrated in Figure 12. To measure unspecific binding of either of the radiolabelled antibodies, cells in 2 of the vials were incubated at room temperature for 15 minutes with 20μg (100 μg/ml) of the respective unlabelled mAb. In all 5 vials, 8 ng (40 ng/ml) of RIC was added and incubated at room temperature for 1 hour with gentle agitation at 350 rpm. After incubation, the cells were measured in the gamma counter and washed 3 times with 0.5 ml of 0.5 % (w/v) bovine serum albumin (BSA) in PBS to remove unbound activity. After wash, the activity in the cells was once again measured. Immunoreactive fraction of the RIC was calculated as specific cell-bound radioactivity using equations 2.1 to 2.3.

An IRF output above 60 % was acceptable for validation of the RIC for experimental use. Anything below 60 % was discarded as the functional efficacy of the RIC was considered compromised.

$$Total\ binding = Non\ blocked\ sample \left(\frac{Activity\ after\ wash}{Activity\ before\ wash} \right)$$

$$Non\ specific\ binding = \ Blocked\ sample\ (\frac{Activity\ after\ wash}{Activity\ before\ wash})$$

$$Specific\ binding = (Total\ binding - Non\ specific\ binding)$$
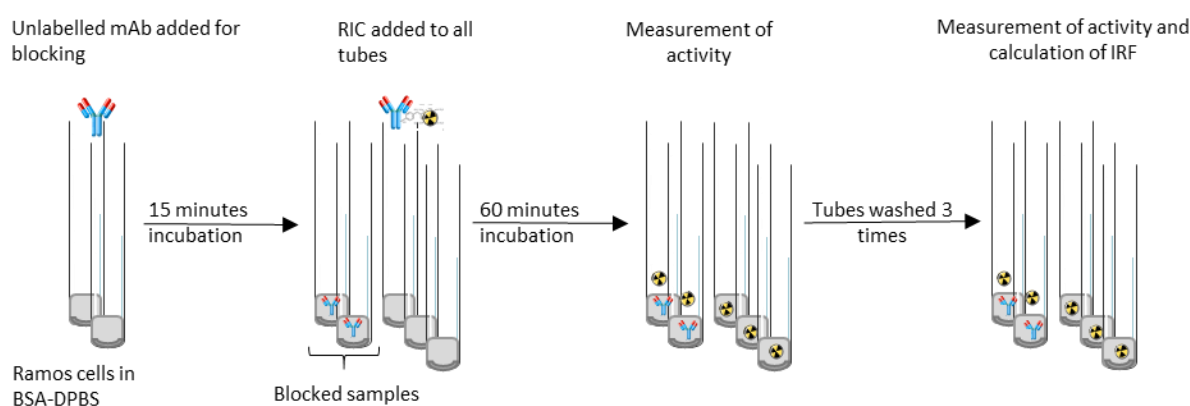
Figure 12. Schematic representation of the IRF procedure.

4.3 *In vitro* **studies**

In the development and screening of pharmaceuticals, *in vitro* studies provide important insights into the potential biological effects of the drugs on specific cellular and molecular mechanisms. These studies make it possible to evaluate a series of experiments under similarly controlled conditions.

Outcomes of *in vitro* studies facilitate a correlative understanding of *in vivo* responses, thereby providing a reference point for clinically viable data. Additionally, the use of *in vitro* models replaces, reduces and refines the use of animal models. When compared to *in vivo* studies, *in vitro* studies are a cost-effective and rapid approach to answering multiple biological questions.

However, a notable limitation of *in vitro* studies using basic cell culture setups is the biased misrepresentation of the tumour microenvironment. The homeostatic regulation of cell in culture is altered by the depletion of nutrients, accumulation of waste products and less than optimal oxygen levels in the cell culture medium in comparison

to *in vivo* homeostasis. This makes data extrapolation to *in vivo* setups rather challenging, but not impossible.

4.3.1 Experimental optimisation

Optimisation of experimental conditions is fundamental for the robust reproducibility of experimental outcomes.

Since the use of cells in culture is primary to *in vitro* studies, cell proliferation patterns of the cell lines used in this thesis were evaluated under different controlled experimental setups. This included evaluation of cell growth rates using different cell concentrations and different sized culture flasks and well plates over a period of time. The optimal cell culture conditions were thereafter used for further experimental work.

To identify the concentration of rituximab to use in assessing CD20 upregulation, the cells were exposed to escalating concentrations of rituximab and the maximal binding concentration was identified as 30 µg/ml. This was the concentration of rituximab used in the flow cytometry experiments.

To identify the optimal effector to target cell ratio to use in the ADCC assay, multiple cell ratios were assessed and 2:1 was found to be optimal for use in the ADCC assay.

4.3.2 Flow cytometry

Flow cytometry is a robust and accurate technique for assessing multiparametric characteristics of cells in suspension. It allows for single-cell analysis through the hydrodynamic focusing of a fluid stream of cells tagged with fluorescent probes through a beam of laser light, causing light scatter and emission of light at varying wavelengths. The point of laser focus is surrounded by multiple detectors that collect and quantify the scattered and emitted light to determine the quantity and type of components present in cell samples.

Rituximab was directly conjugated with either Alexa 488 or Alexa 647 fluorescent dye: (Invitrogen, MA, USA). The dyes have a succinimidyl ester moiety that reacts efficiently with primary amines of proteins to form stable dye-protein conjugates.

In paper I, the effect on CD20/ rituximab binding after treatment of Daudi and Rec-1 cells with either lilotomab, EBR or Betalutin® was evaluated. At various timepoints

within the experiment, Alexa conjugated rituximab was incubated with the cells and rituximab binding on surface CD20 evaluated as described in the paper.

In paper II, Raji and Raji 2R cells were treated with either PBS, lilotomab or Betalutin, and the CD20/rituximab binding was evaluated in these cells 3 and 6 days after treatment. Here, we implemented the barcoding method to maximise robustness by minimising on staining variations, pipetting errors and antibody consumption while enabling the simultaneous acquisition of data.

Raji cells were first stained with a DNA staining dye; Hoechst 33342. The Raji cells were then pooled with Raji 2R cells then labelled with Alexa conjugated mAb. The Hoechst signal allowed for the distinctive identification of Raji from Raji 2R cells and appropriate gating of live cell population.

Cells contain naturally fluorescing substances such as reduced pyridine nucleotides and oxidised flavins which are detected as a fluorescent signal. For this reason, the fluorescence intensity of unstained controls was subtracted from the intensity of the stained samples.

4.3.3 ADCC assay

As elaborated in section 2.3.1, ADCC is an important mechanism of action for many mAbs.

In paper II we incorporated an assay that reported on ADCC, using a bioluminescent ADCC reporter assay kit (Promega Corporation, WI, USA) for quantifying rituximab induced cytotoxicity in Raji and Raji 2R cells after treatment with either PBS or Betalutin. While the primary endpoint of classical ADCC *in vivo* is cell death, the reporter assay uses an alternative endpoint occurring earlier in the ADCC process. In this assay, Jurkat cells engineered to stably express FcγRIIIa and a luciferase reporter driven by nuclear factor of activated T-cells (NFAT) are used as effector cells. Crosslinking of rituximab with FcγRIIIa on the effector cells initiates NFAT activation and subsequently luciferase activity (169).

ADCC activity of rituximab in the treated cells was quantified with luminescence readout of luciferase activity in the effector cells. The detailed experimental procedure is described in the paper.

4.3.4 Cell proliferation assay

Cell proliferation analysis is essential in determining the toxicity of compounds directed against tumour cells. This analysis is typically based on measurement of cellular DNA content or cellular metabolism. Here, cell proliferation assays were performed to evaluate the pharmacodynamic interactions of combining Humalutin with olaparib and with venetoclax. Cell viability after cell exposure to the drugs was evaluated in real time over a period of 48 hours (1, 24 and 48 hours), using the RealTime-Glo™ MT Cell Viability Assay (Promega Corporation). This assay measures the reducing potential of metabolically active cells on the cell permeant substrate; MT Cell Viability substrate. This process generates a membrane diffusing substrate; NanoLuc® Luciferase. On exiting the cell, the substrate is consumed by the NanoLuc® enzyme, producing a luminescent signal proportional to the number of viable cells.

Dose-response curves were fitted for analysis and visualization of relative cell viability. Preliminary studies were performed on the cell lines: DOHH-2, SU-DHL-4, WSU-DLCL-2, OCI-LY-10, U-2932, Granta-519 and Rec-1 to determine the toxicity of dimethyl sulfoxide (DMSO), a cytotoxic agent and the solvent used to dissolve the test drugs: olaparib and venetoclax. Cell viability after cell exposure to escalating concentrations of DMSO was evaluated. The cytotoxic limit of DMSO for which the cells would be exposed to without influencing the outcome of exposure to the test drugs was found to be between 0.3 % to 0.6 % (v/v*)* depending on the cell line.

Additionally, the cell lines were evaluated for their growth rate at different cell concentrations in 96- and 384-well plate. The experimental cell concentrations were optimised to try maintaining the cells at an exponential log growth phase during the course of the experiment.

The edges of the well plates were filled with only cell medium and were not included in the data output. Additionally, the drug concentrations were added to the cells in a randomised fashion using the D300e digital drug printer. These were done in order to decrease spatial bias leading to systematic errors that increase the false positive and false negative rates.

To identify the drug concentration that exerted 50 % inhibitory effect on cell viability (IC_{50}) for each of the 3 drugs on individual cell lines, the cells were treated with escalating drug concentrations in an experimental setup illustrated in Figure 13.
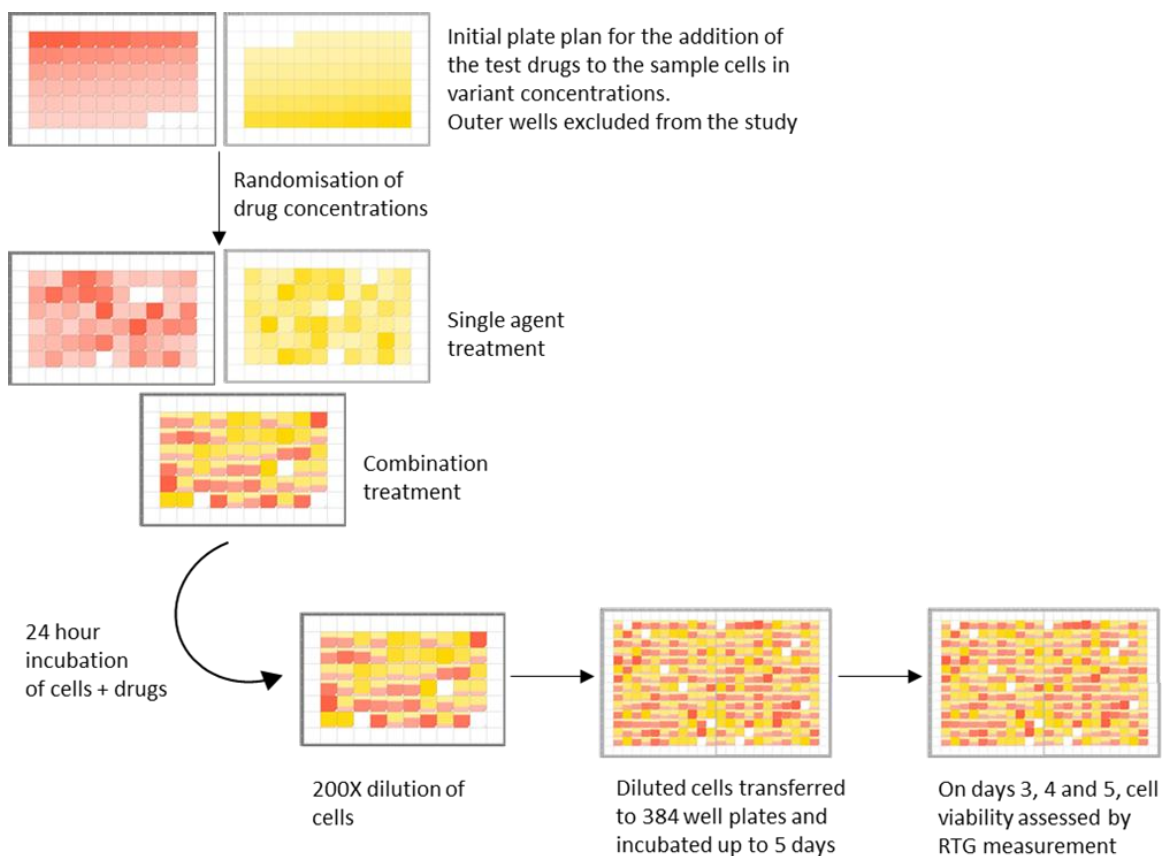
Figure 13. Experimental setup for the treatment of cells with Humalutin, olaparib and venetoclax as single agents or the combination of Humalutin with either olaparib or venetoclax.

Cell viability relative to the untreated controls were plotted against the drug concentrations and sigmoid dose-response curves fitted using the four-parameter logistic equation in GraphPad Prism 8.0 The obtained IC_{50}s are listed in

Table *2*.

Screening of drug combination platforms are influenced by multiple components which could determine whether the resulting pharmacodynamic interaction is synergistic, additive or antagonistic. While identification of the optimal drug concentration is

paramount, the sequence to which drugs are added can influence the combination outcome. We therefore tested the effect of the combination treatments on cell viability when either olaparib or venetoclax was added to the cells 4 hours before adding Humalutin, simultaneously with Humalutin or 24 hours after incubation with Humalutin. Interestingly, the effect exerted by either schedule was similar and therefore simultaneous addition of the test drugs was selected for further studies.

Table 2. IC$_{50}$ of Humalutin, olaparib and venetoclax in the 7 cell lines

Cell line	Humalutin (ng/ml)	Olaparib (μM)	Venetoclax (nM)
DOHH-2	138.4	1.31	12.05
GRANTA-519	189	0.86	150
OCI-LY-10	40.55	0.89	3.5
REC-1	286.7	12.66	1200
SU-DHL-4	177.2	2.36	6.3
U-2932	110.5	1.31	3.6
WSU-DLCL-2	233.8	5.66	21.2

In paper III, the effect of combining ^{177}Lu-NNV003 with either olaparib or venetoclax was investigated, using a fixed ratio ray design, based on the predetermined IC$_{50}$ of individual drugs as described by Straetemans et. al. (170). The test drugs were combined at a constant proportion about the IC$_{50}$ of the individual drugs, dictated by a mixture factors (f) that takes on values between 0 and 1.

The fixed ratio combined drugs are assumed to now be a new drug. Rays made up of mixture factors entailing a series of multiple drug concentrations were mapped. The mixture factors assigned: 0.25, 0.5 and 0.75, were rays each with 9 combined drug concentrations calculated using equation 3.

Rays with factors 0.25 and 0.75 had inverse drug proportions in the combinations, factor 0.5 had equal drug proportions while those assigned 0 and 1 were rays containing individual drugs alone as illustrated in Figure 14.

$$Z = f \bullet IC_{50}Humalutin + (1 - f) \bullet IC_{50}SMI$$

where:

Z is the combined drug mixture

f is the mixture factor

IC_{50} Humalutin is the IC_{50} of Humalutin

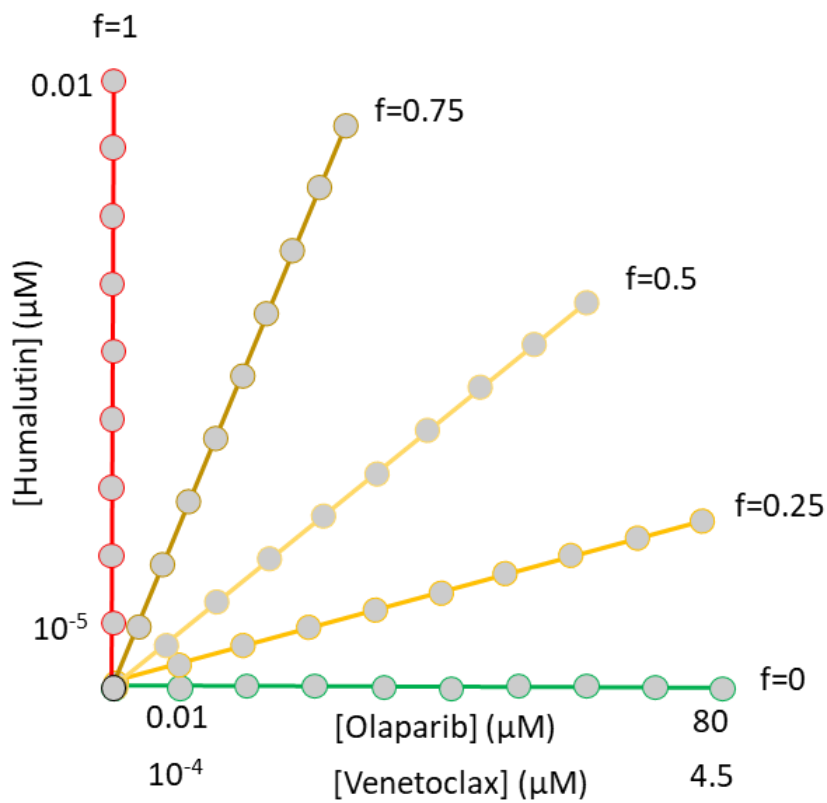IC_{50} SMI is the IC_{50} of olaparib or venetoclax

Figure 14. Schematic of fixed ratio ray design of drug combinations The X-axis corresponds to the concentration of the SMIs; olaparib and venetoclax, while the Y-axis corresponds to the concentration of Humalutin. Each line represents a different ray with a specific f value and the dots represent the concentrations within each ray

Statistical determination of in vitro pharmacodynamic interactions

Using the relative proportion of cells killed as a marker of drug effects, sigmoidal dose response curves were fitted for each ray using a three-parameter logistic equation by a global fitting, assuming that the minimum and maximum effects of the rays were identical. To account for this assumption, the variance of effects for each dose was estimated. SAS/ STAT14.1 (SAS V 9.4, PROCNLMIXED) was used for this analysis.

Ideally, the combination index (CI) for each dose combination across the rays are computed based on the Loewe additivity model defined by equation 4 (171), to determine the pharmacodynamic interactions of the test drugs in combination. This is by comparing the full dose-response curves of the combination treatment to those of the single- agent treatment.

Based on the principle of dose equivalence, the Loewe's additivity model assumes parallelism of the dose-response curves on the notion that the drugs have a constant potency ratio and equal maximum effects.

The combination interactions are defined as: CI < 1 is synergy CI = 1 is additivity and CI > 1 is antagonism.

$$CI = \frac{a}{A} + \frac{b}{B}$$

(Eqn. 4)

where:

a is the concentration of drug A in the combination

b is the concentration of drug B in the combination

B is concentration of drug B alone giving the same effect as a+b

A is concentration of drug A alone giving the same effect as a+b

However, our data presented unequal maximum effects and non-parallel slopes of the dose-response curves making the assumptions towards equation 4 a limitation of the Loewe additivity model. Therefore, a model coined by Grabovsky and Tallarida (172) based on unequal maximum effect and drug potency was used to estimate the CI for each combination concentration.

In situations where the effect of the combination was below the maximum effect of the drugs alone, equation 5 was used to compute the CI. In situations where the combination effect was between the maximum individual effects, then the CI was computed using equation 6.

$$CI = \frac{b}{B} + \frac{IC_{50}B}{B\left[\frac{E_{Bmax}}{E_{Amax}}\left(1 + \frac{IC_{50}A^p}{a^p}\right) - 1\right]^{1/q}}$$

(Eqn. 5)

$$CI = \frac{b}{B} + \frac{1}{B}\left(\frac{1}{\frac{1}{B_A^q} + \frac{\gamma}{a^p}}\right)^{1/q}$$

(Eqn. 6)

where:

$IC_{50}A$ is the half maximum effective dose of drug A

$IC_{50}B$ is the half maximum effective dose of drug B

E_{Amax} is the maximum effect of drug A

E_{Bmax} is the maximum effect of drug B

B_A is the dose of drug B that produces the maximum effect of drug A

p is the hillslope for drug A

q is the hillslope for drug B

$$\gamma = \left(\frac{E_{Bmax}\, A_{50}{}^p}{E_{Amax}\, B_{50}{}^q}\right)$$

CI values <0.85 were considered synergistic and statistical significance defined by 95 % confidence interval <1, while those >1.15 were antagonistic interactions, defined by the aforementioned confidence interval.

If the CI was <0.85 or >1.15 and the 95 % confidence interval included 1, they were categorised as non-significantly synergistic or non-significantly antagonistic.

CI at concentrations that gave approximately 0 % cell death were regarded as irrelevant.

4.4 *In vivo* studies

Animal models used in *in vivo* studies are instrumental in developing and testing therapeutics within the complexity of living systems, as a surrogate for human patients. However, translation of their therapeutic predictive value for human outcomes must acknowledge the physiological and genetic differences between animal models and humans (173).

4.4.1 Animal models

The use of animal models for this thesis was approved by The Norwegian Animal Research Authority (NARA, ID:8591) and the Icelandic Food and Veterinary Authority (MAST). Animal studies were performed in compliance with regulations from NARA, MAST and the Federation of European Laboratory Animal Science Associations (FELASA).

In papers I and II, female athymic nude mice and CB17 SCID mice were the choice animal models for the studies.

Athymic nude mice are an immunodeficient mouse homozygous for the nude spontaneous mutation $Foxn1^{nu}$. They lack a thymus and thus do not develop thymus derived T-cells. They have reduced B-cell function due to a lack of T-cell produced cytokines which mediate B-cell differentiation and activation. Nude mice are characteristically hairless as a result of altered winged helix/forkhead transcription factor arising from the defective development of thymic epithelium. These mice have an unaltered innate immune system therefore expressing a high density of activated NK cells (174). The presence of activated NK cells might undercut the take and growth of inoculated tumour cells. Nude mice have a high tolerance for radiation, with the maximum tolerated dose of Betalutin being approximately 500 MBq/kg (175).

CB17 SCID mice have severe combined immunodeficiency, lacking both B and T lymphocytes. This makes the SCID mouse an appropriate model for disseminated disease. These mice have normal NK cell function. They are homozygous for the $Prkdc^{scid}$ allele, consequently having impaired V(D)J recombination making the mice characteristically radiosensitive with a maximum tolerated dose of Betalutin between 50 and 100 MBq/kg (128, 174).

In preparation for the therapy study, the nude mice received i.p injections of anti-asialo GM1 prior to cell inoculation and for the rest of the study. This was done to reduce NK cells activity in-order to improve the tumour take in the mice after cell inoculation (176). Once the established tumours attained the desired tumour volume, the mice received a dosing of IgG, 1 day prior to treatment with Betalutin. This was done to improve the biodistribution of Betalutin by blocking unspecific FcRn and Fcγ receptor binding and thereby decreasing non-specific binding of the RIC in organs such as the spleen.

The endpoint criteria in the animal studies was based on tumour size and mouse body weight gain > 10 % or loss > 20 % from normal weight, tumour ulceration and any observable signs of discomfort or reduced general condition.

4.4.2 Therapy studies

In paper I, Daudi BL xenografts and Rec-1 MCL disseminated disease were established in nude mice and SCID mice respectively. The mice were i.v injected with either saline, Betalutin or rituximab and depending on their allocated treatment cohort, they received the choice combination agent of either saline or rituximab in single or multiple doses. A comparative study to that in paper I was performed using nude mice with s.c Daudi xenografts and substituting rituximab for obinutuzumab. The obinutuzumab dose was adjusted to 5 mg/kg, a dose we considered suboptimal from reported therapeutic doses (104, 177, 178).

For paper II, nude mice with established Raji 2R BL xenografts were treated with 2 different doses of Betalutin as a monotherapy or in combination with rituximab in 4 subsequent doses using the dosing schedule shown in Figure 15.

In all these studies, anti-tumour efficacy of the treatments was determined as a function of changes in tumour size, body weight and survival time.

Tumour volume in paper I was determined by measuring the shortest (A) and perpendicular longer diameter (B) using an electronic calliper and calculated using equation 7.

Injection days	1	2	3	4	5	6
-1	Mice with similar sized tumours assigned to 6 treatment cohorts (N=10)					
0	0.9% NaCl	0.9% NaCl	150 MBq/kg ^{177}Lu-lilotomab	150 MBq/kg ^{177}Lu-lilotomab	350 MBq/kg ^{177}Lu-lilotomab	350 MBq/kg ^{177}Lu-lilotomab
3	0.9% NaCl	10 mg/kg rituximab	0.9% NaCl	10 mg/kg rituximab	0.9% NaCl	10 mg/kg rituximab
6	0.9% NaCl	rituximab	0.9% NaCl	10 mg/kg rituximab	0.9% NaCl	10 mg/kg rituximab
10	0.9% NaCl	10 mg/kg rituximab	0.9% NaCl	10 mg/kg rituximab	0.9% NaCl	10 mg/kg rituximab
14	0.9% NaCl	10 mg/kg rituximab	0.9% NaCl	10 mg/kg rituximab	0.9% NaCl	10 mg/kg rituximab
70	Termination of study					

Figure 15. Schematic representation of the treatment scheduling and dosing in nude mice with established s.c Raji 2R xenografts.

$$Tumour\ volume = \frac{A^2 \times B}{2}$$

(Eqn. 7)

However, a study performed to compare the calculated tumour volume in 2-dimensions using equation 7 and in 3-dimensions using equation 8 with the tumour height showed a better estimation of tumour volume when the tumour volume was calculated in 3-dimensions. This new approach was used in paper II as it also accurately represented the elliptical shape of the s.c tumour.

$$Tumour\ volume\ (mm^3) = \frac{\pi}{6} \times l \times w \times h$$

(Eqn. 8)

where:

l is the length

w is the width

h is the height

46

Statistical determination of in vivo pharmacodynamic interactions

Survival analysis to determine the effect of the treatments on changes in the time-to-event of death were performed and visualised using the Kaplan-Meier method and log-rank tests. Kaplan-Meier method computes the survival fraction using product limit method, taking into account censored events. The log-rank test compares the observed number of events in each cohort to what would be expected if the survival curves were identical (179). The data analysis software, Sigmaplot, was used for calculation of Kaplan-Meier survival estimates and log-rank tests. Holm- Sidak multiple comparison test was used for the correction of sampling error.

In paper I, pharmacodynamic interactions of the combination were determined using the Cox proportional-hazards model. This evaluated the effect of the given treatments on survival by calculating the probability of the event of death (hazard) in the treated cohort, relative that of the control group, generally termed as the hazard ratio (HR).

An interaction term of the combination treatment HR evaluating the extent to which the effect of the combination treatments exceeded the product of the effects of the monotherapy treatments was calculated using equation 9.

$$HR_{\gamma} = HR_{BvsN} \bullet HR_{RvsN} \bullet HR_{Int}$$

(Eqn. 9)

where:

$HR\gamma$ is the hazard ratio of the combination

HR_{BvsN} is the hazard ratio of Betalutin vs NaCl

HR_{RvsN} is the hazard ratio of rituximab vs NaCl

HR_{Int} is the hazard ratio interaction between rituximab and Betalutin

In paper II, the Bliss independence model was used to compute the pharmacodynamic interactions in the combination of Betalutin and rituximab. This model uses an effect-based approach that directly compares the effects of individual drugs in a combination as independent yet competing components using equation 10.

$$f = f_1 + f_2 - f_1 \cdot f_2$$

<div align="right">(Eqn. 10)</div>

where:

f_1 is the monotherapy effect of rituximab

f_2 is the monotherapy effect of Betalutin

Bliss analysis of tumour volume was performed using extrapolation of tumour volumes and was restricted to the first 20 days of the study. This was because there were no control animals beyond study day 13 and also any analysis beyond day 20 would impose uncertainty as the tumour sizes become infeasibly large.

The tumour volumes were log transformed and data for mice withdrawn before study day 20 were extrapolated by linear regression. Difference from baseline was calculated on the log scale and all statistical analysis were performed on the log-transformed data. A mixed effects linear model was used including fixed effects of each of the treatments (referred to as between group factors) and the associated interaction between these factors. Additionally, study day was included as a within animal fixed effect. All the interactions between the group factors and study day were included. Animal within group and the side of the tumour were included as random effects in the model. An autoregressive correlation structure was assumed. The effects of treatment with and without rituximab were evaluated separately at each dose of Betalutin (control, 150 MBq/kg and 350 MBq/kg), for each study day. The size of these effects was compared for 150 MBq/kg Betalutin against the control and 350 MBq/kg Betalutin against the control using the interaction test of the Bliss independence model using SAS 9.4 (SAS Institute, NC, USA). Interaction values less than 1 were considered synergistic and statistical significance defined by $p < 0.05$ and an interaction value $\pm$ 90 % confidence interval <1.

5 Summary of papers

5.1 Paper I

Combination of ^{177}Lu-lilotomab with rituximab significantly improves the therapeutic outcome in pre-clinical models of non-Hodgkin's lymphoma

We hypothesised that ^{177}Lu-lilotomab could upregulate CD20 in NHL cell lines and therefore interact synergistically with rituximab to improve the therapeutic outcome of mice with s.c NHL xenografts.

Our main findings were:

1) ^{177}Lu-lilotomab significantly increased CD20/ rituximab binding *in vitro* in NHL cell lines.
2) *In vivo* combination treatment with ^{177}Lu-lilotomab and rituximab resulted in increased suppression of tumour growth and prolonged survival time.
3) The therapeutic interaction between ^{177}Lu-lilotomab and rituximab in the *in vivo* model can be synergistic.

Conclusion:

[177]Lu-lilotomab modulates CD20/rituximab binding which results in therapeutic synergy when in combination with rituximab for the treatment of NHL.

5.2 Paper II

[177]Lu-lilotomab satetraxetan has the potential to counteract resistance to rituximab in non-Hodgkin's lymphoma

Having previously demonstrated that ^{177}Lu-lilotomab increased CD20/ rituximab binding in rituximab sensitive NHL cell lines, we hypothesised that ^{177}Lu-lilotomab could reverse rituximab resistance when directed towards a rituximab resistant NHL cell line and animal model.

Our main findings were:

1) *In vitro* treatment of a rituximab resistant BL cell line with ^{177}Lu-lilotomab significantly increased CD20/ rituximab binding and rituximab-induced ADCC.
2) *In vivo* treatment of a rituximab resistant NHL model with the combination of ^{177}Lu-lilotomab and rituximab synergistically increased the suppression of tumour growth.
3) Treatment with ^{177}Lu-lilotomab potentiated the therapeutic efficacy of rituximab, prolonging survival time when the two drugs were given in combination.

Conclusion:

Combination therapy with ^{177}Lu-lilotomab and rituximab could potentially reverse rituximab resistance.

5.3 Paper III

Anti-CD37 radioimmunotherapy with ^{177}Lu-NNV003 synergize with the PARP inhibitor olaparib in treatment of non-Hodgkin lymphoma in vitro

We hypothesised that combination of radiation induced DNA damage by ^{177}Lu-NNV003 and inhibition of DNA damage repair by olaparib could result in synergistic interactions in DLBCL and MCL cell lines.

Our main findings were:

1) Cells responded synergistically to the combination of ^{177}Lu-NNV003 and olaparib, showing dose dependency among different drug concentrations and ratios.
2) Synergistic interactions were prominent in four of seven cell lines while one cell line prominently responded with antagonism.
3) Gene expression was influenced by the drug combination but unsupervised clustering of the genes did not give any correlation to the combination outcome.

Conclusion:

Combination of Humalutin with olaparib is synergistic depending on the cell line, the combination concentration and the proportion of each drug in the combination.

6 Discussion

Tumour response to therapy is variable across patient populations due to tumour heterogeneity. This contributes to subpar responses to targeted therapy, drug resistance and disease progression.

Combination therapy employs the use of interdependent drugs with different mechanisms of action at sublethal doses. This can synergistically improve the therapeutic efficacy while maintaining a low toxicity profile and decreasing the likelihood of drug resistance associated with optimal dosing given as monotherapies. Pre-clinical drug combination studies are an important guide to understanding the pharmacodynamic interactions: synergistic, additive and antagonistic, thus providing the rationale for translation into the clinic.

In this thesis, we investigated the pre-clinical therapeutic potential of combining Betalutin with anti-CD20 mAbs: rituximab and obinutuzumab in rituximab responding and rituximab resistant models. Additionally, the therapeutic potential of combining Humalutin with SMIs: olaparib and venetoclax was investigated, assessing the gene expression changes in response to the combination of Humalutin and olaparib.

6.1.1 The role of Betalutin in CD20 modulation

Paper I and II explored the effects of combining Betalutin with rituximab in NHL models. To give precedence to this, *in vitro* evaluation was done to determine the capability of radiation to modulate CD20 expression.

In paper I, Daudi and Rec-1 cells exposed to either EBR or Betalutin; at doses of the same order of magnitude at the start of the experiment, showed increased rituximab binding in comparison to their respective control cells treated with non-radiolabelled lilotomab. This was a clear indicator that the increased binding of rituximab to CD20, a function of CD20 upregulation, was radiation specific. The extent of the increase in rituximab binding was unique for each cell line. Moreover, it was distinctively dependent on the type and dose of the radiation as well as time. The increase in rituximab binding was substantially prolonged in cells exposed to Betalutin than in cells exposed to EBR.

Although external beam irradiation of Daudi and Rec-1 cells resulted in increased rituximab binding, exposure of the cells to Betalutin resulted in a substantial increase than in similar cells exposed to EBR. Studies have shown that irradiation of cells results in radiation induced oxidative stress, generating ROS which mediates the increase of antigen expression by transient *de novo* protein synthesis (180, 181). This suggests that the increase in rituximab binding is explicitly radiation induced and mediated by intracellular oxidation (180), also because treatment with non-radiolabelled lilotomab had no detectable effect on rituximab binding.

Whereas EBR delivered a one-time high radiation dose to the cells, Betalutin delivered a continuous low-dose of radiation over time. Perhaps, the prolonged exposure to β-radiation extended ROS generation and increasingly modulated CD20 expression in a time-dependent manner. It is noteworthy that, the cumulative absorbed radiation dose in the cells exposed to Betalutin increased over time in attribute to the contribution of the self-absorbed dose from the cell bound RIC, cross-absorbed dose from cells in the vicinity (cross-fire effect) and non-specific absorbed dose from the RIC in the cell culture medium. This means that the absorbed radiation dose between EBR and Betalutin treated cells was different despite the comparable dose estimates at the start of the experiment. This disparity in dosimetry has been discussed at length by Marcatili et. al. (182).

Overall, it is possible that as the radiation decayed over time, the radiation-mediated mechanisms influencing the increase in CD20 expression begun to diminish.

CD37 expression is heterogeneous in different cell lines (128) with Daudi cells expressing approximately three times as much CD37 than Rec-1 cells (128, 135). The level of expression of cell surface antigens can impact the effectiveness of targeted mAb therapy. Accordingly, the number of antigens per cell would tend to correlate with the density of cell-bound RIC and subsequent increase in rituximab binding would be anticipated to be higher in Daudi cells compared to Rec-1 cells.

Paper II was based on the hypothesis that Betalutin in its capacity as a modulator of CD20 expression could be effective in reversing rituximab resistance. Here, we observed increased rituximab binding in both the parental Raji cells and the rituximab-resistant Raji 2R cells treated with Betalutin in a dose and time-dependent manner. Although the increase in rituximab binding was large in Raji 2R cells, it did not sufficiently increase to attain the level of rituximab binding similar to that in Raji cells at baseline.

Binding studies in Raji and rituximab-resistant Raji 2R cells showed comparable CD37 expression between the two cell lines (Table 3). However, the time pattern in which rituximab binding increased in these cells after treatment with Betalutin was different. Raji cells have been shown to have elevated endogenous ROS levels (183), which in addition to ROS generated after Betalutin treatment could be responsible for the observed early increases in rituximab binding reported for Raji cells compared to Raji 2R cells. Perhaps, the complexity of the mechanisms that conferred rituximab resistance in Raji 2R cells alters endogenous mechanisms of ROS production in these cells hence requiring longer time to accumulate adequate amounts of ROS to modulate CD20 protein synthesis. Tsai et al. reported a defect in CD20 protein transport when attempting to re-express surface CD20 in Raji 2R cells, causing a time delay in the CD20 detection in comparison to rituximab sensitive cells (102).

Table 3. Maximum number of CD37 antigens (B_{max}) and equilibrium dissociation constant (K_d) of Betalutin in Raji and Raji 2R cells.

Cell line	Lilotomab (CD37)	
	B_{max} (Antigens/ cell)	K_d (nM)
Raji	67039 ± 17142	7.0 ± 0.9
Raji 2R	93972 ± 22518	7.9 ± 1.1

We additionally evaluated the effects of Betalutin treatment on the ADCC activity of rituximab in Raji and Raji 2R cells. Due to the dose and time dependency in CD20 upregulation observed in these cells after Betalutin treatment, it was important to identify the best suited concentration of Betalutin and the best time for administering rituximab after Betalutin treatment. Since the aim of paper II was to quantify eversion of rituximab resistance in Raji 2R cells relative to Raji cells, the assay was performed using an optimal Betalutin concentration which gave the highest CD20 upregulation while not killing more than 50 % of the cells and at the timepoint with the highest increase in rituximab binding in Raji 2R cells. Here, as a consequence of Betalutin mediated increase in rituximab binding, we observed significant induction of ADCC by rituximab in Raji 2R cells compared to Raji cells.

This observation was confirmation that Betalutin has the potential to sensitise Raji 2R cells to rituximab induced cytotoxicity through increased rituximab binding.

6.1.2 Combination of Betalutin with anti-CD20 mAbs

Combination therapy with Betalutin and rituximab resulted in improved anti-tumour effect and prolonged survival time *in vivo*. This was observed both in the Daudi xenografted nude mice and the SCID mice with Rec-1 disseminated MCL (Paper I) and in Raji 2R xenografted nude mice (Paper II).

The combination effect of Betalutin and rituximab in the Daudi model was synergistic since the hazard ratio i.e. the probability of the event of death relative to the saline control group, in the combination therapy group was lower than the product of the hazard ratios of the single agent monotherapy, although short of statistical significance. This was not the case for the combination therapy in the Rec-1 model, which resulted in an additive effect.

The anti-tumour effect of the combination therapy in the Raji 2R model was synergistic, because the tumour growth was slower than that of the sum of the monotherapy of the individual drugs all when compared to the control group.

A head-to-head comparison of the combination effects between the Raji 2R model and a Raji model would have been ideal in determining the extent of which the Betalutin could potentiate reversal of rituximab resistance. However, an attempt at setting up the comparative study was aborted due to occurrence of severe necrosis on palpable tumours in Raji-xenografted mice.

Since our *in vitro* studies established that Betalutin treatment increased rituximab binding and subsequently ADCC, it is rational to reason that the improved efficacy of the combination treatment *in vivo* is a result of improved ADCC activity of rituximab mediated by NK cells and other effector cells that induce cytotoxic responses such as ADCP mediated by monocytes. This is in addition to the radiation induced biological effects from the mechanisms of action of Betalutin.

Our pre-clinical findings on the combination of Betalutin with rituximab support the rationale for clinical evaluation of the combinations in relapsed/refractory NHL. A phase 1b clinical trial (Archer-1; NCT03806179) is investigating the efficacy of the combination of Betalutin and rituximab in patients with relapsed/refractory FL.

To emulate the strategy tested in paper I, we evaluated whether Betalutin could give similar therapeutic effects when combined with obinutuzumab in a s.c Daudi mouse model.

Contrary to the monotherapy with rituximab, single-agent therapy with obinutuzumab resulted in significant anti-tumour effect (Figure 16) and prolonged survival time (Table 4, Figure 17) when compared to the control group. This observation confirms the superior anti-tumour efficacy of type II mAbs such as obinutuzumab in comparison to type I mAbs like rituximab (3, 55, 184). Monotherapy with Betalutin and its combination with obinutuzumab also resulted in prolonged survival time and improved anti-tumour effect when compared with the control.

Tumour growth was significantly slower in mice cohorts that received obinutuzumab-containing regimens. Survival was prolonged significantly in mice in the combination therapy cohort when compared with those in the obinutuzumab treated cohort.

However, the effect of the combination was not significantly synergistic although the fold change of the tumour volume was lower for the combination treatment than for each treatment alone at 7 to 20 days after start of treatment (Table 5).

The lack of synergism in the combination of obinutuzumab with Betalutin might be a result of the half maximal CD20 binding reported for obinutuzumab in comparison to rituximab binding to CD20.

It might be of interest to pursue this research using varying doses of both Betalutin and obinutuzumab in order to correctly conclude on the combination effect of these two drugs.

It is worth to mention that a lack of synergism can still confer therapeutic benefit as a result of patient-to-patient variability in response to treatment due to disease heterogeneity. This has been comprehensively discussed by Palmer and Sorger (185). A clinical trial currently underway is investigating the efficacy and safety of the combination of obinutuzumab with radiation therapy in patients with FL (NCT03341520) (186).
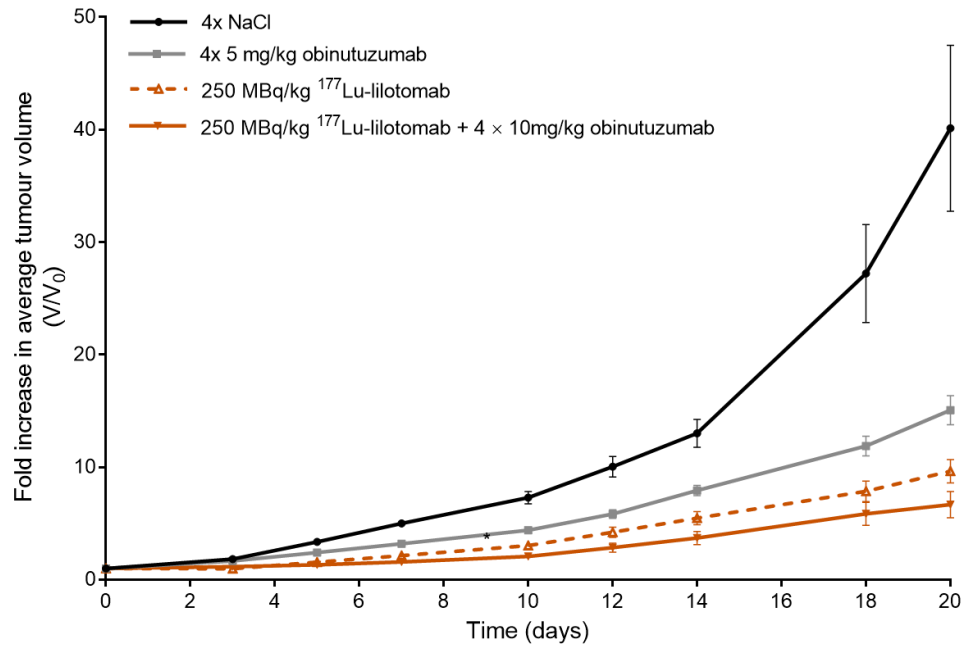
Figure 16. Fold increase in tumour volume after treatment (V), relative to the tumour volume at the point of drug administration (V_0) ± SE in mice treated with NaCl, monotherapy with 4×5 mg/kg obinutuzumab or 250 MBq/kg Betalutin and combination of Betalutin and obinutuzumab at doses similar to the monotherapy. The fold change is determined from tumour volume data extrapolated using log linear regression (N = 10 per treatment cohort).

Table 4. Median survival time of nude mice with s.c Daudi xenografts treated with saline, obinutuzumab, Betalutin and the combination of Betalutin with obinutuzumab. The endpoint in this study was tumour diameter larger than 20 mm (N = 10 mice per cohort)

Treatment Group	Median survival ±SE (days)
4×NaCl	18±2
4×5 mg/kg obinutuzumab	28±3*
250MBq/kg ^{177}Lu-lilotomab	31±1*
250MBq/kg ^{177}Lu-lilotomab + 4×5 mg/kg obinutuzumab	38±8*,†

*Significantly different from NaCl (p<0.01)
†Significantly different from 4x5 mg/kg obinutuzumab (p<0.05)
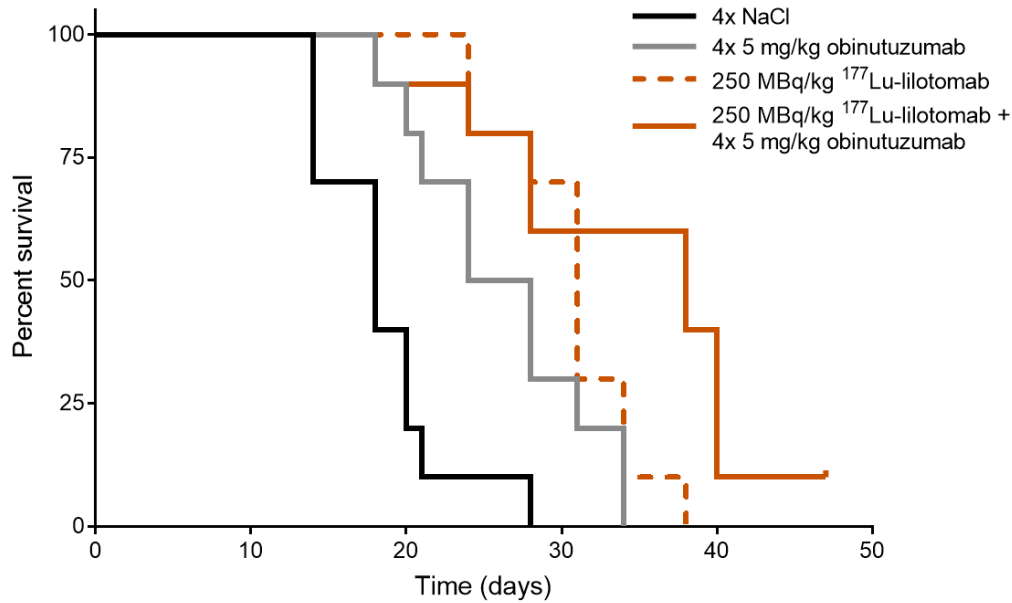
Figure 17. Kaplan-Meier survival curves comparing the survival probability among nude mice with s.c Daudi xenografts treated with saline, obinutuzumab, Betalutin and the combination of Betalutin with obinutuzumab. The endpoint in this study was tumour diameter larger than 20 mm (N = 10 mice per cohort).

Table 5. Fold-change in average tumour volume from baseline of combination therapies vs corresponding monotherapies and Bliss interaction values with 90 % confidence intervals.

Study day	Betalutin (MBq/kg)	Fold-change from day 0		Interaction value (90 % CI)
		without obinutuzumab	with obinutuzumab	
3	0	1.8	1.6	
	250	1.0	1.2	1.35 (1.00, 1.83)
5	0	3.3	2.4	
	250	1.5	1.3	1.24 (0.91, 1.68)
7	0	4.9	3.1*	
	250	2.1	1.6†	1.22 (0.90, 1.65)
10	0	7.1	4.3*	
	250	2.9	2.2†	1.20 (0.89, 1.63)
12	0	9.7	5.7*	
	250	4.0	3.0†	1.29 (0.95, 1.74)
14	0	12.4	7.8*	
	250	5.2	3.9†	1.19 (0.88, 1.61)
18	0	24.0	11.6*	
	250	7.5	6.0	1.68 (1.24, 2.27)
20	0	33.9	14.5*	
	250	9.2	6.9†	1.74 (1.29, 2.36)

* significant obinutuzumab monotherapy effect (p<0.05)
† significant obinutuzumab effect with 250MBq/ kg Betalutin (p<0.05)

58

6.1.3 Combination of Humalutin with olaparib

Paper III explored the *in vitro* interaction effects of combining Humalutin with olaparib. Hypothetically, the combination of these two drugs is anticipated to induce co-operative genotoxic mechanisms with Humalutin inducing DNA damage and olaparib interfering with the repair of the damaged DNA, priming cells for death. Empirically, extensive biochemical and genetic interactions between these mechanisms may contribute to a plethora of interactions that result in either synergistic, additive or antagonistic outcomes. Our results revealed that the combination of Humalutin and olaparib resulted in pharmacodynamic interactions that were dependent on: the concentrations of the drugs, the ratios in which the drugs were combined and the time of assessment. Translation of these dependencies could be of clinical relevance and therapeutic benefit. Additionally, the combination resulted in changes in gene expression some of which could elaborately define the biological implications influencing the observed interaction effects.

With the exception of one cell line, DOHH-2, that presented an antagonistic combination outcome, our study showed that synergistic combination outcomes could be attained at drug concentrations lower than the IC_{50} and having different drug ratios. These results suggest that treatment regimens combining Humalutin with olaparib can be optimised to attain synergy at suboptimal doses lower than the maximum tolerated dose, therefore reducing toxicity and overtreatment of patients.

Treatment with single agents showed that Rec-1 cells were the least sensitive to both olaparib and Humalutin. This was confirmed by the *p53* mutation in the Rec-1 cells identified through RNA sequencing. Mutations in *p53* have been described to interfere with downstream *p53*-dependent effector pathways, causing resistance to anti-cancer therapy (187). When exposed to the combination of the two drugs, we observed a pattern where the probability of synergy was high only when the proportion of Humalutin was equal to or higher than that of olaparib. Perhaps this is as a result of high concentrations of Humalutin inducing a high number of DNA strand breaks which might negatively tip the balance on DNA repair. At this point, it is possible for low concentrations of olaparib to reinforce its inhibitory effect on PARP, resulting in the accumulation of unrepaired radiation-induced DNA damage resulting in increased cell death (153, 154).

A number of clinical trials are exploring the radio-sensitizing effect of olaparib, combining it with (chemo) radiotherapy for evaluation of doses that confer synergistic outcomes with minimal toxicity profiles (188, 189) (NCT01562210, NCT02229656, NCT03532880).

Based on the diverse repertoire of synergistic interactions across the different cell lines, our study provides the rationale to evaluate the therapeutic benefit of the combination of Humalutin with olaparib *in vivo*. If successful, the pre-clinical study can be translated in the clinic as a treatment strategy for patient populations presenting heterogenous disease pathology.

Treatment specific changes in gene expression in response to treatment with Humalutin, Olaparib and a combination of the two were observed in our study.

Genes that were differentially expressed after treatment with the single agents differed between olaparib and Humalutin treatment in the same cell line. Additionally, differentially expressed genes in the cells treated with the single agents differed from those treated with the drug combination. The lack of consistency in gene expression changes between treatments highlights the differences in drug effects of single agent and combination treatments for cell lines. Moreover, using unsupervised clustering of genes expressed at baseline, we did not find any cluster correlation to drug-effect of either treatment, combination outcome or of the NHL subtypes.

Interestingly some differentially expressed genes were upregulated and enriched in the p53 signalling pathway in cells with opposing combination outcomes. The expression levels and complex interactions between the genes are postulated to lead to both antagonistic and synergistic pharmacodynamic interactions. This implies that downstream mechanisms could be involved in the expression patterns of those genes.

Our observations are nonetheless arbitrary due to a mismatch in time of assessment of gene expression and the cellular drug response as well as the drug concentrations used in the two evaluations. Gene expression was evaluated 24 hours after treatment with the drugs at IC_{50} concentrations while the cellular drug-response was evaluated between 3-5 days after treatment with variant concentrations of the drugs about the IC_{50}. Studies have reported temporal changes in gene and mRNA expression in response to irradiation

of lymphoid cells (190-192). Further studies exploring the time factor can be considered to validate our current results.

6.1.4 Combination of Humalutin and venetoclax

Evading apoptosis is a hallmark of B-cell malignancies typically through the over expression of anti-apoptotic proteins or reduced expression of pro-apoptotic proteins. To rebalance the scales, it is rationale to have a therapeutic strategy that can co-operatively release the burden of the pro-survival proteins. Combination of RIT with venetoclax is hypothesised to result in synergy since radiation-induced DNA damage initiates apoptosis and venetoclax facilitates apoptosis by inhibiting Bcl-2 anti-apoptotic proteins.

The combination of Humalutin with venetoclax, like that with olaparib, resulted in pharmacodynamic interactions that were dependent on: the concentrations of the drugs, the ratios in which the drugs were combined and the time of assessment.

We observed that the cells were generally sensitive to venetoclax treatment, with IC_{50} ranging between 3.5-1200 nM. These were well below the plasma concentration of approximately 2.5nM in patients given venetoclax at clinically relevant doses (193).

However, only two of the seven cell lines responded robustly synergistic to the combination of Humalutin and venetoclax while the rest responded in a mixed array of responses between synergistic and antagonistic outcomes (Figure 18).

Sensitivity profiles of the cells to venetoclax treatment matched those documented in literature with the least sensitive Rec-1 cells having overexpression of Bcl-xl anti-apoptotic proteins. Granta-519 cells with slight sensitivity to venetoclax overexpress Bcl-2 anti-apoptotic proteins while the more sensitive U2932 cells had a mix of high Bcl-2 expression and low Bcl-xl expression (162, 164, 194). Bcl-2 protein expression has been shown to positively correlate with sensitivity to venetoclax while Bcl-xl correlates negatively to venetoclax sensitivity (162).

Interestingly, U2932 cells responded antagonistically while Granta-519 cells responded synergistically.

Pham et al. reported on the upregulation Bcl-xl pro-survival proteins in cells after venetoclax treatment as a consequence of activation of components of the AKT

signalling pathway (162). This could explain the prominence of varied combination outcomes observed in our study.

Much more work needs to be done to exhaustively gain more information from this combination study. However, based on our reported combination outcomes and arguments from previous studies, we can conclude that the therapeutic benefit of the combination of RIT with venetoclax may be limited to a patient population with homogenous genetic and phenotypic disease pathology.
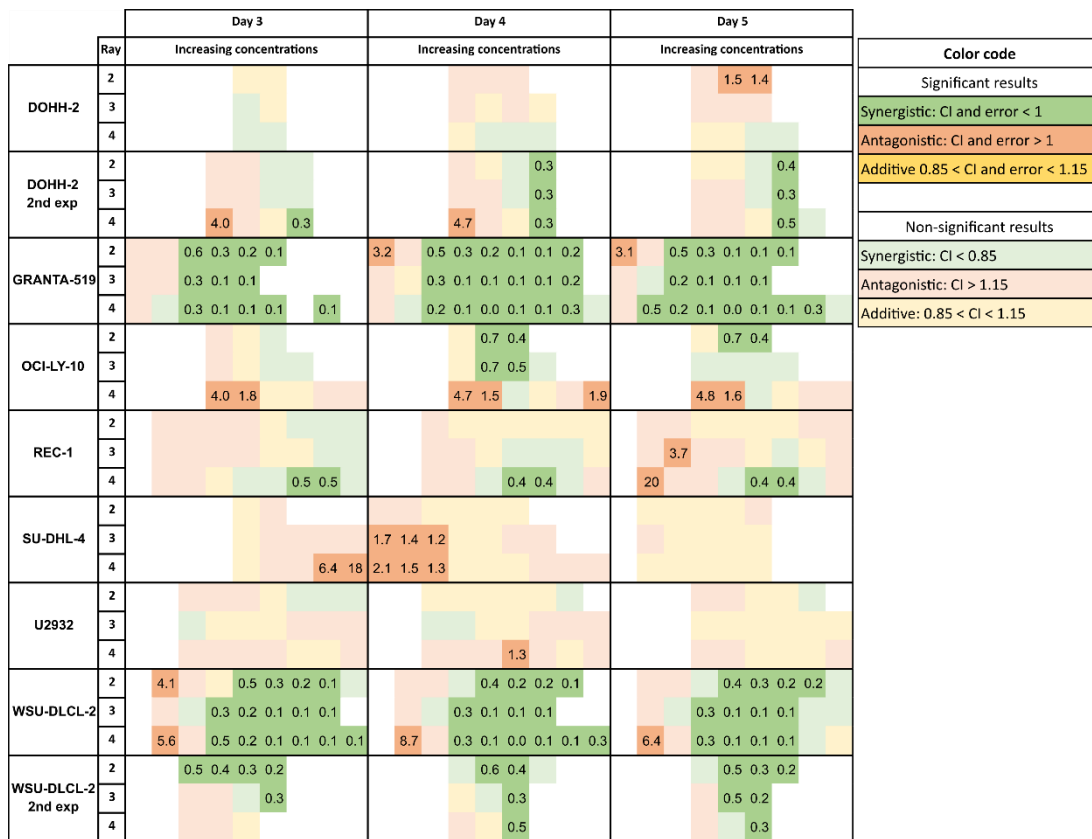

Figure 18. Heat map showing CI of the combination treatments of venetoclax and Humalutin in all 7 cell lines. White squares represent missing data or data non-relevant. The numbers in the square indicate the calculated CI.

7 Conclusion

The overall aim of this thesis was to study the pharmacodynamic interactions of combining the radioimmunotherapies Betalutin and Humalutin, with other drugs in NHL. Indeed, we showed that Betalutin combined synergistically with rituximab in both rituximab responding and resistant models, improving the therapeutic effect and survival in mice. In doing so, we have demonstrated the therapeutic potential of RIT with Betalutin in re-sensitising patients with relapsed and refractory NHL to anti-CD20 immunotherapy. This combination is currently tested in the ongoing Archer-1 clinical trial where three patients in the first cohort all had complete response to the combination treatment.

Additionally, we showed that the combination of Humalutin with SMIs olaparib and venetoclax resulted in both synergistic and antagonistic interactions across MCL and DLBCL cell lines. These interactions were dependent on the concentrations and ratio of the drugs in the combination as well as the time of exposure to the drugs. From these dependencies, we deduce the importance of identifying the 'sweet spot' of parameters where synergy is likely to be the outcome of drug combinations. Also, since synergism is observed at lower combination concentrations, translation into the clinic would mean minimising patient overtreatment and averting undesired treatment related consequences.

8 Future perspectives

The combination of Betalutin with rituximab is currently in a phase 1b clinical trial and the results so far are very promising. Betalutin is also in a pivotal clinical phase 2b trial for treatment of 3rd line FL patients who are resistant to anti-CD20 therapies. To enter 2nd line of therapy, it is necessary to combine Betalutin with another drug and do a randomized phase 3 trial where the combination is compared with an approved drug for 2nd line FL. It is likely that Betalutin will be combined with rituximab in this trial.

Betalutin and obinutuzumab combination did not show significant synergy in the work done in this thesis, but as shown in the combination studies with Humalutin and the SMIs synergism can depend on many factors that were not optimized in the studies performed so far. Furthermore, obinutuzumab may take over the role of rituximab in NHL because of superior results and since rituximab is now out of patent and generic antibodies will enter the market. Therefore, a further investigation of Betalutin in combination with obinutuzumab for instance in other animal models and using varied drug doses might be worth pursuing.

Combination of Humalutin with olaparib and venetoclax gave interesting *in vitro* results and expected continuation of this work will be to do animal studies to validate the findings before clinical studies can be started. Nordic Nanovector has put development of Humalutin on hold so it might be necessary to repeat some of the *in vitro* work with Betalutin before *in vivo* studies can start. The unsupervised cluster analysis of the RNA sequencing data did not give any significant gene profiles that could predict outcome of the combination treatment, but a supervised cluster analysis might give more interesting results. It could also be possible to use machine learning algorithms to analyse the data. If it is decided to test these combinations with Betalutin, then the RNA sequencing studies should also possibly be repeated and more cell lines should be included as well as more assessment timepoints to inherently understand the interactions and treatment outcomes.

9 References

1.   International Agency for Research on Cancer WHO. Non-Hodgkin lymphoma fact sheet 2018 [Available from: https://gco.iarc.fr/today/data/factsheets/cancers/34-Non-hodgkin-lymphoma-fact-sheet.pdf.

2.   Vitolo U, Trneny M, Belada D, Burke JM, Carella AM, Chua N, et al. Obinutuzumab or Rituximab Plus Cyclophosphamide, Doxorubicin, Vincristine, and Prednisone in Previously Untreated Diffuse Large B-Cell Lymphoma. J Clin Oncol. 2017;35(31):3529-37.

3.   Marcus R, Davies A, Ando K, Klapper W, Opat S, Owen C, et al. Obinutuzumab for the First-Line Treatment of Follicular Lymphoma. The New England journal of medicine. 2017;377(14):1331-44.

4.   Coiffier B, Sarkozy C. Diffuse large B-cell lymphoma: R-CHOP failure-what to do? Hematology American Society of Hematology Education Program. 2016;2016(1):366-78.

5.   Pedersen AE, Jungersen MB, Pedersen CD. Monocytes mediate shaving of B-cell-bound anti-CD20 antibodies. Immunology. 2011;133(2):239-45.

6.   Lim SH, Vaughan AT, Ashton-Key M, Williams EL, Dixon SV, Chan HT, et al. Fc gamma receptor IIb on target B cells promotes rituximab internalization and reduces clinical efficacy. Blood. 2011;118(9):2530-40.

7.   Terui Y, Mishima Y, Sugimura N, Kojima K, Sakurai T, Mishima Y, et al. Identification of CD20 C-terminal deletion mutations associated with loss of CD20 expression in non-Hodgkin's lymphoma. Clin Cancer Res. 2009;15(7):2523-30.

8.   Mishima Y, Terui Y, Takeuchi K, Matsumoto-Mishima Y, Matsusaka S, Utsubo-Kuniyoshi R, et al. The identification of irreversible rituximab-resistant lymphoma caused by CD20 gene mutations. Blood cancer journal. 2011;1(4):e15.

9.   Bodet-Milin C, Ferrer L, Pallardy A, Eugene T, Rauscher A, Alain F-C, et al. Radioimmunotherapy of B-Cell Non-Hodgkin's Lymphoma. Frontiers in oncology. 2013;3:177.

10.   Kersten MJ. Radioimmunotherapy in follicular lymphoma: some like it hot. Transfusion and apheresis science : official journal of the World Apheresis Association : official journal of the European Society for Haemapheresis. 2011;44(2):173-8.

11.   Cancer Fact sheets [Internet]. 2018. Available from: http://gco.iarc.fr/today/fact-sheets-cancers.

12.   Elaine JS, Steven SH, James VW. Haematopoietic and lymphoid malignancies. Lyon: World Health Organization; 2014.

13.   Malcolm TI, Hodson DJ, Macintyre EA, Turner SD. Challenging perspectives on the cellular origins of lymphoma. Open biology. 2016;6(9):1-12.

14.   Swerdlow SH, Campo E, Pileri SA, Harris NL, Stein H, Siebert R, et al. The 2016 revision of the World Health Organization classification of lymphoid neoplasms. Blood. 2016;127(20):2375-90.

15.   W.H. S, A. R, C. B. B-Cell Development and Differentiation. In: R. RR, T. FA, C. WM, editors. Clinical Immunology: Principles and Practice. Principles of Immune Response. Fifth ed: Elsevier Ltd.; 2019. p. 107-18.

16.   LeBien TW, Tedder TF. B lymphocytes: how they develop and function. Blood. 2008;112(5):1570-80.

17.   Hatzi K, Melnick A. Breaking bad in the germinal center: how deregulation of BCL6 contributes to lymphomagenesis. Trends in molecular medicine. 2014;20(6):343-52.

18.   Basso K, Dalla-Favera R. Germinal centres and B cell lymphomagenesis. Nature reviews Immunology. 2015;15(3):172-84.

19.   Stefania Pittaluga, Tapan Bhavsar, Jaffe ES. Lymphomas. In: R. RR, T. FA, C. WM, editors. Clinical Immunology: Principles and Practice. Immunology of Neoplasia. Fifth ed: Elsevier; 2019. p. 1065- 72.

20.   Kuppers R. Mechanisms of B-cell lymphoma pathogenesis. Nat Rev Cancer. 2005;5(4):251-62.

21.   Pasqualucci L, Dalla-Favera R. The genetic landscape of diffuse large B-cell lymphoma. Seminars in hematology. 2015;52(2):67-76.

22.   Alizadeh AA, Eisen MB, Davis RE, Ma C, Lossos IS, Rosenwald A, et al. Distinct types of diffuse large B-cell lymphoma identified by gene expression profiling. Nature. 2000;403(6769):503-11.

23.   Huang JZ, Sanger WG, Greiner TC, Staudt LM, Weisenburger DD, Pickering DL, et al. The t(14;18) defines a unique subset of diffuse large B-cell lymphoma with a germinal center B-cell gene expression profile. Blood. 2002;99(7):2285-90.

24.   Ott G, Rosenwald A, Campo E. Understanding MYC-driven aggressive B-cell lymphomas: pathogenesis and classification. Blood. 2013;122(24):3884-91.

25.   Kahl BS. Follicular lymphoma: are we ready for a risk-adapted approach? Hematology American Society of Hematology Education Program. 2017;2017(1):358-64.

26.   Xerri L, Dirnhofer S, Quintanilla-Martinez L, Sander B, Chan JK, Campo E, et al. The heterogeneity of follicular lymphomas: from early development to transformation. Virchows Archiv : an international journal of pathology. 2016;468(2):127-39.

27.   Galteland E, Sivertsen EA, Svendsrud DH, Smedshammer L, Kresse SH, Meza-Zepeda LA, et al. Translocation t(14;18) and gain of chromosome 18/BCL2: effects on BCL2 expression and apoptosis in B-cell non-Hodgkin's lymphomas. Leukemia. 2005;19(12):2313-23.

28.   Gonzalez-Rincon J, Mendez M, Gomez S, Garcia JF, Martin P, Bellas C, et al. Unraveling transformation of follicular lymphoma to diffuse large B-cell lymphoma. PLoS One. 2019;14(2):e0212813.

29.   Schmitz R, Ceribelli M, Pittaluga S, Wright G, Staudt LM. Oncogenic mechanisms in Burkitt lymphoma. Cold Spring Harbor perspectives in medicine. 2014;4(2).

30.   Casulo C, Friedberg JW. Burkitt lymphoma- a rare but challenging lymphoma. Best practice & research Clinical haematology. 2018;31(3):279-84.

31.   Rosenquist R, Bea S, Du MQ, Nadel B, Pan-Hammarstrom Q. Genetic landscape and deregulated pathways in B-cell lymphoid malignancies. Journal of internal medicine. 2017;282(5):371-94.

32.   Bea S, Valdes-Mas R, Navarro A, Salaverria I, Martin-Garcia D, Jares P, et al. Landscape of somatic mutations and clonal evolution in mantle cell lymphoma. Proceedings of the National Academy of Sciences of the United States of America. 2013;110(45):18250-5.

33.   Jares P, Colomer D, Campo E. Molecular pathogenesis of mantle cell lymphoma. The Journal of clinical investigation. 2012;122(10):3416-23.

34.   Ahmed M, Zhang L, Nomie K, Lam L, Wang M. Gene mutations and actionable genetic lesions in mantle cell lymphoma. Oncotarget. 2016;7(36):58638-48.

35.   Friedberg JW. How I treat double-hit lymphoma. Blood. 2017;130(5):590-6.

36.   Smedby KE, Ponzoni M. The aetiology of B-cell lymphoid malignancies with a focus on chronic inflammation and infections. Journal of internal medicine. 2017;282(5):360-70.

37.   t Mannetje A, De Roos AJ, Boffetta P, Vermeulen R, Benke G, Fritschi L, et al. Occupation and Risk of Non-Hodgkin Lymphoma and Its Subtypes: A Pooled Analysis from the InterLymph Consortium. Environmental health perspectives. 2016;124(4):396-405.

38.   Morton LM, Slager SL, Cerhan JR, Wang SS, Vajdic CM, Skibola CF, et al. Etiologic heterogeneity among non-Hodgkin lymphoma subtypes: the InterLymph Non-Hodgkin Lymphoma Subtypes Project. Journal of the National Cancer Institute Monographs. 2014;2014(48):130-44.

39.   Gibson TM, Morton LM, Shiels MS, Clarke CA, Engels EA. Risk of non-Hodgkin lymphoma subtypes in HIV-infected people during the HAART era: a population-based study. AIDS (London, England). 2014;28(15):2313-8.

40.   Wang SS, Vajdic CM, Linet MS, Slager SL, Voutsinas J, Nieters A, et al. Associations of non-Hodgkin Lymphoma (NHL) risk with autoimmune conditions according to putative NHL loci. American journal of epidemiology. 2015;181(6):406-21.

41.   Krishnan B, Morgan GJ. Non-Hodgkin lymphoma secondary to cancer chemotherapy. Cancer epidemiology, biomarkers & prevention : a publication of the American Association for Cancer Research, cosponsored by the American Society of Preventive Oncology. 2007;16(3):377-80.

42.   Yanik EL, Smith JM, Shiels MS, Clarke CA, Lynch CF, Kahn AR, et al. Cancer Risk After Pediatric Solid Organ Transplantation. Pediatrics. 2017;139(5).

43.   Couronne L, Bachy E, Roulland S, Nadel B, Davi F, Armand M, et al. From hepatitis C virus infection to B-cell lymphoma. Annals of oncology : official journal of the European Society for Medical Oncology. 2018;29(1):92-100.

44.   Ponzoni M, Ferreri AJ. Bacteria associated with marginal zone lymphomas. Best practice & research Clinical haematology. 2017;30(1-2):32-40.

45.   Jones SJ, Voong J, Thomas R, English A, Schuetz J, Slack GW, et al. Nonrandom occurrence of lymphoid cancer types in 140 families. Leuk Lymphoma. 2017;58(9):1-10.

46.   Cerhan JR, Slager SL. Familial predisposition and genetic risk factors for lymphoma. Blood. 2015;126(20):2265-73.

47.   Network NCC. NCCN Clinical Practice Guidelines in Oncology. B-cell Lymphomas 2019 [Version 3.2019:[Guidelines]. Available from: https://www.nccn.org/professionals/physician_gls/pdf/nhl.pdf.

48.   Tilly H, Gomes da Silva M, Vitolo U, Jack A, Meignan M, Lopez-Guillermo A, et al. Diffuse large B-cell lymphoma (DLBCL): ESMO Clinical Practice Guidelines for diagnosis, treatment and follow-up. Annals of oncology : official journal of the European Society for Medical Oncology. 2015;26 Suppl 5:v116-25.

49.   Dreyling M, Ghielmini M, Rule S, Salles G, Vitolo U, Ladetto M. Newly diagnosed and relapsed follicular lymphoma: ESMO Clinical Practice Guidelines for diagnosis, treatment and follow-up. Annals of oncology : official journal of the European Society for Medical Oncology. 2017;28(12):3109.

50.   Vitolo U, Seymour JF, Martelli M, Illerhaus G, Illidge T, Zucca E, et al. Extranodal diffuse large B-cell lymphoma (DLBCL) and primary mediastinal B-cell lymphoma: ESMO Clinical Practice Guidelines for diagnosis, treatment and follow-up. Annals of oncology : official journal of the European Society for Medical Oncology. 2016;27(suppl 5):v91-v102.

51.   Dreyling M, Campo E, Hermine O, Jerkeman M, Le Gouill S, Rule S, et al. Newly diagnosed and relapsed mantle cell lymphoma: ESMO Clinical Practice Guidelines for diagnosis, treatment and follow-up. Annals of oncology : official journal of the European Society for Medical Oncology. 2017;28(suppl_4):iv62-iv71.

52.   Mounier N, Briere J, Gisselbrecht C, Emile JF, Lederlin P, Sebban C, et al. Rituximab plus CHOP (R-CHOP) overcomes bcl-2--associated resistance to chemotherapy in elderly patients with diffuse large B-cell lymphoma (DLBCL). Blood. 2003;101(11):4279-84.

53.   Cheson BD, Chua N, Mayer J, Dueck G, Trneny M, Bouabdallah K, et al. Overall Survival Benefit in Patients With Rituximab-Refractory Indolent Non-Hodgkin Lymphoma Who Received Obinutuzumab Plus Bendamustine Induction and

Obinutuzumab Maintenance in the GADOLIN Study. J Clin Oncol. 2018;36(22):2259-66.

54.   Freeman CL, Sehn LH. A tale of two antibodies: obinutuzumab versus rituximab. Br J Haematol. 2018;182(1):29-45.

55.   Herter S, Herting F, Mundigl O, Waldhauer I, Weinzierl T, Fauti T, et al. Preclinical activity of the type II CD20 antibody GA101 (obinutuzumab) compared with rituximab and ofatumumab in vitro and in xenograft models. Mol Cancer Ther. 2013;12(10):2031-42.

56.   Sehn LH, Goy A, Offner FC, Martinelli G, Caballero MD, Gadeberg O, et al. Randomized Phase II Trial Comparing Obinutuzumab (GA101) With Rituximab in Patients With Relapsed CD20+ Indolent B-Cell Non-Hodgkin Lymphoma: Final Analysis of the GAUSS Study. J Clin Oncol. 2015;33(30):3467-74.

57.   Hagemeister FB. Treatment of relapsed aggressive lymphomas: regimens with and without high-dose therapy and stem cell rescue. Cancer chemotherapy and pharmacology. 2002;49 Suppl 1:S13-20.

58.   Lomax ME, Folkes LK, O'Neill P. Biological consequences of radiation-induced DNA damage: relevance to radiotherapy. Clinical oncology (Royal College of Radiologists (Great Britain)). 2013;25(10):578-85.

59.   Zimmermann M, Oehler C, Mey U, Ghadjar P, Zwahlen DR. Radiotherapy for Non-Hodgkin's lymphoma: still standard practice and not an outdated treatment option. Radiation oncology (London, England). 2016;11(1):110.

60.   Tward JD, Wendland MM, Shrieve DC, Szabo A, Gaffney DK. The risk of secondary malignancies over 30 years after the treatment of non-Hodgkin lymphoma. Cancer. 2006;107(1):108-15.

61.   Martins CD, Kramer-Marek G, Oyen WJG. Radioimmunotherapy for delivery of cytotoxic radioisotopes: current status and challenges. Expert opinion on drug delivery. 2018;15(2):185-96.

62.   Price EW, Orvig C. Matching chelators to radiometals for radiopharmaceuticals. Chemical Society reviews. 2014;43(1):260-90.

63.   Sharkey RM, Goldenberg DM. Cancer radioimmunotherapy. Immunotherapy. 2011;3(3):349-70.

64.   Rueda A, Casanova M, Redondo M, Perez-Ruiz E, Medina-Perez A. Has the time to come leave the "watch-and-wait" strategy in newly diagnosed asymptomatic follicular lymphoma patients? BMC cancer. 2012;12:210.

65.   Nicholson LB. The immune system. Essays in biochemistry. 2016;60(3):275-301.

66.   Anu Sharma, Matthew Campbell, Cassian Yee, Sangeeta Goswami, Sharma P. Immunotherapy of Cancer. In: R. RR, T. FA, C. WM, editors. Clinical Immunology: Principles and Practice. Immunology of Neoplasia. Fifth ed: Elsevier; 2019. p. 1033-42.

67.   Paul S, Lal G. The Molecular Mechanism of Natural Killer Cells Function and Its Importance in Cancer Immunotherapy. Frontiers in immunology. 2017;8:1124.

68.   Raval RR, Sharabi AB, Walker AJ, Drake CG, Sharma P. Tumor immunology and cancer immunotherapy: summary of the 2013 SITC primer. Journal for immunotherapy of cancer. 2014;2:14.

69.   Crisci S, Di Francia R, Mele S, Vitale P, Ronga G, De Filippi R, et al. Overview of Targeted Drugs for Mature B-Cell Non-hodgkin Lymphomas. Frontiers in oncology. 2019;9:443.

70.   Maloney GD. Monoclonal antibodies in lymphoid neoplasia: principles for optimal combined therapy. Seminars in hematology. 2000;37(4 Suppl 7):17-26.

71.   Singh S, Kumar NK, Dwiwedi P, Charan J, Kaur R, Sidhu P, et al. Monoclonal Antibodies: A Review. Current clinical pharmacology. 2018;13(2):85-99.

72.   Stern M, Herrmann R. Overview of monoclonal antibodies in cancer therapy: present and promise. Crit Rev Oncol Hematol. 2005;54(1):11-29.

73.   Weiner GJ. Building better monoclonal antibody-based therapeutics. Nat Rev Cancer. 2015;15(6):361-70.

74.   Mathur R, Weiner GJ. Picking the optimal target for antibody-drug conjugates. American Society of Clinical Oncology educational book American Society of Clinical Oncology Annual Meeting. 2013.

75.   Wishart DS, Knox C, Guo AC, Shrivastava S, Hassanali M, Stothard P, et al. DrugBank: a comprehensive resource for in silico drug discovery and exploration. Nucleic acids research. 2006;34(Database issue):D668-72.

76.   Ovacik M, Lin K. Tutorial on Monoclonal Antibody Pharmacokinetics and Its Considerations in Early Development. Clinical and translational science. 2018;11(6):540-52.

77.   Wong JY. Basic immunology of antibody targeted radiotherapy. International journal of radiation oncology, biology, physics. 2006;66(2 Suppl):S8-14.

78.   Geskin LJ. Monoclonal Antibodies. Dermatologic clinics. 2015;33(4):777-86.

79.   Kohler G, Milstein C. Continuous cultures of fused cells secreting antibody of predefined specificity. Nature. 1975;256(5517):495-7.

80.   Parlevliet KJ, Schellekens PT. Monoclonal antibodies in renal transplantation: a review. Transplant international : official journal of the European Society for Organ Transplantation. 1992;5(4):234-46.

81.   Christiansen J, Rajasekaran AK. Biological impediments to monoclonal antibody-based cancer immunotherapy. Mol Cancer Ther. 2004;3(11):1493-501.

82.   Neuberger MS, Williams GT, Mitchell EB, Jouhal SS, Flanagan JG, Rabbitts TH. A hapten-specific chimaeric IgE antibody with human physiological effector function. Nature. 1985;314(6008):268-70.

83.   Jones PT, Dear PH, Foote J, Neuberger MS, Winter G. Replacing the complementarity-determining regions in a human antibody with those from a mouse. Nature. 1986;321(6069):522-5.

84.   Chames P, Van Regenmortel M, Weiss E, Baty D. Therapeutic antibodies: successes, limitations and hopes for the future. British journal of pharmacology. 2009;157(2):220-33.

85.   Ayyar BV, Arora S, O'Kennedy R. Coming-of-Age of Antibodies in Cancer Therapeutics. Trends in pharmacological sciences. 2016;37(12):1009-28.

86.   Ludwig DL, Pereira DS, Zhu Z, Hicklin DJ, Bohlen P. Monoclonal antibody therapeutics and apoptosis. Oncogene. 2003;22(56):9097-106.

87.   Wang W, Erbe AK, Hank JA, Morris ZS, Sondel PM. NK Cell-Mediated Antibody-Dependent Cellular Cytotoxicity in Cancer Immunotherapy. Frontiers in immunology. 2015;6:368.

88.   Weiskopf K, Weissman IL. Macrophages are critical effectors of antibody therapies for cancer. mAbs. 2015;7(2):303-10.

89.   Mamidi S, Hone S, Kirschfink M. The complement system in cancer: Ambivalence between tumour destruction and promotion. Immunobiology. 2017;222(1):45-54.

90.   Janas E, Priest R, Wilde JI, White JH, Malhotra R. Rituxan (anti-CD20 antibody)-induced translocation of CD20 into lipid rafts is crucial for calcium influx and apoptosis. Clinical and experimental immunology. 2005;139(3):439-46.

91.   Cragg MS, Morgan SM, Chan HT, Morgan BP, Filatov AV, Johnson PW, et al. Complement-mediated lysis by anti-CD20 mAb correlates with segregation into lipid rafts. Blood. 2003;101(3):1045-52.

92.   Harjunpaa A, Junnikkala S, Meri S. Rituximab (anti-CD20) therapy of B-cell lymphomas: direct complement killing is superior to cellular effector mechanisms. Scandinavian journal of immunology. 2000;51(6):634-41.

93.   Wang SY, Racila E, Taylor RP, Weiner GJ. NK-cell activation and antibody-dependent cellular cytotoxicity induced by rituximab-coated target cells is inhibited by the C3b component of complement. Blood. 2008;111(3):1456-63.

94.   Tedder TF, Engel P. CD20: a regulator of cell-cycle progression of B lymphocytes. Immunology today. 1994;15(9):450-4.

95.   Cang S, Mukhi N, Wang K, Liu D. Novel CD20 monoclonal antibodies for lymphoma therapy. Journal of hematology & oncology. 2012;5:64.

96.   Agez M, Mandon ED, Iwema T, Gianotti R, Limani F, Herter S, et al. Biochemical and biophysical characterization of purified native CD20 alone and in complex with rituximab and obinutuzumab. Scientific reports. 2019;9(1):13675.

97.   Beum PV, Kennedy AD, Williams ME, Lindorfer MA, Taylor RP. The shaving reaction: rituximab/CD20 complexes are removed from mantle cell lymphoma and chronic lymphocytic leukemia cells by THP-1 monocytes. Journal of immunology (Baltimore, Md : 1950). 2006;176(4):2600-9.

98.   Beum PV, Peek EM, Lindorfer MA, Beurskens FJ, Engelberts PJ, Parren PW, et al. Loss of CD20 and bound CD20 antibody from opsonized B cells occurs more rapidly because of trogocytosis mediated by Fc receptor-expressing effector cells than direct internalization by the B cells. Journal of immunology (Baltimore, Md : 1950). 2011;187(6):3438-47.

99. Czuczman MS, Olejniczak S, Gowda A, Kotowski A, Binder A, Kaur H, et al. Acquirement of rituximab resistance in lymphoma cell lines is associated with both global CD20 gene and protein down-regulation regulated at the pretranscriptional and posttranscriptional levels. Clin Cancer Res. 2008;14(5):1561-70.

100. Golay J, Lazzari M, Facchinetti V, Bernasconi S, Borleri G, Barbui T, et al. CD20 levels determine the in vitro susceptibility to rituximab and complement of B-cell chronic lymphocytic leukemia: further regulation by CD55 and CD59. Blood. 2001;98(12):3383-9.

101. Kennedy AD, Beum PV, Solga MD, DiLillo DJ, Lindorfer MA, Hess CE, et al. Rituximab infusion promotes rapid complement depletion and acute CD20 loss in chronic lymphocytic leukemia. Journal of immunology (Baltimore, Md : 1950). 2004;172(5):3280-8.

102. Tsai PC, Hernandez-Ilizaliturri FJ, Bangia N, Olejniczak SH, Czuczman MS. Regulation of CD20 in rituximab-resistant cell lines and B-cell non-Hodgkin lymphoma. Clin Cancer Res. 2012;18(4):1039-50.

103. Rezvani AR, Maloney DG. Rituximab resistance. Best practice & research Clinical haematology. 2011;24(2):203-16.

104. Mossner E, Brunker P, Moser S, Puntener U, Schmidt C, Herter S, et al. Increasing the efficacy of CD20 antibody therapy through the engineering of a new type II anti-CD20 antibody with enhanced direct and immune effector cell-mediated B-cell cytotoxicity. Blood. 2010;115(22):4393-402.

105. Alduaij W, Ivanov A, Honeychurch J, Cheadle EJ, Potluri S, Lim SH, et al. Novel type II anti-CD20 monoclonal antibody (GA101) evokes homotypic adhesion and actin-dependent, lysosome-mediated cell death in B-cell malignancies. Blood. 2011;117(17):4519-29.

106. Niederfellner G, Lammens A, Mundigl O, Georges GJ, Schaefer W, Schwaiger M, et al. Epitope characterization and crystal structure of GA101 provide insights into the molecular basis for type I/II distinction of CD20 antibodies. Blood. 2011;118(2):358-67.

107. Larson SM, Carrasquillo JA, Cheung NK, Press OW. Radioimmunotherapy of human tumours. Nat Rev Cancer. 2015;15(6):347-60.

108. Tsai WK, Wu AM. Aligning physics and physiology: Engineering antibodies for radionuclide delivery. Journal of labelled compounds & radiopharmaceuticals. 2018;61(9):693-714.

109. Pouget JP, Lozza C, Deshayes E, Boudousq V, Navarro-Teulon I. Introduction to radiobiology of targeted radionuclide therapy. Frontiers in medicine. 2015;2:12.

110. Wessels BW, Meares CF. Physical and chemical properties of radionuclide therapy. Seminars in radiation oncology. 2000;10(2):115-22.

111. DeNardo GL, Kennel SJ, Siegel JA, Denardo SJ. Radiometals as payloads for radioimmunotherapy for lymphoma. Clinical lymphoma. 2004;5 Suppl 1:S5-10.

112. Seidl C. Radioimmunotherapy with alpha-particle-emitting radionuclides. Immunotherapy. 2014;6(4):431-58.

113. Wulbrand C, Seidl C, Gaertner FC, Bruchertseifer F, Morgenstern A, Essler M, et al. Alpha-particle emitting 213Bi-anti-EGFR immunoconjugates eradicate tumor cells independent of oxygenation. PLoS One. 2013;8(5):e64730.

114. Kassis AI. Molecular and cellular radiobiological effects of Auger emitting radionuclides. Radiation protection dosimetry. 2011;143(2-4):241-7.

115. Hall EJ, Giaccia AJ. Radiobiology for the Radiobiologist. Eighth edition ed. Philadelphia Wolters Kluwer; 2019.

116. O'Connor MJ. Targeting the DNA Damage Response in Cancer. Molecular cell. 2015;60(4):547-60.

117. Zhao X, Wei C, Li J, Xing P, Li J, Zheng S, et al. Cell cycle-dependent control of homologous recombination. Acta biochimica et biophysica Sinica. 2017;49(8):655-68.

118. Chang HHY, Pannunzio NR, Adachi N, Lieber MR. Non-homologous DNA end joining and alternative pathways to double-strand break repair. Nature reviews Molecular cell biology. 2017;18(8):495-506.

119. Morales J, Li L, Fattah FJ, Dong Y, Bey EA, Patel M, et al. Review of poly (ADP-ribose) polymerase (PARP) mechanisms of action and rationale for targeting in cancer and other diseases. Critical reviews in eukaryotic gene expression. 2014;24(1):15-28.

120. Hosoya N, Miyagawa K. Targeting DNA damage response in cancer therapy. Cancer science. 2014;105(4):370-88.

121.   Blackford AN, Jackson SP. ATM, ATR, and DNA-PK: The Trinity at the Heart of the DNA Damage Response. Molecular cell. 2017;66(6):801-17.

122.   Maier P, Hartmann L, Wenz F, Herskind C. Cellular Pathways in Response to Ionizing Radiation and Their Targetability for Tumor Radiosensitization. Int J Mol Sci. 2016;17(1).

123.   Eriksson D, Stigbrand T. Radiation-induced cell death mechanisms. Tumour biology : the journal of the International Society for Oncodevelopmental Biology and Medicine. 2010;31(4):363-72.

124.   Campbell KJ, Tait SWG. Targeting BCL-2 regulated apoptosis in cancer. Open biology. 2018;8(5).

125.   Sheard MA. Ionizing radiation as a response-enhancing agent for CD95-mediated apoptosis. International journal of cancer. 2001;96(4):213-20.

126.   Zong WX, Thompson CB. Necrotic death as a cell fate. Genes & development. 2006;20(1):1-15.

127.   Eskian M, Khorasanizadeh M, Zinzani PL, Rezaei N. Radioimmunotherapy as the first line of treatment in non-Hodgkin lymphoma. Immunotherapy. 2018;10(8):699-711.

128.   Dahle J, Repetto-Llamazares AH, Mollatt CS, Melhus KB, Bruland OS, Kolstad A, et al. Evaluating antigen targeting and anti-tumor activity of a new anti-CD37 radioimmunoconjugate against non-Hodgkin's lymphoma. Anticancer research. 2013;33(1):85-95.

129.   Schwartz-Albiez R, Dorken B, Hofmann W, Moldenhauer G. The B cell-associated CD37 antigen (gp40-52). Structure and subcellular expression of an extensively glycosylated glycoprotein. Journal of immunology (Baltimore, Md : 1950). 1988;140(3):905-14.

130.   Lapalombella R, Yeh YY, Wang L, Ramanunni A, Rafiq S, Jha S, et al. Tetraspanin CD37 directly mediates transduction of survival and apoptotic signals. Cancer cell. 2012;21(5):694-708.

131.   Sheng KC, van Spriel AB, Gartlan KH, Sofi M, Apostolopoulos V, Ashman L, et al. Tetraspanins CD37 and CD151 differentially regulate Ag presentation and T-cell co-stimulation by DC. European journal of immunology. 2009;39(1):50-5.

132.   Press OW, Howell-Clark J, Anderson S, Bernstein I. Retention of B-cell-specific monoclonal antibodies by human lymphoma cells. Blood. 1994;83(5):1390-7.

133.   Repetto-Llamazares AH, Larsen RH, Patzke S, Fleten KG, Didierlaurent D, Pichard A, et al. Targeted cancer therapy with a novel anti-CD37 beta-particle emitting radioimmunoconjugate for treatment of non-Hodgkin lymphoma. PLoS One. 2015;10(6):e0128816.

134.   Dash A, Pillai MR, Knapp FF, Jr. Production of (177)Lu for Targeted Radionuclide Therapy: Available Options. Nuclear medicine and molecular imaging. 2015;49(2):85-107.

135.   Pichard A, Marcatili S, Karam J, Constanzo J, Ladjohounlou R, Courteau A, et al. The therapeutic effectiveness of 177Lu-lilotomab in B-cell non-Hodgkin lymphoma involves modulation of G2/M cell cycle arrest. Leukemia. 2019.

136.   Repetto-Llamazares A, Abbas N, Bruland OS, Dahle J, Larsen RH. Advantage of lutetium-177 versus radioiodine immunoconjugate in targeted radionuclide therapy of b-cell tumors. Anticancer research. 2014;34(7):3263-9.

137.   Repetto-Llamazares AH, Larsen RH, Mollatt C, Lassmann M, Dahle J. Biodistribution and dosimetry of (177)Lu-tetulomab, a new radioimmunoconjugate for treatment of non-Hodgkin lymphoma. Current radiopharmaceuticals. 2013;6(1):20-7.

138.   Heyerdahl H, Repetto-Llamazares A, Dahle J. Administration of beta-emitting anti-CD37 radioimmunoconjugate lutetium (177Lu) lilotomab satetraxetan as weekly multiple injections increases maximum tolerated activity in nude mice with non-Hodgkin lymphoma xenografts. J Cancer Biol Therap. 2018;4(1):181-90.

139.   Blakkisrud J, Holtedahl JE, Londalen A, Dahle J, Bach-Gansmo T, Holte H, et al. Biodistribution and dosimetry results from a phase 1 trial of (177)Lu-lilotomab satetraxetan antibody-radionuclide conjugate therapy. J Nucl Med. 2017.

140.   Blakkisrud J, Londalen A, Dahle J, Turner S, Holte H, Kolstad A, et al. Red Marrow-Absorbed Dose for Non-Hodgkin Lymphoma Patients Treated with 177Lu-Lilotomab Satetraxetan, a Novel Anti-CD37 Antibody-Radionuclide Conjugate. J Nucl Med. 2017;58(1):55-61.

141.   Stokke C, Blakkisrud J, Londalen A, Dahle J, Martinsen ACT, Holte H, et al. Pre-dosing with lilotomab prior to therapy with (177)Lu-lilotomab satetraxetan

significantly increases the ratio of tumor to red marrow absorbed dose in non-Hodgkin lymphoma patients. Eur J Nucl Med Mol Imaging. 2018.

142.   Maaland AF, Heyerdahl H, O'Shea A, Eiriksdottir B, Pascal V, Andersen JT, et al. Targeting B-cell malignancies with the beta-emitting anti-CD37 radioimmunoconjugate (177)Lu-NNV003. European journal of nuclear medicine and molecular imaging. 2019;46(11):2311-21.

143.   Sasikumar PG, Ramachandra M. Small-Molecule Immune Checkpoint Inhibitors Targeting PD-1/PD-L1 and Other Emerging Checkpoint Pathways. BioDrugs : clinical immunotherapeutics, biopharmaceuticals and gene therapy. 2018;32(5):481-97.

144.   Gatzka MV. Targeted Tumor Therapy Remixed-An Update on the Use of Small-Molecule Drugs in Combination Therapies. Cancers. 2018;10(6).

145.   Curigliano G, Criscitiello C. Successes and limitations of targeted cancer therapy in breast cancer. Progress in tumor research. 2014;41:15-35.

146.   Fece de la Cruz F, Gapp BV, Nijman SM. Synthetic lethal vulnerabilities of cancer. Annual review of pharmacology and toxicology. 2015;55:513-31.

147.   Bochum S, Berger S, Martens UM. Olaparib. Recent results in cancer research Fortschritte der Krebsforschung Progres dans les recherches sur le cancer. 2018;211:217-33.

148.   Livraghi L, Garber JE. PARP inhibitors in the management of breast cancer: current data and future prospects. BMC Med. 2015;13:188.

149.   Farmer H, McCabe N, Lord CJ, Tutt AN, Johnson DA, Richardson TB, et al. Targeting the DNA repair defect in BRCA mutant cells as a therapeutic strategy. Nature. 2005;434(7035):917-21.

150.   Weston VJ, Oldreive CE, Skowronska A, Oscier DG, Pratt G, Dyer MJ, et al. The PARP inhibitor olaparib induces significant killing of ATM-deficient lymphoid tumor cells in vitro and in vivo. Blood. 2010;116(22):4578-87.

151.   Williamson CT, Muzik H, Turhan AG, Zamo A, O'Connor MJ, Bebb DG, et al. ATM deficiency sensitizes mantle cell lymphoma cells to poly(ADP-ribose) polymerase-1 inhibitors. Mol Cancer Ther. 2010;9(2):347-57.

152.   Gani C, Coackley C, Kumareswaran R, Schutze C, Krause M, Zafarana G, et al. In vivo studies of the PARP inhibitor, AZD-2281, in combination with fractionated

radiotherapy: An exploration of the therapeutic ratio. Radiotherapy and oncology : journal of the European Society for Therapeutic Radiology and Oncology. 2015;116(3):486-94.

153.   Schaefer NG, James E, Wahl RL. Poly(ADP-ribose) polymerase inhibitors combined with external beam and radioimmunotherapy to treat aggressive lymphoma. Nuclear medicine communications. 2011;32(11):1046-51.

154.   Campillo-Marcos I, Lazo PA. Olaparib and ionizing radiation trigger a cooperative DNA-damage repair response that is impaired by depletion of the VRK1 chromatin kinase. Journal of experimental & clinical cancer research : CR. 2019;38(1):203.

155.   Thomas S, Quinn BA, Das SK, Dash R, Emdad L, Dasgupta S, et al. Targeting the Bcl-2 family for cancer therapy. Expert opinion on therapeutic targets. 2013;17(1):61-75.

156.   Adams CM, Clark-Garvey S, Porcu P, Eischen CM. Targeting the Bcl-2 Family in B Cell Lymphoma. Frontiers in oncology. 2018;8:636.

157.   Zhu H, Almasan A. Development of venetoclax for therapy of lymphoid malignancies. Drug design, development and therapy. 2017;11:685-94.

158.   Davids MS, Roberts AW, Seymour JF, Pagel JM, Kahl BS, Wierda WG, et al. Phase I First-in-Human Study of Venetoclax in Patients With Relapsed or Refractory Non-Hodgkin Lymphoma. J Clin Oncol. 2017;35(8):826-33.

159.   Seymour JF, Kipps TJ, Eichhorst B, Hillmen P, D'Rozario J, Assouline S, et al. Venetoclax-Rituximab in Relapsed or Refractory Chronic Lymphocytic Leukemia. The New England journal of medicine. 2018;378(12):1107-20.

160.   Li Q, Cheng L, Shen K, Jin H, Li H, Cheng Y, et al. Efficacy and Safety of Bcl-2 Inhibitor Venetoclax in Hematological Malignancy: A Systematic Review and Meta-Analysis of Clinical Trials. Frontiers in pharmacology. 2019;10:697.

161.   Mihalyova J, Jelinek T, Growkova K, Hrdinka M, Simicek M, Hajek R. Venetoclax: A new wave in hematooncology. Experimental hematology. 2018;61:10-25.

162.   Pham LV, Huang S, Zhang H, Zhang J, Bell T, Zhou S, et al. Strategic Therapeutic Targeting to Overcome Venetoclax Resistance in Aggressive B-cell Lymphomas. Clin Cancer Res. 2018;24(16):3967-80.

163.   Tahir SK, Smith ML, Hessler P, Rapp LR, Idler KB, Park CH, et al. Potential mechanisms of resistance to venetoclax and strategies to circumvent it. BMC cancer. 2017;17(1):399.

164.   O'Steen S, Green DJ, Gopal AK, Orozco JJ, Kenoyer AL, Lin Y, et al. Venetoclax Synergizes with Radiotherapy for Treatment of B-cell Lymphomas. Cancer Res. 2017;77(14):3885-93.

165.   MacLeod RA, Nagel S, Scherr M, Schneider B, Dirks WG, Uphoff CC, et al. Human leukemia and lymphoma cell lines as models and resources. Current medicinal chemistry. 2008;15(4):339-59.

166.   Wilding JL, Bodmer WF. Cancer cell lines for drug discovery and development. Cancer Res. 2014;74(9):2377-84.

167.   Masters JR. Human cancer cell lines: fact and fantasy. Nature reviews Molecular cell biology. 2000;1(3):233-6.

168.   Lindmo T, Boven E, Cuttitta F, Fedorko J, Bunn PA, Jr. Determination of the immunoreactive fraction of radiolabeled monoclonal antibodies by linear extrapolation to binding at infinite antigen excess. Journal of immunological methods. 1984;72(1):77-89.

169.   Parekh BS, Berger E, Sibley S, Cahya S, Xiao L, LaCerte MA, et al. Development and validation of an antibody-dependent cell-mediated cytotoxicity-reporter gene assay. mAbs. 2012;4(3):310-8.

170.   Straetemans R, O'Brien T, Wouters L, Van Dun J, Janicot M, Bijnens L, et al. Design and analysis of drug combination experiments. Biometrical journal Biometrische Zeitschrift. 2005;47(3):299-308.

171.   Foucquier J, Guedj M. Analysis of drug combinations: current methodological landscape. Pharmacology research & perspectives. 2015;3(3):e00149.

172.   Grabovsky Y, Tallarida RJ. Isobolographic analysis for combinations of a full and partial agonist: curved isoboles. The Journal of pharmacology and experimental therapeutics. 2004;310(3):981-6.

173.   de Jong M, Maina T. Of mice and humans: are they the same?--Implications in cancer translational research. Journal of nuclear medicine : official publication, Society of Nuclear Medicine. 2010;51(4):501-4.

174.   B. Anne Croy, James P. Di Santo, Marcus Manz, Bankert RB. Mouse Models of Immunodeficiency. In: James G. Fox, Muriel T. Davisson, Fred W. Quimby, Stephen W. Barthold, Christian E. Newcomer, Smith AL, editors. The Mouse in Biomedical Research Second Edition ed2007. p. 275-89.

175.   Repetto-Llamazares AH, Larsen RH, Giusti AM, Riccardi E, Bruland OS, Selbo PK, et al. 177Lu-DOTA-HH1, a novel anti-CD37 radio-immunoconjugate: a study of toxicity in nude mice. PLoS One. 2014;9(7):e103070.

176.   Habu S, Fukui H, Shimamura K, Kasai M, Nagai Y, Okumura K, et al. In vivo effects of anti-asialo GM1. I. Reduction of NK activity and enhancement of transplanted tumor growth in nude mice. Journal of immunology (Baltimore, Md : 1950). 1981;127(1):34-8.

177.   Awasthi A, Ayello J, Van de Ven C, Elmacken M, Sabulski A, Barth MJ, et al. Obinutuzumab (GA101) compared to rituximab significantly enhances cell death and antibody-dependent cytotoxicity and improves overall survival against CD20(+) rituximab-sensitive/-resistant Burkitt lymphoma (BL) and precursor B-acute lymphoblastic leukaemia (pre-B-ALL): potential targeted therapy in patients with poor risk CD20(+) BL and pre-B-ALL. Br J Haematol. 2015;171(5):763-75.

178.   Herting F, Friess T, Bader S, Muth G, Holzlwimmer G, Rieder N, et al. Enhanced anti-tumor activity of the glycoengineered type II CD20 antibody obinutuzumab (GA101) in combination with chemotherapy in xenograft models of human lymphoma. Leuk Lymphoma. 2014;55(9):2151-5160.

179.   Rich JT, Neely JG, Paniello RC, Voelker CC, Nussenbaum B, Wang EW. A practical guide to understanding Kaplan-Meier curves. Otolaryngology--head and neck surgery : official journal of American Academy of Otolaryngology-Head and Neck Surgery. 2010;143(3):331-6.

180.   Gupta D, Crosby ME, Almasan A, Macklis RM. Regulation of CD20 expression by radiation-induced changes in intracellular redox status. Free Radic Biol Med. 2008;44(4):614-23.

181.   Wattenberg MM, Kwilas AR, Gameiro SR, Dicker AP, Hodge JW. Expanding the use of monoclonal antibody therapy of cancer by using ionising radiation to upregulate antibody targets. Br J Cancer. 2014;110(6):1472-80.

182.   Marcatili S, Pichard A, Courteau A, Ladjohounlou R, Navarro-Teulon I, Repetto-Llamazares A, et al. Realistic multi-cellular dosimetry for 177Lu-labelled antibodies: model and application. Phys Med Biol. 2016;61(19):6935-52.

183.   Hu ZY, Xu F, Sun R, Chen YF, Zhang DS, Fan YH, et al. Apogossypolone induces reactive oxygen species accumulation and controls cell cycle progression in Raji Burkkit's lymphoma cells. Molecular medicine reports. 2015;12(1):337-44.

184.   Elias S, Kahlon S, Kotzur R, Kaynan N, Mandelboim O. Obinutuzumab activates FcgammaRI more potently than other anti-CD20 antibodies in chronic lymphocytic leukemia (CLL). Oncoimmunology. 2018;7(6):e1428158.

185.   Palmer AC, Sorger PK. Combination Cancer Therapy Can Confer Benefit via Patient-to-Patient Variability without Drug Additivity or Synergy. Cell. 2017;171(7):1678-91.e13.

186.   Konig L, Dreyling M, Durig J, Engelhard M, Hohloch K, Viardot A, et al. Therapy of nodal Follicular Lymphoma (WHO grade 1/2) in clinical stage I/II using response adapted Involved Site Radiotherapy in combination with Obinutuzumab (Gazyvaro) - GAZAI Trial (GAZyvaro and response adapted Involved-site Radiotherapy): a study protocol for a single-arm, non-randomized, open, national, multi-center phase II trial. Trials. 2019;20(1):544.

187.   Mantovani F, Collavin L, Del Sal G. Mutant p53 as a guardian of the cancer cell. Cell death and differentiation. 2019;26(2):199-212.

188.   Fulton B, Short SC, James A, Nowicki S, McBain C, Jefferies S, et al. PARADIGM-2: Two parallel phase I studies of olaparib and radiotherapy or olaparib and radiotherapy plus temozolomide in patients with newly diagnosed glioblastoma, with treatment stratified by MGMT status. Clinical and translational radiation oncology. 2018;8:12-6.

189.   de Haan R, van Werkhoven E, van den Heuvel MM, Peulen HMU, Sonke GS, Elkhuizen P, et al. Study protocols of three parallel phase 1 trials combining radical radiotherapy with the PARP inhibitor olaparib. BMC cancer. 2019;19(1):901.

190.   Lyng H, Landsverk KS, Kristiansen E, DeAngelis PM, Ree AH, Myklebost O, et al. Response of malignant B lymphocytes to ionizing radiation: gene expression and genotype. International journal of cancer. 2005;115(6):935-42.

191.   Falt S, Holmberg K, Lambert B, Wennborg A. Long-term global gene expression patterns in irradiated human lymphocytes. Carcinogenesis. 2003;24(11):1837-45.

192.   Li S, Zhang QZ, Zhang DQ, Feng JB, Luo Q, Lu X, et al. GDF-15 gene expression alterations in human lymphoblastoid cells and peripheral blood lymphocytes following exposure to ionizing radiation. Molecular medicine reports. 2017;15(6):3599-606.

193.   Salem AH, Agarwal SK, Dunbar M, Enschede SL, Humerickhouse RA, Wong SL. Pharmacokinetics of Venetoclax, a Novel BCL-2 Inhibitor, in Patients With Relapsed or Refractory Chronic Lymphocytic Leukemia or Non-Hodgkin Lymphoma. Journal of clinical pharmacology. 2017;57(4):484-92.

194.   Chiron D, Dousset C, Brosseau C, Touzeau C, Maiga S, Moreau P, et al. Biological rational for sequential targeting of Bruton tyrosine kinase and Bcl-2 to overcome CD40-induced ABT-199 resistance in mantle cell lymphoma. Oncotarget. 2015;6(11):8750-9.

10 Publications

Papers I, II and III

I

ORIGINAL ARTICLE

WILEY Haematology

Combination of ^{177}Lu-lilotomab with rituximab significantly improves the therapeutic outcome in preclinical models of non-Hodgkin's lymphoma

Ada H. V. Repetto-Llamazares[1] [ID] | Marion M. Malenge[1,2,3] | Adam O'Shea[1] | Bergthóra Eiríksdóttir[4] | Trond Stokke[2] | Roy H. Larsen[5] | Jostein Dahle[1]

[1]Nordic Nanovector ASA, Oslo, Norway

[2]Department of Radiation Biology, Institute for Cancer Research, Oslo University Hospital, Oslo, Norway

[3]Institute of Clinical Medicine, Faculty of Medicine, University of Oslo, Oslo, Norway

[4]ArcticLAS Ltd. CRO, Reykjavík, Iceland

[5]Sciencons AS, Oslo, Norway

Correspondence
Ada H. V. Repetto-Llamazares, Nordic Nanovector ASA, Kjelsåsveien 168B, 0884 Oslo, Norway.
Email: arepetto@nordicnanovector.com

Abstract

Objectives: To investigate the therapeutic potential of the next-generation anti-CD37 radioimmunoconjugate ^{177}Lu-lilotomab satetraxetan (^{177}Lu-lilotomab) in combination with the anti-CD20 antibody rituximab for treatment of mice with non-Hodgkin's lymphoma (NHL) xenografts.

Methods: Nude mice with subcutaneous (s.c.) Burkitt's lymphoma Daudi xenografts and SCID mice intravenously (i.v.) injected with Mantle cell lymphoma Rec-1 cells were treated with either ^{177}Lu-lilotomab or rituximab alone or with the combination of both treatments. Tumour volume, body weight, blood counts and clinical status were monitored. CD20 expression was measured using flow cytometry with fluorescence-labelled rituximab.

Results: The combination of ^{177}Lu-lilotomab and rituximab was synergistic for treatment of nude mice with s.c. Daudi xenografts while it was additive for treatment of SCID mice with i.v. injected Rec-1 cells. Binding of rituximab to NHL cells in-vitro was increased by pretreatment with ^{177}Lu-lilotomab.

Conclusions: Treatment of mice with NHL xenografts with ^{177}Lu-lilotomab synergistically increased tumour suppression of subsequent anti-CD20 immunotherapy and improved survival. If the same effect is confirmed in a recently started clinical study, it could change the way radioimmunotherapy and CD20 immunotherapy would be used in the future.

KEYWORDS
betalutin, CD37, lilotomab, lutetium, lymphoma, non-Hodgkin's, preclinical, radioimmunotherapy, rituximab, synergy

1 | INTRODUCTION

Immunotherapy has been an area of great interest and strong research efforts in the last decades. The anti-CD20 monoclonal antibody rituximab has been used in combination treatment regimens with chemotherapy as first line, maintenance and salvage therapies for non-Hodgkin's lymphoma (NHL).[1-5] This has resulted in significantly improved response rate and survival in patients with CD20 positive B-cell lymphoproliferative disease. However, not every patient responds to rituximab and many relapse after an initial response.[6,7] Therefore, it is necessary to develop new strategies that will enhance the biological activity of rituximab in these patients.

We have recently developed a next-generation radioimmunoconjugate (RIC) based on the beta-emitting radionuclide ^{177}Lu chelated to p-SCN-Bn-DOTA (satetraxetan) conjugated to the anti-CD37 antibody lilotomab (^{177}Lu-lilotomab satetraxetan, referred also as ^{177}Lu-lilotomab, trade name Betalutin®). [177]Lu has a half-life of 6.7 days, and the beta particles emitted have a maximum value in tissue of 1.76 mm [8] which allows for cross-irradiation, i.e. untargeted cells can be killed by ^{177}Lu-lilotomab bound to neighbouring cells. CD37 is an internalising transmembrane glycoprotein strongly expressed on mature B lymphocytes, including normal and neoplastic cells.[9-12] ^{177}Lu-lilotomab has shown strong anti-tumour effect in preclinical models [9,13] and in a completed phase 1/2a clinical trial.[14]

To be effective, rituximab depends on selective expression of a sufficient number of CD20 antigens per cell.[1-4] Treatment with high-dose External Beam Radiation (EBR) upregulates antigens such as HER2, EGFR and CD20 in cancer cells,[15-17] and an increase in the antigen expression is correlated with an increase in anti-tumour activity of immunotherapies targeting these antigens.[15,18,19] Patients treated with low-dose EBR immediately prior to anti-CD20 radioimmunotherapy (RIT) with ibritumomab tiuxetan conjugated to Yttrium-90 had longer freedom from progression (FFP) than patients only treated with RIT with no additional toxicity.[20] The authors hypothesised that the superior therapeutic effect of anti-CD20 RIT after EBR was due to surface upregulation of CD20 after EBR. We wanted to study if the selectively delivered low-dose rate radiation from ^{177}Lu-lilotomab affected the CD20 expression of NHL cells and subsequently altered the efficacy of rituximab. Indeed, we found that the combination of ^{177}Lu-lilotomab with rituximab synergistically increased the therapeutic effect in nude mice with NHL xenografts and rituximab bound to a higher extent to NHL cells treated with ^{177}Lu-lilotomab than to un-treated cells.

2 | MATERIALS AND METHODS

2.1 | Labelling of lilotomab with [177]Lu

The chelator (p-SCN-Bn-DOTA, Macrocyclics, TX, USA) was dissolved in 0.005 M HCl, added to the antibody in a 6:1 ratio and pH-adjusted to approximately 8.5 using carbonate buffer. After 45 minutes of incubation at 37°C, the reaction was stopped by the addition of 50 µL per mg of Ab of 0.2 mol/L glycine solution. To remove free p-SCN-Bn-DOTA, the conjugated antibody was washed using Vivaspin 20 centrifuge tubes (Sartorius Stedim Biotech, Göttingen Germany) 4-5 times with NaCl 0.9%. Before labelling with ^{177}Lu, the pH was adjusted to 5.3 ± 0.3 using 0.25 mol/L ammonium acetate buffer. Between 120 and 220 MBq of [177]Lu (ITG, Garching, Germany) was added to 1 mg of satetraxetan-Ab and incubated for 15-30 minutes at 37°C. The radiochemical purity (RCP) of the conjugate was evaluated using instant thin-layer chromatography. If RCP was below 95% the conjugate was purified by elution through a Sephadex G-25 PD-10 column (GE Healthcare Bio-Sciences AB, Uppsala, Sweden).

2.2 | Cell lines

Cell suspensions of lymphoma cell lines Daudi (Burkitt's lymphoma), and Rec-1 (Mantle Cell Lymphoma, both acquired from ATCC) were grown in RPMI 1640 medium (PAA, Linz, Austria) supplemented with 10% heat-inactivated FCS (PAA), 1% L-glutamine (PAA) and 1% penicillin-streptomycin (PAA) in a humid atmosphere with 95% air/5% CO_2 and maintained in exponential growth phase through sub-culturing every 2-4 days.

2.3 | Immunoreactive fraction of ^{177}Lu-lilotomab

The immunoreactivity of the radioimmunoconjugates was measured using NHL Ramos cells and a one point modified Lindmo method.[21,22] The cell concentration used was 75 million cells/mL. The immunoreactivity of the conjugates was between 60% and 82%.

2.4 | Animal models

A subcutaneous Daudi model was established in the Institute for Comparative Medicine, Radium Hospital, Oslo, Norway. Institutionally bred female athymic nude Foxn1nu mice that were between 6 and 8 weeks old and had body weights between 18 and 24 g at the start of the study were used. All mice had 1-2 weeks for acclimation before the studies began. The animals were maintained under pathogen-free conditions with a 12-hour lighting cycle at a room temperature of 23°C and air relative humidity of 55% in plastic cages. Food and water were supplied ad libitum, and bedding was changed regularly. All procedures and experiments involving animals in this study were approved by The Norwegian Animal Research Authority (NARA). The Department of Comparative Medicine institutional veterinarian has established the rules for feeding, monitoring, handling and sacrifice of animals in compliance with regulations set by the Ministry of Agriculture of Norway and "The European Convention for the Protection of Vertebrate Animals used for Experimental and other Scientific Purposes." The institutional veterinarian has delegated authority from the Norwegian Animal Research Authority (NARA). The laboratory animal facilities are subject to a routine health-monitoring programme and tested for infectious organisms according to a modification of Federation of European Laboratory Animal Science Associations (FELASA) recommendations. Mice were injected subcutaneously in both flanks with 100 µL of 100 million Daudi cells/mL using a 1:1 Matrigel dilution.

An intravenous Rec-1 model was established in ArcticLAS, Reykjavik, Iceland. Female CB17-SCID mice, 6 weeks of age, weighing no less than 15 g, were ordered from Taconic in Denmark and allowed for one week of acclimation prior to study start. SCID mice were chosen because it was not possible to establish a disseminated model in nude mice. In this type of models, tumours are of microscopic dimensions at injection of treatment. Due to the SCID mutation, this mouse strain tolerates less radiation than nude mice.[23] The mice were weighed and earmarked in the acclimation week. The animals were housed in an IVC-rack (individually ventilated cages). Five mice

TABLE 1 Study groups and treatment schedule in the study of ^{177}Lu-liltomab and rituximab combination in nude mice with s.c. Daudi xenografts

| Group name | Study day[a] | | | | | Tumour volume[b] (mm^3) |
	0	3	6	10	13	
NaCl × 5	NaCl	NaCl	NaCl	NaCl	NaCl	216 ± 83
[177]Lu-lilotomab + 4 × NaCl	^{177}Lu-lilotomab (250 MBq/kg)	NaCl	NaCl	NaCl	NaCl	322 ± 110
[177]Lu-lilotomab + 4 × Rituximab	^{177}Lu-lilotomab (250 MBq/kg)	Rituximab (10 mg/kg)	Rituximab (10 mg/kg)	Rituximab (10 mg/kg)	Rituximab (10 mg/kg)	302 ± 101
[177]Lu-lilotomab + 1 × Rituximab	^{177}Lu-lilotomab (250 MBq/kg)	Rituximab (40 mg/kg)	-	-	-	313 ± 120
NaCl + 4 × Rituximab	NaCl	Rituximab (10 mg/kg)	Rituximab (10 mg/kg)	Rituximab (10 mg/kg)	Rituximab (10 mg/kg)	305 ± 89
NaCl + 1 × Rituximab	NaCl	Rituximab (40 mg/kg)	-	-	-	264 ± 119

[a]Mice were inoculated at day -15.

[b]Average ± SD at injection of first treatment (day 0).

were housed per cage (Euro-standard Type-II). Cages, water bottles, nesting material and hideaways were autoclaved at ArcticLAS prior to use. Cages were changed once a week. The mice were provided with autoclaved drinking water. Water bottles were changed every other day. The mice were fed with irradiated rodent diet (Altromin NIH#31 M -from Brogarden, Denmark). The animals were provided with irradiated-Tapevei aspen bedding from Brogarden, Denmark. Mice were injected intravenously with 100 µL containing 10 million Rec-1 cells via their lateral tail vein. The animal studies were approved by the national committee for animal experiments prior to study start. ArcticLAS animal facility works under authorisation and approval from the Food and Veterinary authority in Iceland (MAST). The facility is inspected regularly by the District veterinary office.

2.5 | Therapy studies

The therapeutic effect of the combination of ^{177}Lu-lilotomab and rituximab in the s.c. Daudi model was studied using one injection of 250 MBq/kg ^{177}Lu-lilotomab, one dose of 40 mg/kg rituximab, four doses of 10 mg/kg rituximab or NaCl (Table 1). The activity of ^{177}Lu-lilotomab used was approximately 50% of the maximum tolerated dosage (MTD) [24] and was chosen so that the therapeutic effect of the single treatment was suboptimal in order to be able to detect an increased effect of the combination with rituximab. The same thinking guided the choice of rituximab dosage which was chosen based on published data on similar animal models.[25-30] Pre-dosing with 200 µg IgG2$_a$ was given one day before the first treatment injection to reduce non-specific uptake of mAbs. Treatments were given every 3-4 days. Nine to ten mice (bearing a total of 16-18 tumours) were used per group. Tumour volumes were measured 2-3 times a week, and weekly after study day 100 by measuring the shortest (a) and longest (b) perpendicular diameters using an electronic calliper and the equation: Volume = (a^{2}b)/2. Body weight was measured every 2-3 days and

weekly after study day 100 or more often when mice showed signs of sickness. Mice that were still alive at the end of the study (day 222) were necropsied, and key organs (lungs, liver, spleen, kidneys, stomach, ovaries, brain, femur and skull) were harvested for histopathological evaluation.

The therapeutic effect of the combination in the Rec-1 i.v. model was performed in a blinded study using one injection of 40 MBq/kg ^{177}Lu-lilotomab, one injection of 100 µg of rituximab per mouse (around 5 mg/kg for a 20 g mouse) or NaCl (Table 2). The activity of ^{177}Lu-lilotomab used was approximately 50% of the maximum tolerated dosage (MTD) [24] and was chosen so that the therapeutic effect of the single treatment was suboptimal in order to be able to detect an increased effect of the combination with rituximab. The same thinking guided the choice of rituximab dosage which was chosen based on published data on similar animal models.[31,32] Nine to ten mice were used per group. Mice were administered with the first treatment on day 8; study day 0 was set at injection of tumour cells. The second treatment was given 5 days later. The mice were weighed at least twice a week, and they were inspected at least once daily for clinical signs of disease. When clinical signs of the disease were apparent, an abdominal palpation for tumours was preformed once/twice a week. At termination, all mice were necropsied and the following organs were collected for histopathological evaluation: skull, brain, femur, liver, spleen, easily accessible lymph nodes, uterus, ovaries, the whole vertebrae and tumours. The organs were fixed in 10% buffered formalin and further processed for histopathological evaluation. Blood was drawn from the animals every 3 weeks until week 9 for haematology analysis. Blood samples (no more than 10% of the total blood volume) were drawn from vena facialis and collected into 100 µL EDTA-coated tubes (Microvette®100 K3E, Sarsted). The tubes were turned/swirled for around 1 minute to ensure all EDTA was mixed well with the blood. White blood cells, platelets and red blood cells were counted on an automated haematology analyzer (MS4 analyzer from Melet Schloeing Laboratories, France).

TABLE 2 Study groups and treatment schedule in the study of ^{177}Lu-lilotomab and rituximab combination in SCID mice with i.v. injected Rec-1 cells

	Study day[a]	
Group name	Day 8	Day 13
[177]Lu-lilotomab + Rituximab	^{177}Lu-lilotomab (40 MBq/kg)	Rituximab (100 μg)
NaCl + NaCl	NaCl	NaCl
[177]Lu-lilotomab + NaCl	^{177}Lu-lilotomab (40 MBq/kg)	NaCl
NaCl + Rituximab	NaCl	Rituximab (100 μg)

[a]Days after cell inoculation.

The end-points in the i.v. Rec-1 model and in the s.c. Daudi model were weight loss of more than 10% over a period of one week or of 20% from highest recorded weight, respectively, signs of substantial discomfort or tumour size equal to 20 mm in diameter.

2.6 | Statistical analysis

Survival analysis was performed using log-rank test and the Holm-Sidak method for all multiple pairwise comparisons (Sigma Plot 12.5, Systat Software Inc., San Jose, California, USA). In addition, the Cox proportionial hazards regression model was used for the analysis of the s.c. Daudi survival data. The hazard ratio HR of the combination and of the interaction (Equation 1) was used to assess if there was a synergistic effect of the combination treatment.[33] A HR of 1 indicates no effect and a value <1 indicates lower risk for event.

$$HR_T = HR_{BvsN} \cdot HR_{RvsN} \cdot HR_{Int} \qquad (1)$$

In equation 1, HR_T is the HR of the combination treatment, HR_{Bvs} and HR_{RvsN} are the HR of ^{177}Lu-lilotomab and rituximab alone vs NaCl, respectively, and HR_{Int} is the HR of the interaction between ^{177}Lu-lilotomab and rituximab. The multiplication of HR_{Bvs} by HR_{RvsN} gives the HR of the combination when both treatments are additive (no interaction; HR_{Int} = 1). The lower the HR_{Int} value, the stronger the interaction effect and thus the synergy between the treatments. The threshold for statistical significance for the synergy was set at a P-value associated with HR_{Int} lower than 0.05.

2.7 | Expression of cell surface CD20 in-vitro

The expression of the CD20 antigen was measured in the cell lines Daudi and Rec-1 at various time-points after treatment with naked lilotomab, ^{177}Lu-lilotomab or external beam radiation (EBR). An X-ray machine Faxitron CP160 was used as source of External Beam Radiation (maximum energy of 160 keV with a current of 6.3 mA

and a linear energy distribution). To avoid the lowest energies, 2 filters were used: 0.5 mm Cu and 0.8 mm Be. Dose rate was 1 Gy/min. Non-irradiated cells were used as controls. Treatment with radio-immunotherapy was given by incubating cells for 18 hours with either 0.44 or 0.88 MBq/mL of ^{177}Lu-lilotomab. Control cells were incubated for the same period of time with an equivalent amount of naked lilotomab. After the incubation time, cells were washed 3 times and resuspended in fresh medium. The surface expression of CD20 was estimated by incubating the cells with Alexa 488- or Alexa 647-labelled rituximab and measuring Mean Fluorescence Intensity (MFI) with a Guava EasyCyte 12HT (Merck KGaA, Darmstadt, Germany). Rituximab was labelled with Alexa 488 or Alexa 647 using labelling kits and protocols supplied by Invitrogen, Oregon, US. Binding to CD20 was measured every 1-5 days and up to 3 days in Rec-1 and 13 days in Daudi (duplicates). The absorbed dose by ^{177}Lu-lilotomab to the cells was estimated by assuming a homogeneous distribution of the RIC in the cell suspension during the 18 hours of incubation time, which gives an estimated absorbed dose to the cells of 0.5 Gy for 0.44 MBq/mL ^{177}Lu-lilotomab and 1.5 Gy for 0.88 MBq/mL ^{177}Lu-lilotomab treatments. This might underestimate the actual dose received by the cells. Based on the results reported by Marcatilli et al [34] for Ramos cells incubated with ^{177}Lu-lilotomab for 18 hours and maintained in culture for 5 days, the absorbed doses to the cells were around 0.8 Gy for 0.44 Mq/mL ^{177}Lu-lilotomab and 1.5 Gy for 0.88 MBq/mL ^{177}Lu-lilotomab.

3 | RESULTS

3.1 | Synergistic effect of ^{177}Lu-lilotomab and rituximab in nude mice with s.c. Daudi xenografts

[177]Lu-lilotomab treatment in combination with rituximab showed stronger anti-tumour effect compared to the control groups and each of the treatments alone in mice bearing s.c. Daudi xenografts (Figure 1). Doubling time of the average tumour volume was more than 3 times longer in the combination treatment than the sum of the treatments alone (Table 3). The plateaus observed in Figure 1 are due to 2 reasons: (a) tumour volume after euthanasia was maintained constant in the calculations of average tumour volume and (b) mice reaching complete remission had constant tumour volumes equal to 0. The median survival of mice given the combination treatment was statistically significantly longer (>222 days, $P < 0.05$, Log-Rank test) than the survival of each of the treatments alone (31-60 days; Figure 2, Table 3). There was no significant difference between a single 40 mg/kg injection of rituximab and 4 times injection of 10 mg/kg rituximab ($P = 0.219$, Log-Rank test) nor between the groups receiving ^{177}Lu-lilotomab in combination with one or 4 doses of rituximab ($P = 0.343$, Log-Rank test). A Cox proportional hazards regression model evaluating the interaction effect of the two treatments showed that there was a strong synergistic effect when the two treatments were given in combination (pooled data for groups receiving one dose or 4 doses of rituximab alone, and for groups

FIGURE 1 Average volume ± SE of s.c. Daudi xenografts in nude mice after treatment with ^{177}Lu-lilotomab, rituximab or the combination. N = 16-18 tumours (9-10 mice) per group
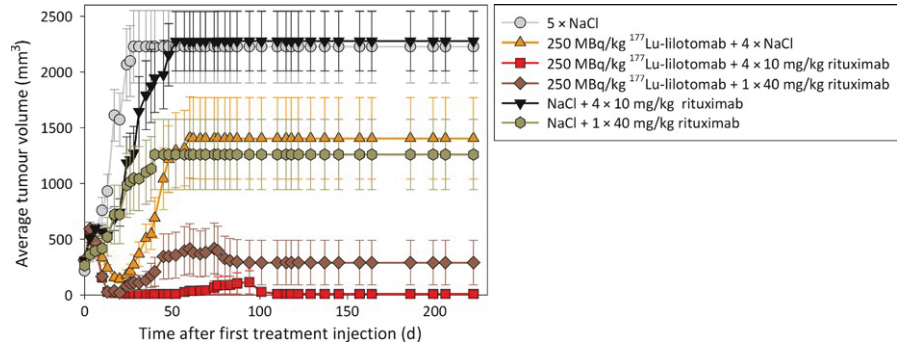
TABLE 3 Median survival with end-point tumour diameter of 20 mm and doubling time of average tumour volume of mice with s.c. Daudi xenografts

Treatment	Median survival ± SE (days)	Doubling time of average tumour volume (days)
5 × NaCl	24 ± 5	4
^{177}Lu-lilotomab + 4 × NaCl	60 ± 9	42
^{177}Lu-lilotomab + 4 × Rituximab	>222[a]	Not Reached
^{177}Lu-lilotomab + 1 × Rituximab	>222[a]	Not Reached
NaCl + 4 × Rituximab	31 ± 5	15
NaCl + 1 × Rituximab	40 ± 11	15

[a]Significantly different from 5 × NaCl and NaCl + 4 × Rituximab (P < 0.05, Log-Rank).

FIGURE 2 Survival of nude mice with s.c. Daudi xenografts after treatment with ^{177}Lu-lilotomab, rituximab or the combination. End-point: tumour diameter equal to or larger than 20 mm
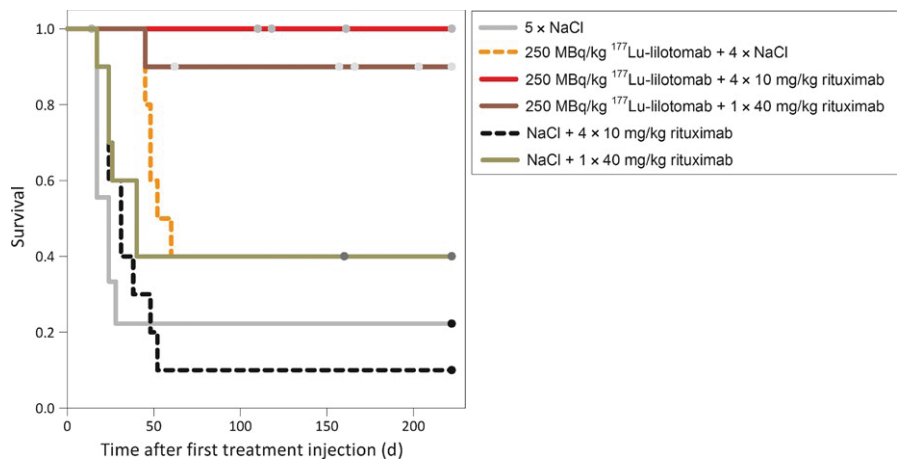
receiving ^{177}Lu-lilotomab in combination with one or 4 doses of rituximab). The expected HR of the combination group given an additive effect was 0.186 (HR_{BvsN} · HR_{RvsN}, Table 4) vs NaCl, whereas HR_T for the combination group was 0.024 (HR_{BvsN} · HR_{RvsN} · HR_{Int}) vs NaCl. Due to the low number of events (ie mice never reaching tumour diameter >20 mm and thus being censored at the end of the study) in the combination group, the test for interaction did not reach the threshold for significance (P = 0.078). In addition, the spread in the survival of mice treated with only rituximab and the dependence of HR with time might have also contributed to the lack of statistical significance.

Average body weight was similar in all treatment groups (data not shown). There were, however, some mice in the combination groups that experienced body weight loss and other clinical symptoms of sickness and discomfort (Table 5). Histopathological analysis of mice euthanised at the end of the study showed no evidence of long-term toxicity associated with the combination treatments. The body weight loss observed after day 100 was probably due to normal aging of the mice.

3.2 | Additive effect of ^{177}Lu-lilotomab and rituximab in SCID mice with i.v. injected Rec-1 cells

There was an increased survival of SCID mice with Rec-1 i.v. injected cells treated with the combination of ^{177}Lu-lilotomab and rituximab as compared with mice treated with either treatment alone or with NaCl (Figure 3). However, the differences were only statistically significant for the comparison with NaCl (Table 6). The median survival

TABLE 4 Output from cox regression model from study in nude mice with s.c. Daudi xenografts and tumour diameter equal or larger than 20 mm as end-point and from study in SCID mice with i.v. injected Rec-1 cells and euthanasia due to sickness, discomfort or palpable tumour diameter equal to 20 mm as end-point

	s.c. Daudi			i.v. Rec-1		
	Hazard ratio	95% CI	P-value	Hazard Ratio	95% CI	P-value
^{177}Lu-lilotomab vs NaCl (HR$_{BvsN}$)	0.30	(0.10-0.90)	0.032	0.30	(0.11-0.87)	0.027
Rituximab[a] vs NaCl (HR$_{RvsN}$)	0.62	(0.25-1.53)	0.298	0.46	(0.16-1.31)	0.147
Interaction of ^{177}Lu-lilotomab and Rituximab[b] (HR$_{Int}$)	0.13	(0.01-1.26)	0.078	0.75	(0.14-4.09)	0.736

[a]Pooled data from both groups receiving rituximab alone.
[b]Pooled data from both groups receiving ^{177}Lu-lilotomab in combination with 4 doses of 10 mg/kg rituximab and one dose of 40 mg/kg rituximab.

TABLE 5 Number of mice with s.c. Daudi xenografts euthanised due to body weight loss and general state of sickness during the study, at end of study or due to tumour size equal or larger than 20 mm

Treatment	Number/ % of mice euthanised due to body weight loss	Study day of euthanasia due to body weight loss	Number/% of mice alive at end of study (222 days)	Number/% of mice euthanised due to tumour size
5 × NaCl	0/0%	Not Applicable	2/22%	7/78%
^{177}Lu-lilotomab + 4 × NaCl	0/0%	Not Applicable	4/40%	6/60%
^{177}Lu-lilotomab + 4 × Rituximab	5/50%	14, 110, 118 and 2 at 161 days	5/50%	0/0%
^{177}Lu-lilotomab + 1 × Rituximab	4/40%	157, 166 and 2 at 203 days	4/40%	2/20%
NaCl + 4 × Rituximab	0/0%	Not Applicable	1/10%	9/90%
NaCl + 1 × Rituximab	1/10%	160 days	3/30%	6/60%
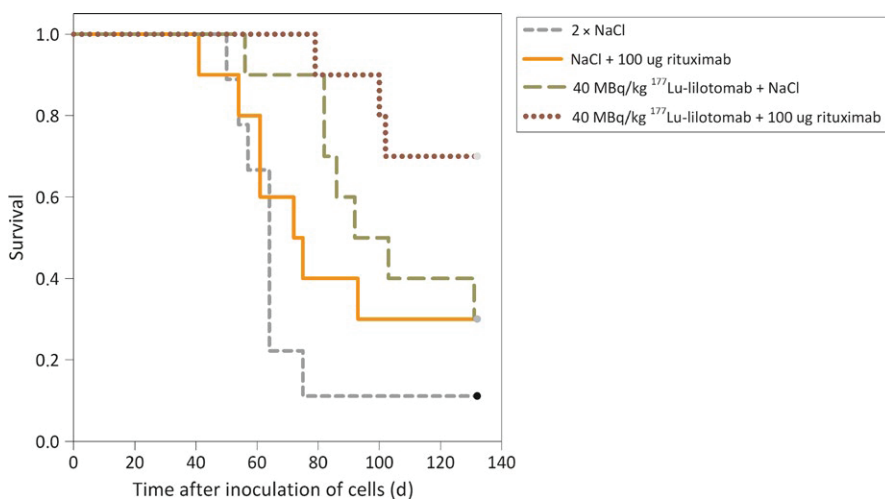
FIGURE 3 Survival of SCID mice intravenously injected with Rec-1 cells. End-point: weight loss of more than 10% over a period of one week, signs of substantial discomfort or tumour size equal to 20 mm in diameter

was more than 132 days (106% increase as compared to NaCl control) for the combination while it was 92 days (44% increase) for ^{177}Lu-lilotomab alone and 75 days (15% increase) for rituximab alone (Table 6). The HR$_T$ found using the Cox proportional hazards regression model was 0.104 (Table 4) which was close to the HR of the combination if only an additive effect is considered (HR$_{BvsN}$ · HR$_{RvsN}$ = 0.138). In addition, the *P*-value associated to HR$_{Int}$ was substantially higher than the statistical threshold, which makes us conclude that the combination of ^{177}Lu-lilotomab and rituximab in this study was additive.

It is worth noticing that at necropsy, 2 of the 7 mice surviving until the end of the study in the combination treatment group showed pathological signs of tumours and therefore a total of 5 animals of 10 in this group had clear pathological signs of tumours. No sign of treatment toxicity was observed in the mice. Platelet (THR), and red blood cell (RBC) counts were within or close to the established reference interval and similar to the control group during the whole study (data not shown). Average body weight of all treatment groups followed that of the control group, showing severe body weight loss close to euthanasia due to the disease (data not shown).

TABLE 6 Median survival of SCID mice intravenously injected with Rec-1 cells after treatment with ^{177}Lu-lilotomab, rituximab or the combination

Treatment	Median Survival (days) ± SE	% Increased Survival vs control
NaCl + NaCl	64 ± 2	NA
NaCl + Rituximab	75 ± 11	14.5
[177]Lu-lilotomab + NaCl	92[a] ± 13	43.8
[177]Lu-lilotomab + Rituximab	>132[a]	>106.3

[a]Statistically significant different from the NaCl + NaCl control group ($P < 0.05$, log-rank).

It took 40 days or more for tumours to be palpable, or for animals to start showing signs of disease in this animal model. Macroscopic tumours found at euthanasia were commonly located in the skull, ventral vertebral muscles of the thorax or abdomen, in the mediastinum, ovaries or mesovarium, uterus or mesometrium, in skeletal muscles and superficial lymph nodes. Other less common locations were in the abdominal cavity where tumours were seen around the kidneys or stomach, or as large tumours pendulating from the dorsal abdomen.

3.3 | Expression of cell surface CD20 in-vitro

The cell lines showed increased binding of rituximab after treatment with either EBR or ^{177}Lu-lilotomab as compared to untreated cells or cells treated with naked lilotomab (Figure 4). This may indicate an increased expression or upregulation of the CD20 antigen. Daudi cells showed the highest increase, increasing up to 356% compared to control, 5 days after treatment. The upregulation lasted up to 13 days which was the last time-point measured. The amount of increased binding and the length of the increase when treating with the RIC ^{177}Lu-lilotomab was superior to that found when the same cells were treated with similar doses of EBR.

4 | DISCUSSION

The use of radioimmunotherapy has been approved as a therapeutic option in cancer therapy for several years.[35] Today radioimmunotherapy is mainly used in those patients experiencing relapse from chemotherapy and immunotherapy. We have previously shown that ^{177}Lu-lilotomab can target and deliver radiation selectively to lymphoma tumour cells and xenografts,[9,13,36] and the treatment is currently being tested clinically for treatment of both aggressive and indolent NHL. In this study, we showed that ^{177}Lu-lilotomab can interact synergistically with rituximab to give an increased antitumour effect, prolonging the survival of mice with s.c. NHL xenografts. There are several mechanisms that can lead to the observed synergy. Among them is the upregulation of CD20, which would lead to increased binding of rituximab. It has previously been shown that high-dose rate External Beam Radiation (EBR) can cause a reactive oxygen species (ROS) mediated increase of CD20 in B cells and that the effect can last for up to 2-3 days.[15-17] We have shown both a
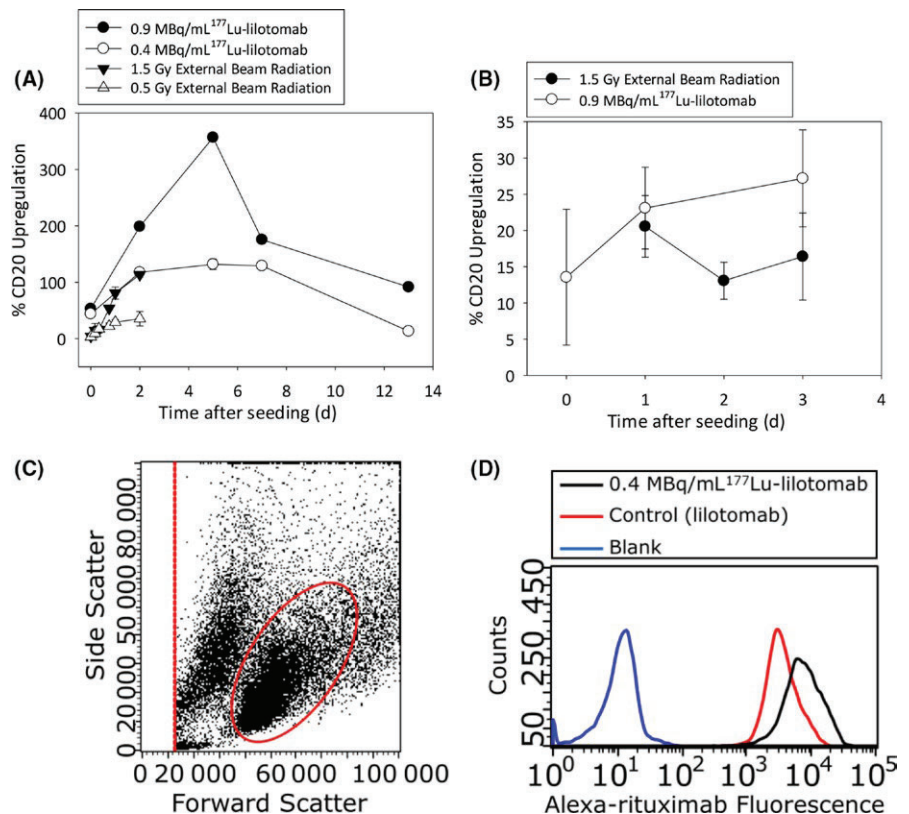

FIGURE 4 Percentage increase in CD20 expression for A, Daudi, B, Rec-1 cells as compared to naked lilotomab (control), 0.4 or 0.9 MBq/mL ^{177}Lu-lilotomab or 0.5 or 1.5 Gy external beam radiation for different time-points after start of treatment. C, Example of gating used to acquire the FC histograms presented in (D). D, Example of histograms acquired through Flow Cytometry using Daudi cells 2 days after treatment with naked lilotomab or ^{177}Lu-lilotomab stained with fluorescently-labelled rituximab or without staining (blank)
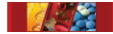
stronger and more prolonged increase in rituximab binding by radio-immunotherapy with ^{177}Lu-lilotomab as compared to EBR. It could be speculated that the prolonged and stronger effect could be related to increased formation of ROS induced by the continuous, low-dose rate beta-irradiation from ^{177}Lu-lilotomab in contrast to the short, high-dose rate gamma-irradiation from the EBR treatment. Consequently, anti-CD37 radioimmunotherapy with ^{177}Lu-lilotomab can be used to both deliver short-range beta-radiation selectively and continuously to tumour cells, minimising irradiation of healthy tissues and increase CD20 binding in those cells that are not killed by the radiation dose delivered and make these cells more susceptible for subsequent rituximab treatment.

There might be other mechanisms behind the synergistic effect. Radioimmunotherapy has been shown to increase the permeability of tumour vasculature [37] which might lead to better tumour uptake of antibodies. Moreover, CD20 binding of rituximab has shown to improve internalisation of an anti-CD37 antibody drug conjugate (ADC) thereby enhancing its efficacy.[38] The efficacy of ^{177}Lu-lilotomab might therefore be also increased if the same enhanced internalisation occurs. In addition, it has been shown that radiation induces immunogenic modulation of tumour cells.[39-41]

There might be several reasons for the lower effect of the combination of ^{177}Lu-lilotomab and rituximab in the model using SCID mice with i.v. injected Rec-1 cells: (a) Rec-1 cells showed around 10 times lower CD20 upregulation than Daudi cells (b) SCID mice were treated with a lower dose of ^{177}Lu-lilotomab than the nude mice which might further decrease the CD20 upregulation since the degree of upregulation has shown to be dose dependent in our in vitro studies and (c) the effect of increased vascularity would be negligible in a disseminated model where tumours would be of microscopic size at treatment injection compared to the bulky s.c. model which may further decrease the synergistic effect of the combination treatment.

It is important to notice that ^{177}Lu-lilotomab does not bind to murine CD37 (data not shown) and rituximab does not bind to murine CD20.[42,43] Therefore, in the mouse models, there is not non-specific binding to normal B cells, which is not the case in human patients. The lack of binding to normal B cells in the mouse models represents a perfect scenario in human patients where all normal B cells have been either blocked by pre-dosing with unlabelled lilotomab, or depleted by previous treatment with rituximab, which would decrease treatment associated toxicity and increase treatment efficacy.

CD20 downregulation after treatment with rituximab has been repeatedly observed in rituximab resistant patients [44-46] although the exact mechanism for development of rituximab resistance is not yet known. It could be potentially mediated by alterations in CD20 expression or signalling, both by genetic or epigenetic changes, elevated apoptotic threshold, modulation of complement activity or diminished cellular cytotoxicity.[47,48] In addition treatment with molecular targeting therapeutics such as ibrutinib,[49] lenalidomide [50] and bortezomib [51] downregulate CD20. Given that ^{177}Lu-lilotomab has been shown to increase rituximab binding to NHL cells, we hypothesise that treatment with ^{177}Lu-lilotomab could be potentially used to revert downregulation of CD20 and resistance to rituximab. Further studies using rituximab resistant cell lines will be performed to explore this hypothesis.

5 | CONCLUSION

We have shown that treatment of NHL in vivo with ^{177}Lu-lilotomab results in an increased tumour suppression of anti-CD20 immunotherapy and improved survival. We have also shown that the interaction can be synergistic. If the same effect is confirmed in clinical studies, it could change the way RIT and CD20 immunotherapy would be used in the future.

ORCID

Ada H. V. Repetto-Llamazares http://orcid.org/0000-0001-5390-0692

REFERENCES

1. Maloney DG, Grillo-Lopez AJ, White CA, et al. IDEC-C2B8 (Rituximab) anti-CD20 monoclonal antibody therapy in patients with relapsed low-grade non-Hodgkin's lymphoma. *Blood.* 1997;90(6):2188-2195.
2. Coiffier B, Haioun C, Ketterer N, et al. Rituximab (anti-CD20 monoclonal antibody) for the treatment of patients with relapsing or refractory aggressive lymphoma: a multicenter phase II study. *Blood.* 1998;92(6):1927-1932.
3. Coiffier B, Thieblemont C, Den Van, et al. Long-term outcome of patients in the LNH-98.5 trial, the first randomized study comparing rituximab-CHOP to standard CHOP chemotherapy in DLBCL patients: a study by the Groupe d'Etudes des Lymphomes de l'Adulte. *Blood.* 2010;116(12):2040-2045.

4. Cheung MC, Haynes AE, Meyer RM, Stevens A, Imrie KR, Members of the Hematology DSGotCCOPiE-BC. Rituximab in lymphoma: a systematic review and consensus practice guideline from Cancer Care Ontario. *Cancer Treat Rev.* 2007;33(2):161-176.

5. NCCN Guidelines Non-Hodgkin's Lymphomas, version 3. 2017.

6. Casulo C, Byrtek M, Dawson KL, et al. Early relapse of follicular lymphoma after rituximab plus cyclophosphamide, doxorubicin, vincristine, and prednisone defines patients at high risk for death: an analysis from the National LymphoCare Study. *J Clin Oncol.* 2015;33(23):2516-2522.

7. Abdollahi S, Chong EA, Olin RL, et al. The impact of rituximab resistance on overall survival rate in low-grade follicular lymphoma. *Blood.* 2008;112(11):3783.

8. Berger MJ Coursey JS, Zucker M A, Chang J. Stopping-power and range tables for electrons, protons, and helium ions (NIST), 2009 [cited 2016 July]; Available from: http://www.nist.gov/pml/data/star/

9. Dahle J, Repetto-Llamazares AH, Mollatt CS, et al. Evaluating antigen targeting and anti-tumor activity of a new anti-CD37 radioimmunoconjugate against non-Hodgkin's lymphoma. *Anticancer Res.* 2013;33(1):85-95.

10. Barrena S, Almeida J, Yunta M, et al. Aberrant expression of tetraspanin molecules in B-cell chronic lymphoproliferative disorders and its correlation with normal B-cell maturation. *Leukemia.* 2005;19(8):1376-1383.

11. Wang W, Li Y, Gao L, et al. Significance of CD37 expression in malignant B cells. *Zhongguo Shi Yan Xue Ye Xue Za Zhi.* 2014;22(3):644-647.

12. Zhao X, Ybarra S, Durkin L, et al. CD37 Is a Potential Therapeutic Target for B-Cell Non-Hodgkin Lymphoma. *Blood.* 2010;116(21):3098.

13. Repetto-Llamazares AH, Larsen RH, Patzke S, et al. Targeted cancer therapy with a novel anti-CD37 beta-particle emitting radioimmunoconjugate for treatment of non-hodgkin lymphoma. *PLoS ONE.* 2015;10(6):e0128816.

14. Kolstad A, Matsbu U, Dahle J, et al. A phase I Study of ^{177}Lu-DOTA-HH1 (BetalutinTM) Radioimmunotherapy in Patients with Relapsed CD37 + Non-Hodgkin B-Cell Lymphoma. 56th ASH Annual Meeting, San Francisco, CA, Dec 6-9 2014; 2014.

15. Wattenberg MM, Kwilas AR, Gameiro SR, Dicker AP, Hodge JW. Expanding the use of monoclonal antibody therapy of cancer by using ionising radiation to upregulate antibody targets. *Br J Cancer.* 2014;110(6):1472-1480.

16. Gupta D, Crosby ME, Almasan A, Macklis RM. Regulation of CD20 expression by radiation-induced changes in intracellular redox status. *Free Radic Biol Med.* 2008;44(4):614-623.

17. Kunala S, Macklis RM. Ionizing radiation induces CD20 surface expression on human B cells. *Int J Cancer.* 2001;96(3):178-181.

18. Shimizu R, Kikuchi J, Wada T, Ozawa K, Kano Y, Furukawa Y. HDAC inhibitors augment cytotoxic activity of rituximab by upregulating CD20 expression on lymphoma cells. *Leukemia.* 2010;24(10):1760-1768.

19. Tsai PC, Hernandez-Ilizaliturri FJ, Bangia N, Olejniczak SH, Czuczman MS. Regulation of CD20 in rituximab-resistant cell lines and B-cell non-Hodgkin lymphoma. *Clin Cancer Res.* 2012;18(4):1039-1050.

20. Abuodeh Y, Ahmed K, Echevarria M, et al. Priming radioimmunotherapy with external beam radiation in patients with relapsed low grade non-Hodgkin lymphoma. *Ther Adv Hematol.* 2017;8(4):129-138.

21. Lindmo T, Boven E, Cuttitta F, Fedorko J, Bunn PA Jr. Determination of the immunoreactive fraction of radiolabeled monoclonal antibodies by linear extrapolation to binding at infinite antigen excess. *J Immunol Methods.* 1984;72(1):77-89.

22. Lindmo T, Bunn PA Jr. Determination of the true immunoreactive fraction of monoclonal antibodies after radiolabeling. *Methods Enzymol.* 1986;121:678-691.

23. Fulop GM, Phillips RA. The scid mutation in mice causes a general defect in DNA repair. *Nature.* 1990;347(6292):479-482.

24. Repetto-Llamazares AH, Larsen RH, Giusti AM, et al. 177Lu-DOTA-HH1, a Novel Anti-CD37 Radio-Immunoconjugate: a Study of Toxicity in Nude Mice. *PLoS ONE.* 2014;9(7):e103070.

25. Dalle S, Dupire S, Brunet-Manquat S, Reslan L, Plesa A, Dumontet C. In vivo model of follicular lymphoma resistant to rituximab. *Clin Cancer Res.* 2009;15(3):851-857.

26. Schliemann C, Palumbo A, Zuberbuhler K, et al. Complete eradication of human B-cell lymphoma xenografts using rituximab in combination with the immunocytokine L19-IL2. *Blood.* 2009;113(10):2275-2283.

27. DiJoseph JF, Dougher MM, Kalyandrug LB, et al. Antitumor efficacy of a combination of CMC-544 (inotuzumab ozogamicin), a CD22-targeted cytotoxic immunoconjugate of calicheamicin, and rituximab against non-Hodgkin's B-cell lymphoma. *Clin Cancer Res.* 2006;12(1):242-249.

28. Gopal AK, Pagel JM, Hedin N, Press OW. Fenretinide enhances rituximab-induced cytotoxicity against B-cell lymphoma xenografts through a caspase-dependent mechanism. *Blood.* 2004;103(9):3516-3520.

29. Pagel JM, Laugen C, Bonham L, et al. Induction of apoptosis using inhibitors of lysophosphatidic acid acyltransferase-beta and anti-CD20 monoclonal antibodies for treatment of human non-Hodgkin's lymphomas. *Clin Cancer Res.* 2005;11(13):4857-4866.

30. Kita A, Mitsuoka K, Kaneko N, et al. Sepantronium bromide (YM155) enhances response of human B-cell non-Hodgkin lymphoma to rituximab. *J Pharmacol Exp Ther.* 2012;343(1):178-183.

31. Frys S, Simons Z, Hu Q, et al. Entinostat, a novel histone deacetylase inhibitor is active in B-cell lymphoma and enhances the anti-tumour activity of rituximab and chemotherapy agents. *Br J Haematol.* 2015;169(4):506-519.

32. Chu TW, Zhang R, Yang J, Chao MP, Shami PJ, Kopecek J. A two-step pretargeted nanotherapy for CD20 crosslinking may achieve superior anti-lymphoma efficacy to rituximab. *Theranostics.* 2015;5(8):834-846.

33. Dale Rein I, Solberg Landsverk K, Micci F, Patzke S, Stokke T. Replication-induced DNA damage after PARP inhibition causes G2 delay, and cell line-dependent apoptosis, necrosis and multinucleation. *Cell Cycle.* 2015;14(20):3248-3260.

34. Marcatili S, Pichard A, Courteau A, et al. Realistic multi-cellular dosimetry for 177Lu-labelled antibodies: model and application. *Phys Med Biol.* 2016;61(19):6935-6952.

35. Stevens PL, Oluwole O, Reddy N. Advances and application of radioimmunotherapy in non-Hodgkin lymphoma. *Am J Blood Res.* 2012;2(2):86-97.

36. Repetto-Llamazares AH, Larsen RH, Mollatt C, Lassmann M, Dahle J. Biodistribution and dosimetry of (177)Lu-tetulomab, a new radioimmunoconjugate for treatment of non-Hodgkin lymphoma. *Curr Radiopharm.* 2013;6(1):20-27.

37. Heyerdahl H, Roe K, Brevik EM, Dahle J. Modifications in dynamic contrast-enhanced magnetic resonance imaging parameters after alpha-particle-emitting (2)(2)(7)Th-trastuzumab therapy of HER2-expressing ovarian cancer xenografts. *Int J Radiat Oncol Biol Phys.* 2013;87(1):153-159.

38. Hicks SW, Lai KC, Gavrilescu LC, et al. The antitumor activity of IMGN529, a CD37-targeting antibody-drug conjugate, is potentiated by rituximab in non-Hodgkin lymphoma models. *Neoplasia.* 2017;19(9):661-671.

39. Chakraborty M, Abrams SI, Camphausen K, et al. Irradiation of tumor cells up-regulates Fas and enhances CTL lytic activity and CTL adoptive immunotherapy. *J Immunol.* 2003;170(12):6338-6347.

40. Chakraborty M, Abrams SI, Coleman CN, Camphausen K, Schlom J, Hodge JW. External beam radiation of tumors alters phenotype of
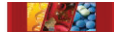
tumor cells to render them susceptible to vaccine-mediated T-cell killing. *Cancer Res*. 2004;64(12):4328-4337.

41. Reits EA, Hodge JW, Herberts CA, et al. Radiation modulates the peptide repertoire, enhances MHC class I expression, and induces successful antitumor immunotherapy. *J Exp Med* 2006;203(5):1259-1271.

42. Klein C, Lammens A, Schafer W, et al. Epitope interactions of monoclonal antibodies targeting CD20 and their relationship to functional properties. *MAbs*. 2013;5(1):22-33.

43. Huang H, Benoist C, Mathis D. Rituximab specifically depletes short-lived autoreactive plasma cells in a mouse model of inflammatory arthritis. *Proc Natl Acad Sci USA*. 2010;107(10):4658-4663.

44. Musto P, D'Auria F. The clinical and biological role of CD20 membrane antigen modulation under immunotherapy with anti-CD20 monoclonal antibody rituximab in lymphoproliperative neoplastic disorders. *Expert Opin Biol Ther*. 2011;11(5):551-557.

45. Bellesso M, Xavier FD, Costa RO, Pereira J, Siqueira SA, Chamone DA. Disease progression after R-CHOP treatment associated with the loss of CD20 antigen expression. *Rev Bras Hematol Hemoter*. 2011;33(2):148-150.

46. Kennedy GA, Tey SK, Cobcroft R, et al. Incidence and nature of CD20-negative relapses following rituximab therapy in aggressive B-cell non-Hodgkin's lymphoma: a retrospective review. *Br J Haematol*. 2002;119(2):412-416.

47. Smith MR. Rituximab (monoclonal anti-CD20 antibody): mechanisms of action and resistance. *Oncogene*. 2003;22(47):7359-7368.

48. Tomita A. Genetic and epigenetic modulation of CD20 expression in B-cell malignancies: molecular mechanisms and significance to rituximab resistance. *J Clin Exp Hematop*. 2016;56(2):89-99.

49. Skarzynski M, Niemann CU, Lee YS, et al. Interactions between Ibrutinib and Anti-CD20 antibodies: competing effects on the outcome of combination therapy. *Clin Cancer Res*. 2016;22(1):86-95.

50. Lapalombella R, Yu B, Triantafillou G, et al. Lenalidomide down-regulates the CD20 antigen and antagonizes direct and antibody-dependent cellular cytotoxicity of rituximab on primary chronic lymphocytic leukemia cells. *Blood*. 2008;112(13):5180-5189.

51. Bil J, Winiarska M, Nowis D, et al. Bortezomib modulates surface CD20 in B-cell malignancies and affects rituximab-mediated complement-dependent cytotoxicity. *Blood*. 2010;115(18):3745-3755.

II

[177]Lu-lilotomab satetraxetan has the potential to counteract resistance to rituximab in non-Hodgkin's lymphoma

Marion M. Malenge[1,2,3], Sebastian Patzke[1,2], Anne H. Ree[3,4], Trond Stokke[2,] Peter Ceuppens[5], Brian Middleton[5], Jostein Dahle[1] and Ada H. V. Repetto-Llamazares[1].

[1]Nordic Nanovector ASA, Oslo, Norway.

[2]Department of Radiation Biology, Institute for Cancer Research, Oslo University Hospital, Norway

[3]Institute of Clinical Medicine, University of Oslo, Norway

[4]Department of Oncology, Akershus University Hospital, Norway

[5]Inferstats Consulting Ltd, Cheshire, UK

Correspondence:

Jostein Dahle

Kjelsåsveien 168B, 0884 Oslo, Norway

Telephone: +4722183301

jdahle@nordicnanovector.com

First author:

Marion M. Malenge, PhD student

mmalenge@nordicnanovector.com

Running title: ^{177}Lu-lilotomab RIT for NHL

ABSTRACT

Background: Patients with NHL who are treated with rituximab may develop resistant-disease, often associated with changes in expression of CD20. The next generation β-particle emitting radioimmunoconjugate ^{177}Lu-lilotomab-satetraxetan (Betalutin®) was shown to up-regulate CD20 expression in different rituximab-sensitive NHL cell lines and to act synergistically with rituximab in a rituximab-sensitive NHL animal model. We hypothesized that ^{177}Lu-lilotomab-satetraxetan may be used to reverse rituximab-resistance in NHL.

Methods: The rituximab-resistant Raji 2R and the parental Raji cell lines were used. CD20 expression was measured by flow cytometry. ADCC was measured by a bioluminescence reporter assay. The efficacies of combined treatments with ^{177}Lu-lilotomab-satetraxetan (150 MBq/kg or 350 MBq/kg) and rituximab (4×10mg/kg) were compared with those of single agents or saline in a Raji 2R-xenograft model. Cox-regression and the Bliss independence model were used to assess synergism.

Results: Rituximab-binding in Raji 2R cells was $36\pm5\%$ of that in the rituximab-sensitive Raji cells. ^{177}Lu-lilotomab-satetraxetan treatment of Raji 2R cells increased the binding to $53\pm3\%$ of the parental cell line. Rituximab ADCC-induction in Raji 2R cells was $20\pm2\%$ of that induced in Raji cells, while treatment with ^{177}Lu-lilotomab-satetraxetan increased the ADCC-induction to $30\pm3\%$ of Raji cells, representing a 50% increase ($p<0.05$). The combination of rituximab with 350 MBq/kg ^{177}Lu-lilotomab-satetraxetan synergistically suppressed Raji 2R tumor growth in athymic Foxn1^{nu} mice.

Conclusion: ^{177}Lu-lilotomab-satetraxetan has the potential to reverse rituximab-resistance; it can increase rituximab-binding and ADCC-activity *in-vitro* and can synergistically improve anti-tumor efficacy *in-vivo*.

Keywords: Lutetium-177, Radioimmunotherapy, NHL, rituximab-resistance

INTRODUCTION

Non-Hodgkin's lymphoma (NHL) is the most common hematological malignancy and had the eleventh highest mortality-rate of all malignancies worldwide in 2018 (*1,2*). B-lymphocytes are predominantly the origin of NHL, with malignant B-cells expressing a high density of specific antigens such as CD20 and CD37 on their surface (*3*). These antigens provide a platform for antibody-based targeted therapies (*4*). Immunotherapy with the CD20-directed antibody rituximab inhibits cell proliferation by inducing antibody-dependent cellular cytotoxicity (ADCC) and complement-dependent cytotoxicity (*5*). Although rituximab alone and in combination with chemotherapy are a mainstay of NHL treatment (*6-8*), the efficacy is variable (*9*). Some patients are reported to have disease progression after initial response to rituximab (*10*). Conversely, rituximab-naïve patients have been reported with primarily rituximab-refractory disease (*11*).

The mechanisms of rituximab-resistance are not completely understood (*9,12*). Rituximab-resistance is postulated to be a result of down-regulation of the CD20 gene, internalization, lysosomal degradation and shaving off of rituximab/CD20 complexes (*13-18*). Strategies to counteract rituximab-resistance include combination therapies and targeting of alternative antigens. Previous studies have described the ability of ionizing radiation to potentiate immunotherapy through the generation of reactive-oxygen species that mediates an increase in antigen expression (*19-21*), consequently improving on antibody-dependent toxicity in addition to the direct cytotoxic radiation effect (*21,22*). Anti-CD20 antibody binding increased up to two-fold, 20-120 hours after irradiation (*19,20,23*). Radioimmunotherapy delivers targeted short-range radiation that effectively ablates malignant cells and with limited toxicity to normal tissues (*24,25*).

The anti-CD37 radioimmunoconjugate ^{177}Lu-lilotomab-satetraxetan (^{177}Lu-lilotomab), consisting of the β-emitting isotope lutetium-177 ($T_{1/2} = 6.7$ days) chelated to a chemical linker p-SCN-benzyl-DOTA (satetraxetan) conjugated to the murine antibody lilotomab, has shown robust anti-tumor activity and low toxicity in preclinical models (*26,27*). ^{177}Lu-lilotomab is currently in clinical trials for relapsed/ refractory lymphomas (NCT01796171, NCT02658968) (*25,28*).

We have recently shown that pre-treatment of rituximab-sensitive NHL cells with ^{177}Lu-lilotomab increases CD20 binding *in-vitro* and synergistically increases the anti-tumor effect when combined with rituximab *in-vivo* (*23*). Currently, ^{177}Lu-lilotomab is tested in

combination with rituximab in patients with previously treated follicular lymphoma (NCT03806179).

Here, we hypothesized that ^{177}Lu-lilotomab can reverse rituximab-resistance in NHL. We employed a rituximab-resistant NHL cell line and animal model and explored the mechanism of synergy by measuring rituximab-binding and ADCC-induction and apoptosis.

MATERIALS AND METHODS

Cell Lines

Burkitt lymphoma cell lines Raji and Raji 2R, from Roswell Park Institute *(16)*, were cultured in RPMI medium (Thermofisher, USA) supplemented with Glutamax, 10% heat inactivated fetal bovine serum and 1% penicillin-streptomycin at 37˚C with 5% CO_2.

Radiolabeling of Antibodies with ^{177}Lu

Lilotomab-satetraxetan was pH-adjusted using ammonium acetate then radiolabeled with ^{177}Lu (ITG, Germany) at 37˚C for 15–30 minutes. The specific activity for all *in-vitro* studies was 600 MBq/mg, while 200 MBq/mg was chosen for *in-vivo* studies. The radiochemical purity and immunoreactive fraction of the conjugate were determined using instant thin layer chromatography and by a modified Lindmo method*(29)* respectively.

Measurement of CD20 Binding

Cells at a concentration of 2.5×10^6cells/ml were incubated for 18 hours with 0-20µg/ml of either lilotomab, ^{177}Lu-lilotomab or saline (PBS, control) at 37°C. The cells were then washed, resuspended in fresh medium to a concentration of 0.5×10^6cells/ml and cultured up to 6 days, with fresh medium added on day 3. On days 3 and 6, the cells were prepared for flow cytometric assays using rituximab (Roche, Switzerland) conjugated to Alexa-Fluor647 tetra fluorophenyl ester (Thermofisher) according to the manufacturer's instructions. The cell concentration was adjusted to 1×10^6cells/ml and Raji cells stained with 0.4µg/ml Hoechst 33342 (Life technologies, USA) for identity barcoding, at 37°C for 20 minutes then washed using ice-cold PBS. To assess the effect of ^{177}Lu-lilotomab treatment on CD20 binding, the cells were incubated at 4°C with 30µg/ml rituximab-Alexa647 for 30 minutes. To estimate the background signal, cells were incubated with 100-fold excess of non-fluorescent rituximab before addition of rituximab-Alexa647.

Cells were washed and fluorescence was read by flow cytometry (Guava® easyCyte12HT, Millipore). Changes in rituximab-binding on ^{177}Lu-lilotomab treated cells relative to control cells for each cell line were assessed using equation 1.

$$Increase\ in\ rituximab\ binding = \frac{Rituximab\ binding\ (treated - control)cells}{Rituximab\ binding\ (control)cells} \times 100$$

(1)

Rituximab-binding in rituximab-resistant Raji 2R cells (control and treated cells) was compared to rituximab-binding in untreated (control) rituximab-sensitive Raji cells using equation 2.

$$Relative\ rituximab\ binding = \frac{Rituximab\ binding\ of\ Raji2R}{Rituximab\ binding\ of\ Raji\ (control)} \times 100$$

(2)

Measurement of ADCC

The cells at a concentration of 2.5×10^6cells/ml were incubated with 1µg/ml of either lilotomab, ^{177}Lu-lilotomab or controls at 37°C for 18 hours. All cells were washed and adjusted to 0.5×10^6cells/ml in fresh medium before further incubated . After 6 days, rituximab-induced ADCC-activity was measured using ADCC reporter bioassay kits (Promega, USA) containing Jurkat cells engineered to stably express FcγRIIIa receptor ([30]) as effector cells. These cells have a firefly luciferase gene driven by a nuclear factor of activated T-cells response element reporting the activation of the gene by producing luciferase quantified as luminescence signal. The cells were co-incubated with 0.68-40µg/ml rituximab and effector cells for 22 hours at a 2:1 effector:target cells ratio. ADCC-activity was measured as the luminescence of cell-bound effector cells. Change in ADCC-induction by rituximab in ^{177}Lu-lilotomab treated cells relative to control cells was obtained using equation 3.

$$Increase\ in\ ADCC\ induction = \frac{ADCC\ induction\ in\ cells\ (treated - control)}{ADCC\ induction\ in\ cells\ (control)} \times 100$$

(3)

Relative ADCC-induction by rituximab in Raji 2R control and ^{177}Lu-lilotomab treated cells to Raji control cells was obtained using equation 4.

$$Relative\ ADCC\ induction = \frac{ADCC\ induction\ in\ Raji2R}{ADCC\ induction\ in\ Raji\ (control)} \times 100$$

(4)

In-vivo **Xenograft Model**

All procedures in this study were approved by The Norwegian Animal Research Authority (NARA) and performed in accordance to NARA regulations and Federation of European Laboratory Animal Science Associations (FELASA) recommendations. Female athymic nude Foxn1[nu] mice bred at the Institute for Comparative Medicine, Oslo University Hospital, Norway were used.

The mice, aged 4-5 weeks old with an average weight of 21±2g, were injected subcutaneously in both flanks with 10×10^6 Raji 2Rcells/flank using a 1:1 Matrigel dilution ratio. Mice were injected intraperitoneally with 50µl of anti-asialo GM1 (Wako Chemicals, USA) after dilution per manufacturers recommendation, 24 hours prior to cell inoculation and once every week thereafter for the rest of the study. This was administered to increase tumor-take and prevent spontaneous tumor regressions by decreasing the natural killer (NK) cell population in the mice. On attaining tumor diameter between 4mm and 11mm, the mice were placed into treatment groups of 10 mice each, ensuring similar average tumor volumes per group.

Therapy Study

Raji 2R-xenografted mice were administered with *i)* NaCl, *ii)* rituximab monotherapy administered as 4 subsequent doses every 3-4 days (4×10mg/kg), *iii)* 150 MBq/kg of ^{177}Lu-lilotomab as monotherapy, *iv)* 350 MBq/kg of ^{177}Lu-lilotomab as monotherapy, *v)* combination therapy of 150 MBq/kg ^{177}Lu-lilotomab and rituximab (4×10mg/kg) and *vi)* combination therapy of 350 MBq/kg ^{177}Lu-lilotomab and rituximab (4×10mg/kg). The dosing concentrations of ^{177}Lu-lilotomab were below the maximum tolerated dose (around 550 MBq/kg) in nude mice (*27*). The 2 chosen dosing concentrations were considered to be therapeutically suboptimal without the combination with rituximab, which would make it feasible to observe any synergistic effect of the combination.

Caliper measurements of the tumors in 3-dimensions were recorded 2-3 times a week. Tumor volume was calculated as $\frac{\pi}{6}(Length \times Width \times Height)$. Animal health status was monitored for the length of the study and animals were euthanized by cervical dislocation when tumor diameter was >20mm or animals were observed to experience severe poor health, tumor-necrosis or ulceration, weight gain or loss >10% from maximum or minimum recorded weight or any other signs of discomfort. During euthanasia, the animal was dissected to observe for any anatomical anomalies.

Statistical Analysis

In-vitro data was analyzed in SigmaPlot 13.0 (Systat, USA) and Prism 8 (GraphPad, USA) using two-tailed t-tests on either complete data sets or paired averaged data, to compare the different groups, cell lines and timepoints. Data is presented as mean ±standard error (SE) and $p < 0.05$ was considered statistically significant.

Mouse survival was defined as time to the event of death due to tumor diameter >20mm (representative of disease progression). The analysis was performed in SigmaPlot using the Log-rank test reporting statistical significance by Holm-Sidak test for multiple comparisons.

Tumor volume was computed in two different ways: as average ±SE for each group, maintaining tumor volume constant after euthanasia along the 70 days of the study and by extrapolation of tumor volume after euthanasia which is considered a better representation of the data but can only be performed up to 20 days due to tumor volumes becoming infeasibly large. SAS 9.4 (SAS, USA) was used for these calculations.

Bliss independence model was used to evaluate synergy in the in-vivo study using the extrapolated tumor volumes. Difference from baseline was calculated on the log-scale and all statistical analysis were performed on the log-transformed data.

Bliss analysis of mice survival was performed by fitting a Cox Proportional-Hazard model to the survival data. The Bliss definition of synergy was assessed by the interaction of the combination treated groups with the rituximab and respective ^{177}Lu-lilotomab monotherapy groups. Interaction values lower than 1 were considered synergistic and statistical significance defined both by $p < 0.05$ and an interaction value ±90% confidence interval <1. R (2019) with survival package was used for these calculations.

RESULTS

Increased Rituximab-Binding by ^{177}Lu-lilotomab

Exposure of Raji and Raji 2R cells to ^{177}Lu-lilotomab resulted in a dose-dependent increase in rituximab-binding as compared with control cells (Fig. 1). Increase in rituximab-binding (equation 1) was fitted using a regression line based on the two-parameter exponential rise to maximum equation (R^2 values between 0.71 and 0.90). Rituximab-binding in ^{177}Lu-lilotomab treated Raji cells continuously increased when compared to the control, reaching

78% 3 days after treatment (Fig. 1A). Six days after treatment, rituximab-binding showed an initial exponential increase from the control, followed by a plateau at 31% for ^{177}Lu-lilotomab concentrations above 0.5µg/ml. The same was observed in Raji 2R cells with a plateau at 25% for 3 days and at 68% for 6 days after ^{177}Lu-lilotomab treatment (Fig.1B). The increase in rituximab-binding at 3 days was significantly different from that at 6 days in both cell lines (p<0.01). Binding in Raji cells was highest at 3 days after treatment while in Raji 2R cells it was highest at 6 days.

In order to compare the relative rituximab-binding of Raji 2R versus Raji cells (equation 2), the maximum asymptote of the fitted curves in Fig. 1B were used. Rituximab-binding in Raji 2R cells was on average 36±5% of the binding in Raji cells when no ^{177}Lu-lilotomab was given (equation 2, Fig. 1C).

After treatment with ^{177}Lu-lilotomab the relative binding to Raji 2R cells compared to untreated Raji cells increased to 47 ±1% (p<0.01) at 3 days and 53 ±3% (p<0.01) at 6 days. In contrast, treatment with unlabelled lilotomab or PBS had no effect on rituximab-binding (data not shown).

Enhanced ADCC by Rituximab after ^{177}Lu-lilotomab Treatment

ADCC-induction was assessed by measurement of effector-cell binding of cell-bound rituximab in cells previously treated with ^{177}Lu-lilotomab or PBS (control). There was no significant change in effector-cell binding of rituximab in Raji cells after treatment with ^{177}Lu-lilotomab (Fig. 2A, p>0.05). Conversely, treatment of Raji 2R cells with ^{177}Lu-lilotomab significantly augmented effector-cell binding (p<0.05, Fig. 2B). The maximum asymptote of the fitted curves from Figs. 2A and B were used to calculate the increase in ADCC-induction and the relative increase in ADCC-induction in Raji 2R vs Raji cells (equations 3 and 4 respectively). Effector-cell binding increased by 47±4% in ^{177}Lu-lilotomab treated Raji 2R cells compared with untreated Raji 2R cells (equation 3). Effector-cell binding in ^{177}Lu-lilotomab treated Raji 2R cells was 43% higher than in untreated Raji 2R cells relative to untreated Raji cells (30 ±3% versus 21 ±2%, equation 4, p<0.05, Fig. 2C). Unlabelled lilotomab did not modulate effector-cell binding (data not shown).

Synergistic Anti-tumor Efficacy of the Combination of ^{177}Lu-lilotomab and Rituximab

Treatment of Raji 2R-xenografted mice with rituximab alone did not suppress tumor growth compared to that in mice treated with saline (Fig. 3). However, treatment with ^{177}Lu-lilotomab alone or in combination with rituximab showed inhibition of tumor growth when

compared to the saline and rituximab-treated tumors. This inhibition was reflected in the lower fold change in tumor volume from baseline at various time points after start of treatment with the combination of 150 MBq/kg or 350 MBq/kg ^{177}Lu-lilotomab and rituximab compared with monotherapy of the respective treatments (p<0.05, Table 1). The Bliss independence model indicated significant synergism in combining 350 MBq/kg ^{177}Lu-lilotomab with rituximab (p<0.05 for tumor volumes measured 17 and 20 days after treatment), while the combination of 150 MBq/kg ^{177}Lu-lilotomab and rituximab did not reach statistical significance for any time point (Fig. 3A). When analyzing the tumor volume data in the duration of the study (by maintaining last tumor volume after euthanasia) a significant difference was found between the 350 MBq/kg ^{177}Lu-lilotomab monotherapy and the respective combination with rituximab (Fig. 3B, p<0.05), indicating that ^{177}Lu-lilotomab potentiated the rituximab-effect.

Treatment with ^{177}Lu-lilotomab alone and in combination with rituximab significantly prolonged time-to-event compared to saline and rituximab-treatment (Fig. 4, Table 2). The median survival time of mice treated with the combination of 350 MBq/kg ^{177}Lu-lilotomab and rituximab was doubled when compared to survival of mice given 350 MBq/kg ^{177}Lu-lilotomab monotherapy and it was 5 times longer than for mice given rituximab monotherapy.

Bliss independence analysis did not provide statistically significant results (Table 3). The lack of significance might be due to the large number of censored animals and the poor Proportional-Hazards assumption in the Cox model (p=0.048).

A total of 14 mice out of 60 included in the study were euthanized due to tumor-ulceration (Fig. 5). Most of the ulcers appeared in mice given ^{177}Lu-lilotomab monotherapy or the combination with rituximab. These mice were regarded as censored in the survival analysis since the tumors did not reach the primary end point (tumor diameter >20mm).

An alternative time-to-event analysis using tumor diameter >20mm or tumor-ulceration as end point was performed (Supplemental Fig. 3). Median survival times were slightly different (Supplemental Table 1) but the outcome of Bliss independence analysis did not provide statistically significant results (Supplemental Table 2).

DISCUSSION

Although immunotherapy with rituximab has been widely successful, rituximab-resistance in subsets of NHL patients remains a challenge in clinical management of the disease. In the present study, we demonstrated that *in-vitro* treatment of rituximab-resistant

Raji 2R cells with ^{177}Lu-lilotomab increased both rituximab-binding and ADCC-activity. In addition, we showed that *in-vivo* combination of ^{177}Lu-lilotomab with rituximab can synergistically suppress tumor growth in Raji 2R-xenografted mice.

Evidence supports that ADCC-activity may be the predominant *in-vivo* mechanism of action of rituximab (*31,32*).We have therefore explored if ^{177}Lu-lilotomab can restore ADCC by rituximab in the rituximab-resistant Raji 2R cell line. Our findings show that partial restoration can be reached. The increased ADCC may be caused by the significant time-dependent increase in rituximab-binding, an observation in line with results presented by Hiraga et al. (*13*), who hypothesized the delay to be due to altered transcriptional regulation resulting from persistent rituximab-treatment during acquisition of resistance. In agreement with observations by van Meerten et al. (*33*) the direct cytotoxic or apoptotic effect of rituximab in the rituximab-sensitive Raji cells was negligible (Supplemental Fig. 1 and 2) and therefore it was not possible to study the sensitization of rituximab-resistant cells to rituximab by ^{177}Lu-lilotomab using this model. Further studies using other rituximab-resistant cell lines are warranted.

Translation of the *in-vitro* results to a clinical setting is limited. The dose delivered from ^{177}Lu-lilotomab to cells in the *in-vitro* studies is a function of both specific and non-specific irradiation of the cells during the 18hours incubation time (*34*). Given that CD20 upregulation is mediated by intracellular redox regulation and is dose-dependent (*19,23*), we expect that treatment with a non-specific radioimmunoconjugate will produce a similar increase in CD20 binding and subsequent ADCC increase in this experimental set-up. However, in an *in-vivo* or clinical setting, ^{177}Lu-lilotomab would have an important advantage over a non-specific radioimmunoconjugate due to its capability to deliver targeted radiation to tumor while sparing the healthy tissues.

Although the time-to-event for mice treated with the combination of ^{177}Lu-lilotomab and rituximab was not significantly synergistic, there was significant synergy in tumor growth delay. We have shown that *in-vivo* combination therapy with ^{177}Lu-lilotomab and rituximab has the potential to synergistically suppress tumor growth in Raji 2R-xenografted mice. The increased rituximab-binding and enhanced ADCC shown in our *in-vitro* studies are among the mechanisms of action that that could lead to the observed synergy.

Other mechanisms that might contribute to the observed synergy are improved complement-dependent cytotoxicity by colocalization of CD37 and CD20 on the cell membrane (*35*), radiation-induced permeability of tumor vasculature (*36*), radiation-induced immunogenic

modulation of tumor cells (*37-39*), rituximab-induced sensitization of tumor cells to ionizing radiation (*40*) and rituximab-induced increased internalization of CD37 (*41*) leading to increased cellular retention of ^{177}Lu and thus to a higher cellular absorbed radiation dose (*25*).

In order to have good tumor-take and growth, our animal model required use of anti-asialo antibody to decrease the amount of NK cells, which are the classical mediators of ADCC. This intentional decrease in NK cell numbers might have led to a reduced ADCC effect. The observed ADCC effect in our animal studies was probably exerted by the remaining NK cells and other effector cells such as neutrophils and monocytes. The observed tumor-ulceration seemed to be related to treatment efficacy. Only one ulcer was observed in the control mice and no ulcers were observed in the rituximab-treated mice while the number of ulcers increased with increasing dose of ^{177}Lu-lilotomab. Ulceration could therefore be due to the accelerated tumor necrosis caused by the therapy. The probable cause of the observed ulceration is the proximity of the s.c tumor xenografts to the mouse skin.

We have shown in previous studies that ^{177}Lu-lilotomab can synergize with rituximab in rituximab-sensitive cell lines. In the current study we have taken the analysis one step further and shown that synergy can also be observed in rituximab-resistant cell lines and that rituximab-resistance might be partially reversed by combining rituximab with ^{177}Lu-lilotomab. Further studies using different rituximab-resistant cell lines and animal models with an intact immune system might be of interest in order to generalize our findings and gain deeper insight into the mechanisms of action behind the observed synergy.

The current results further support the rationale underlying the current clinical phase 1b trial (Archer-1; NCT03806179) of combination treatment of patients with relapsed/refractory follicular lymphoma and suggest that in the future ^{177}Lu-lilotomab radioimmunotherapy could potentially be used for re-sensitization of relapsed/ refractory NHL patients to CD20 targeting therapy.

CONCLUSION

In this present work, we have demonstrated that radioimmunotherapy with ^{177}Lu-lilotomab has the potential to reverse rituximab-resistance through increased rituximab-binding and ADCC-activity in rituximab-resistant NHL models.

DISCLOSURE

KEYPOINTS

QUESTION: Can ^{177}Lu-lilotomab reverse rituximab-resistance and improve efficacy of rituximab-therapy?

PERTINENT FINDINGS: ^{177}Lu-lilotomab significantly increases rituximab-binding and rituximab-mediated ADCC-activity and when in combination with rituximab, has the potential to synergistically suppressed tumor growth in an NHL mouse model.

IMPLICATIONS FOR PATIENT CARE: ^{177}Lu-lilotomab could potentially be used for re-sensitization of relapsed/ refractory NHL patients to CD20 targeting therapy.

REFERENCES

1.   Siegel RL, Miller KD, Jemal A. Cancer Statistics, 2017. *CA Cancer J Clin.* 2017;67:7-30.

2.   Bray F, Ferlay J, Soerjomataram I, Siegel RL, Torre LA, Jemal A. Global cancer statistics 2018: GLOBOCAN estimates of incidence and mortality worldwide for 36 cancers in 185 countries. *CA Cancer J Clin.* 2018;68:394-424.

3.   Malcolm TI, Hodson DJ, Macintyre EA, Turner SD. Challenging perspectives on the cellular origins of lymphoma. *Open Biol.* 2016;6:1-12.

4.   Del Bufalo F, Merli P, Alessi I, Locatelli F. B-cell depleting immunotherapies: therapeutic opportunities and toxicities. *Expert Rev Clin Immunol.* 2019;15:497-509.

5.   Reff ME, Carner K, Chambers KS, et al. Depletion of B cells in vivo by a chimeric mouse human monoclonal antibody to CD20. *Blood.* 1994;83:435-445.

6.   Mounier N, Briere J, Gisselbrecht C, et al. Rituximab plus CHOP (R-CHOP) overcomes bcl-2--associated resistance to chemotherapy in elderly patients with diffuse large B-cell lymphoma (DLBCL). *Blood.* 2003;101:4279-4284.

7.   Petryk M, Grossbard ML. Rituximab therapy of B-cell neoplasms. *Clin Lymphoma.* 2000;1:186-194.

8.   Davis TA, Grillo-Lopez AJ, White CA, et al. Rituximab anti-CD20 monoclonal antibody therapy in non-Hodgkin's lymphoma: safety and efficacy of re-treatment. *J Clin Oncol.* 2000;18:3135-3143.

9.   Rezvani AR, Maloney DG. Rituximab resistance. *Best Pract Res Clin Haematol.* 2011;24:203-216.

10.   Davis TA, Czerwinski DK, Levy R. Therapy of B-cell lymphoma with anti-CD20 antibodies can result in the loss of CD20 antigen expression. *Clin Cancer Res.* 1999;5:611-615.

11.   Colombat P, Salles G, Brousse N, et al. Rituximab (anti-CD20 monoclonal antibody) as single first-line therapy for patients with follicular lymphoma with a low tumor burden: clinical and molecular evaluation. *Blood.* 2001;97:101-106.

12.   Duman BB, Sahin B, Ergin M, Guvenc B. Loss of CD20 antigen expression after rituximab therapy of CD20 positive B cell lymphoma (diffuse large B cell extranodal marginal zone lymphoma combination): a case report and review of the literature. *Med Oncol.* 2012;29:1223-1226.

13.   Hiraga J, Tomita A, Sugimoto T, et al. Down-regulation of CD20 expression in B-cell lymphoma cells after treatment with rituximab-containing combination chemotherapies: its prevalence and clinical significance. *Blood.* 2009;113:4885-4893.

14.   Miyoshi H, Arakawa F, Sato K, et al. Comparison of CD20 expression in B-cell lymphoma between newly diagnosed, untreated cases and those after rituximab treatment. *Cancer Sci.* 2012;103:1567-1573.

15.   Tokunaga T, Tomita A, Sugimoto K, et al. De novo diffuse large B-cell lymphoma with a CD20 immunohistochemistry-positive and flow cytometry-negative phenotype: molecular mechanisms and correlation with rituximab sensitivity. *Cancer Sci.* 2014;105:35-43.

16.   Czuczman MS, Olejniczak S, Gowda A, et al. Acquirement of rituximab resistance in lymphoma cell lines is associated with both global CD20 gene and protein down-regulation regulated at the pretranscriptional and posttranscriptional levels. *Clin Cancer Res.* 2008;14:1561-1570.

17.   Beers SA, French RR, Chan HT, et al. Antigenic modulation limits the efficacy of anti-CD20 antibodies: implications for antibody selection. *Blood.* 2010;115:5191-5201.

18.   Beum PV, Kennedy AD, Williams ME, Lindorfer MA, Taylor RP. The shaving reaction: rituximab/CD20 complexes are removed from mantle cell lymphoma and chronic lymphocytic leukemia cells by THP-1 monocytes. *J Immunol.* 2006;176:2600-2609.

19.   Gupta D, Crosby ME, Almasan A, Macklis RM. Regulation of CD20 expression by radiation-induced changes in intracellular redox status. *Free Radic Biol Med.* 2008;44:614-623.

20.   Kunala S, Macklis RM. Ionizing radiation induces CD20 surface expression on human B cells. *Int J Cancer.* 2001;96:178-181.

21.   Wattenberg MM, Kwilas AR, Gameiro SR, Dicker AP, Hodge JW. Expanding the use of monoclonal antibody therapy of cancer by using ionising radiation to upregulate antibody targets. *Br J Cancer.* 2014;110:1472-1480.

22.   Weber T, Botticher B, Mier W, et al. High treatment efficacy by dual targeting of Burkitt's lymphoma xenografted mice with a (177)Lu-based CD22-specific radioimmunoconjugate and rituximab. *Eur J Nucl Med Mol Imaging.* 2016;43:489-498.

23.   Repetto-Llamazares AHV, Malenge MM, O'Shea A, et al. Combination of (177) Lu-lilotomab with rituximab significantly improves the therapeutic outcome in preclinical models of non-Hodgkin's lymphoma. *Eur J Haematol.* 2018;101:522-531.

24. Multani P. Development of radioimmunotherapy for the treatment of non-Hodgkin's lymphoma. *Int J Hematol.* 2002;76:401-410.

25. Dahle J, Repetto-Llamazares AH, Mollatt CS, et al. Evaluating antigen targeting and anti-tumor activity of a new anti-CD37 radioimmunoconjugate against non-Hodgkin's lymphoma. *Anticancer Res.* 2013;33:85-95.

26. Repetto-Llamazares AH, Larsen RH, Patzke S, et al. Targeted cancer therapy with a novel anti-CD37 beta-particle emitting radioimmunoconjugate for treatment of non-Hodgkin lymphoma. *PLoS One.* 2015;10:e0128816.

27. Repetto-Llamazares AH, Larsen RH, Giusti AM, et al. 177Lu-DOTA-HH1, a novel anti-CD37 radio-immunoconjugate: a study of toxicity in nude mice. *PLoS One.* 2014;9:e103070.

28. Kolstad A, Madsbu U, Beasley M, et al. Lymrit 37-01: Updated results of a phase I/II study of 177Lu-lilotomab satetraxetan, a novel CD37-targeted antibody-radionuclide-conjugate in relapsed NHL patients. *Hematol Oncol.* 2017;35:269-270.

29. Lindmo T, Boven E, Cuttitta F, Fedorko J, Bunn PA, Jr. Determination of the immunoreactive fraction of radiolabeled monoclonal antibodies by linear extrapolation to binding at infinite antigen excess. *J Immunol Methods.* 1984;72:77-89.

30. Parekh BS, Berger E, Sibley S, et al. Development and validation of an antibody-dependent cell-mediated cytotoxicity-reporter gene assay. *MAbs.* 2012;4:310-318.

31. Clynes RA, Towers TL, Presta LG, Ravetch JV. Inhibitory Fc receptors modulate in vivo cytotoxicity against tumor targets. *Nat Med.* 2000;6:443-446.

32. Hernandez-Ilizaliturri FJ, Jupudy V, Ostberg J, et al. Neutrophils contribute to the biological antitumor activity of rituximab in a non-Hodgkin's lymphoma severe combined immunodeficiency mouse model. *Clin Cancer Res.* 2003;9:5866-5873.

33. van Meerten T, van Rijn RS, Hol S, Hagenbeek A, Ebeling SB. Complement-induced cell death by rituximab depends on CD20 expression level and acts complementary to antibody-dependent cellular cytotoxicity. *Clin Cancer Res.* 2006;12:4027-4035.

34. Marcatili S, Pichard A, Courteau A, et al. Realistic multi-cellular dosimetry for 177Lu-labelled antibodies: model and application. *Phys Med Biol.* 2016;61:6935-6952.

35. Oostindie SC, van der Horst HJ, Lindorfer MA, et al. CD20 and CD37 antibodies synergize to activate complement by Fc-mediated clustering. *Haematologica.* 2019;104:1841-1852.

36.   Heyerdahl H, Abbas N, Sponheim K, Mollatt C, Bruland O, Dahle J. Targeted alpha therapy with 227Th-trastuzumab of intraperitoneal ovarian cancer in nude mice. *Curr Radiopharm.* 2013;6:106-116.

37.   Chakraborty M, Abrams SI, Camphausen K, et al. Irradiation of tumor cells up-regulates Fas and enhances CTL lytic activity and CTL adoptive immunotherapy. *J Immunol.* 2003;170:6338-6347.

38.   Chakraborty M, Abrams SI, Coleman CN, Camphausen K, Schlom J, Hodge JW. External beam radiation of tumors alters phenotype of tumor cells to render them susceptible to vaccine-mediated T-cell killing. *Cancer Res.* 2004;64:4328-4337.

39.   Reits EA, Hodge JW, Herberts CA, et al. Radiation modulates the peptide repertoire, enhances MHC class I expression, and induces successful antitumor immunotherapy. *J Exp Med.* 2006;203:1259-1271.

40.   Kapadia NS, Engles JM, Wahl RL. In vitro evaluation of radioprotective and radiosensitizing effects of rituximab. *J Nucl Med.* 2008;49:674-678.

41.   Hicks SW, Lai KC, Gavrilescu LC, et al. The antitumor activity of IMGN529, a CD37-targeting antibody-drug conjugate, is potentiated by rituximab in non-Hodgkin lymphoma Models. *Neoplasia.* 2017;19:661-671.
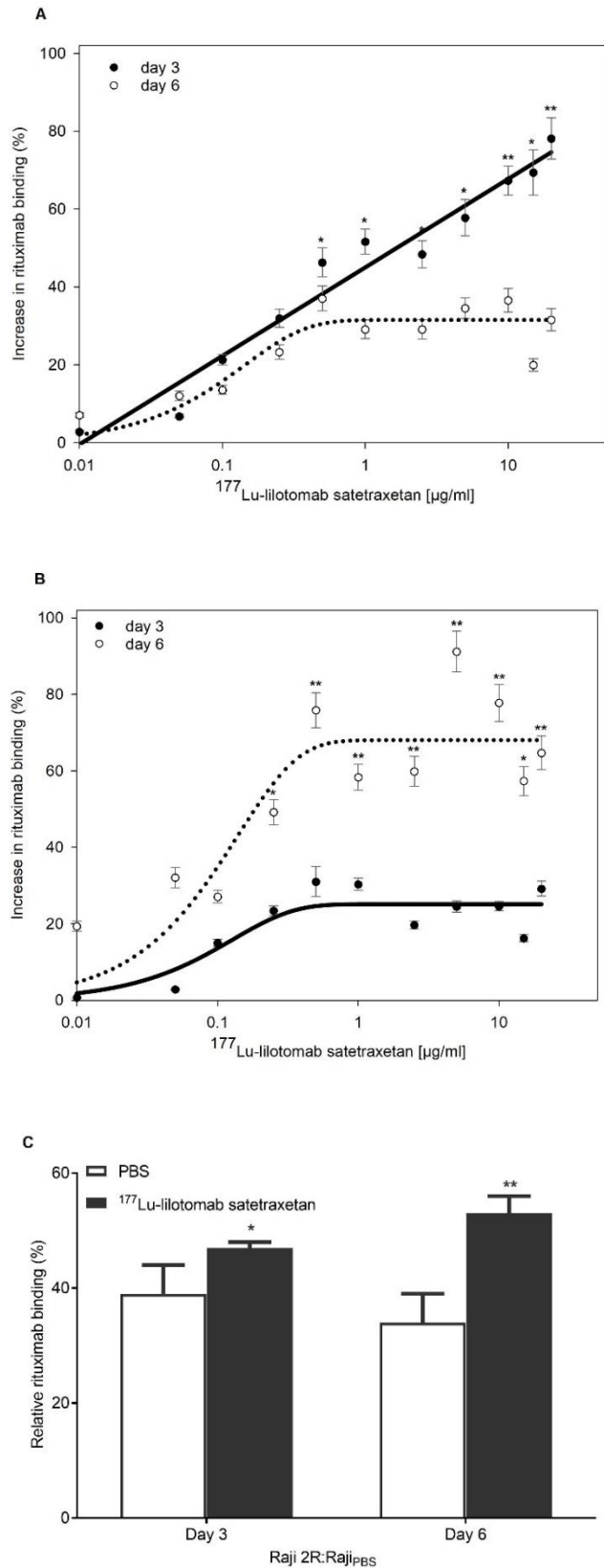
FIGURES

Fig. 1 Increase in rituximab-binding on days 3 (solid lines) and 6 (dotted lines) after treatment with escalating doses of ^{177}Lu-lilotomab in (A) Raji cells and (B) Raji 2R cells. (C) Rituximab-binding in Raji 2R cells relative to untreated Raji cells when considering the average of the horizontal plateau from Fig. B. *p<0.05 and **p<0.005, N=3.
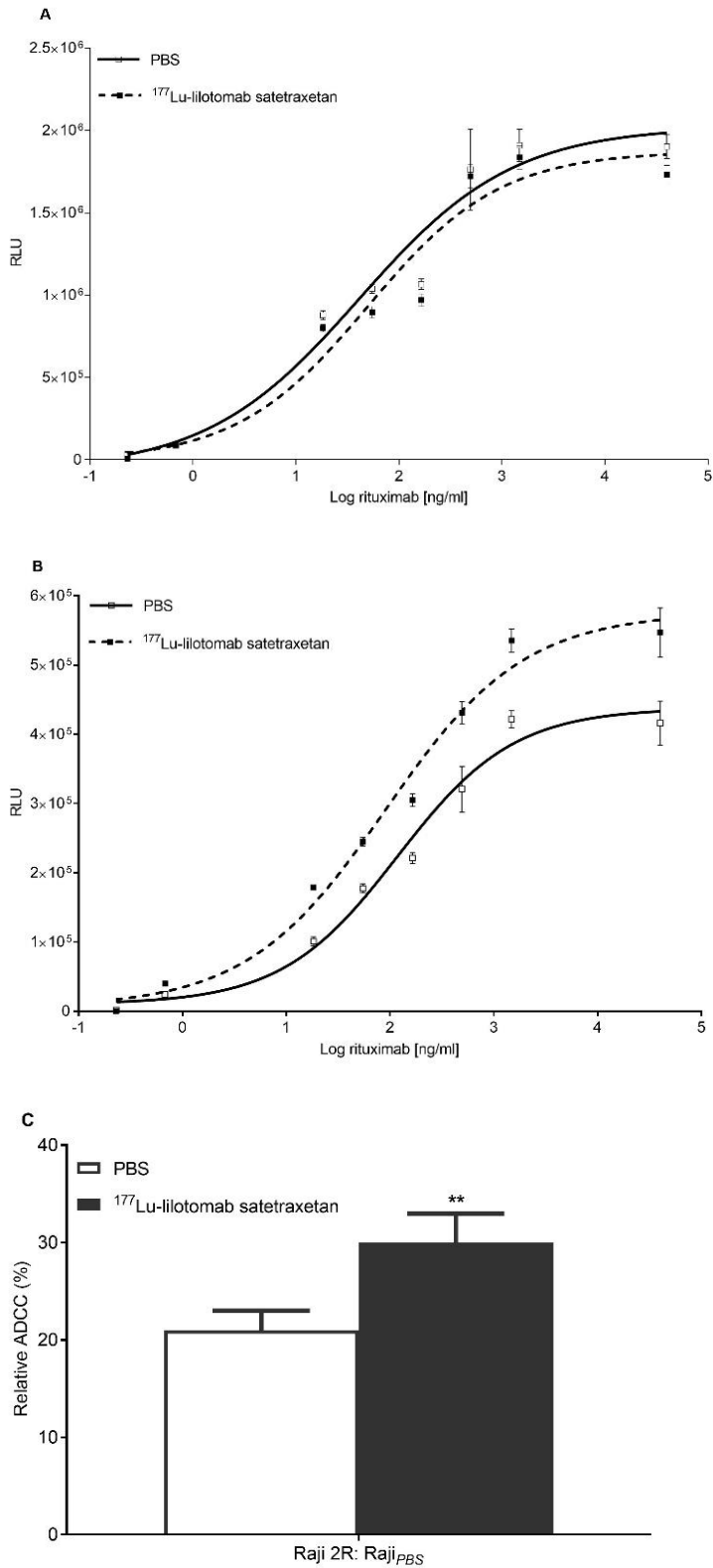
Fig. 2 Luminescence (RLU) representative of effector-cell binding to rituximab in (A) Raji and (B) Raji 2R cells treated with 1µg/ml ^{177}Lu-lilotomab or PBS (untreated). (C) Relative change in effector-cell binding to rituximab in untreated and in 1µg/ml ^{177}Lu-lilotomab treated Raji 2R cells relative to untreated Raji cells, **p<0.05, N=3-4.

Fig. 3 Average tumor volume±SE in Raji 2R-xenografted mice treated with saline, rituximab, 150 MBq/kg and 350 MBq/kg ^{177}Lu-lilotomab monotherapy or combination with rituximab. N=10. (A) Curve built using extrapolation of tumor volumes after euthanasia, ♦ timepoints of observed significant synergistic effects (p<0.05) (B) Curve built keeping constant tumor volume after euthanasia, *timepoints observed to be significantly different from ^{177}Lu-lilotomab monotherapy (p<0.05).

Fig. 4 Kaplan-Meier survival curves of Raji 2R-xenografted mice treated with saline, rituximab, 150 MBq/kg and 350 MBq/kg ¹⁷⁷Lu-lilotomab monotherapy or combination with rituximab. N=10. End point: tumor diameter larger than 20mm. Gray dots: censored animals.

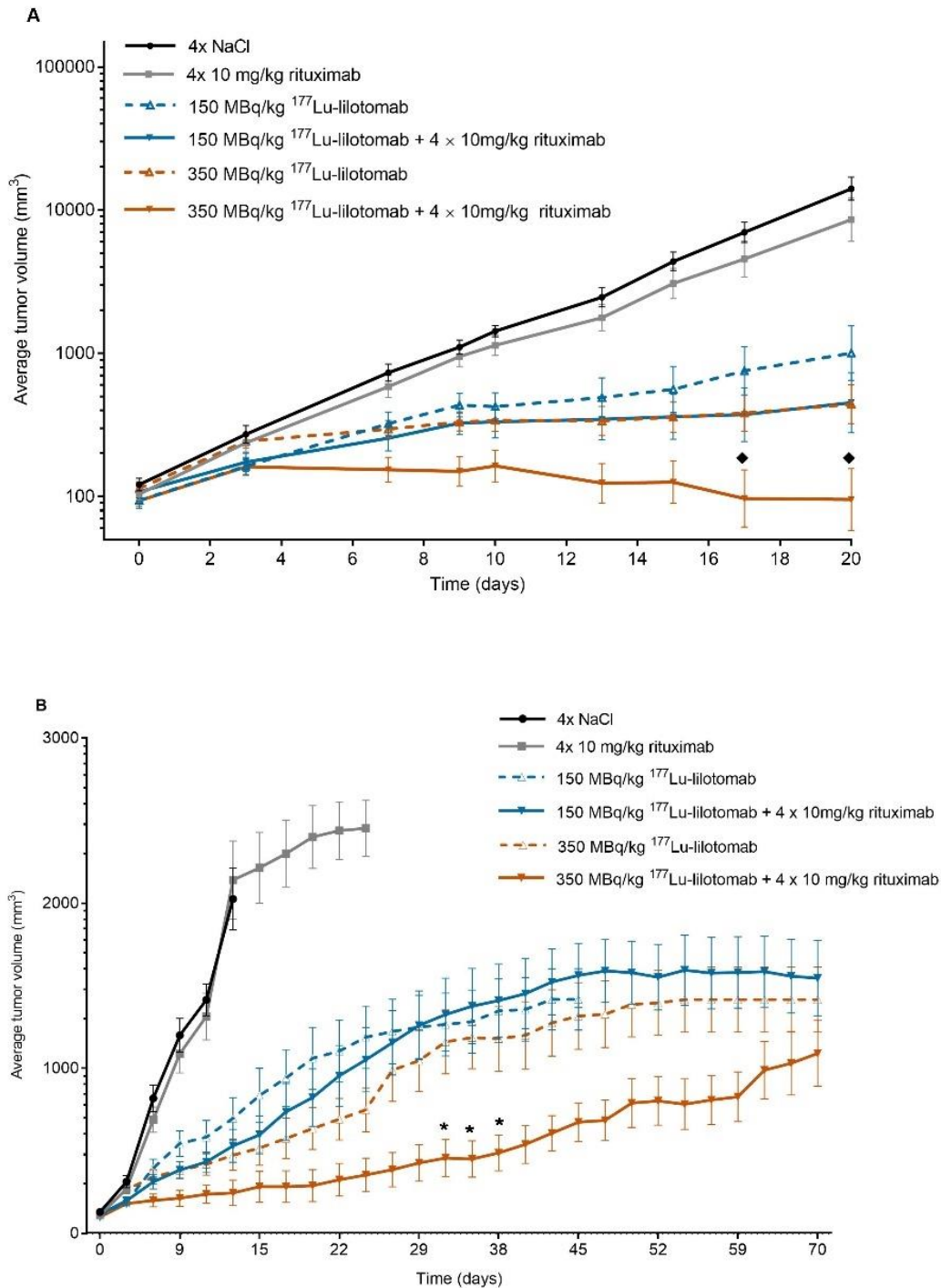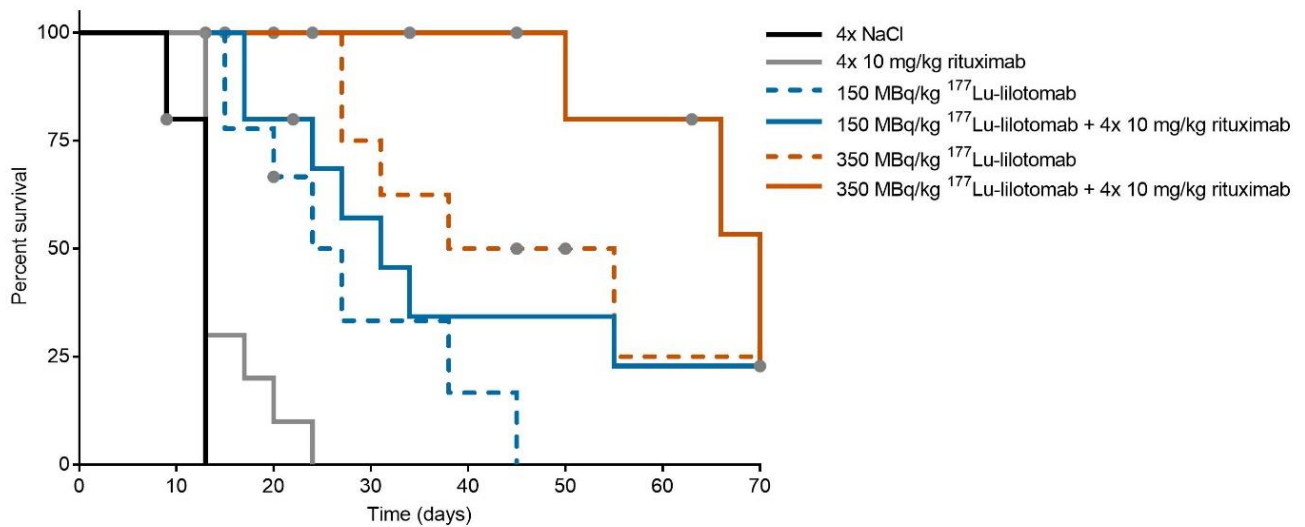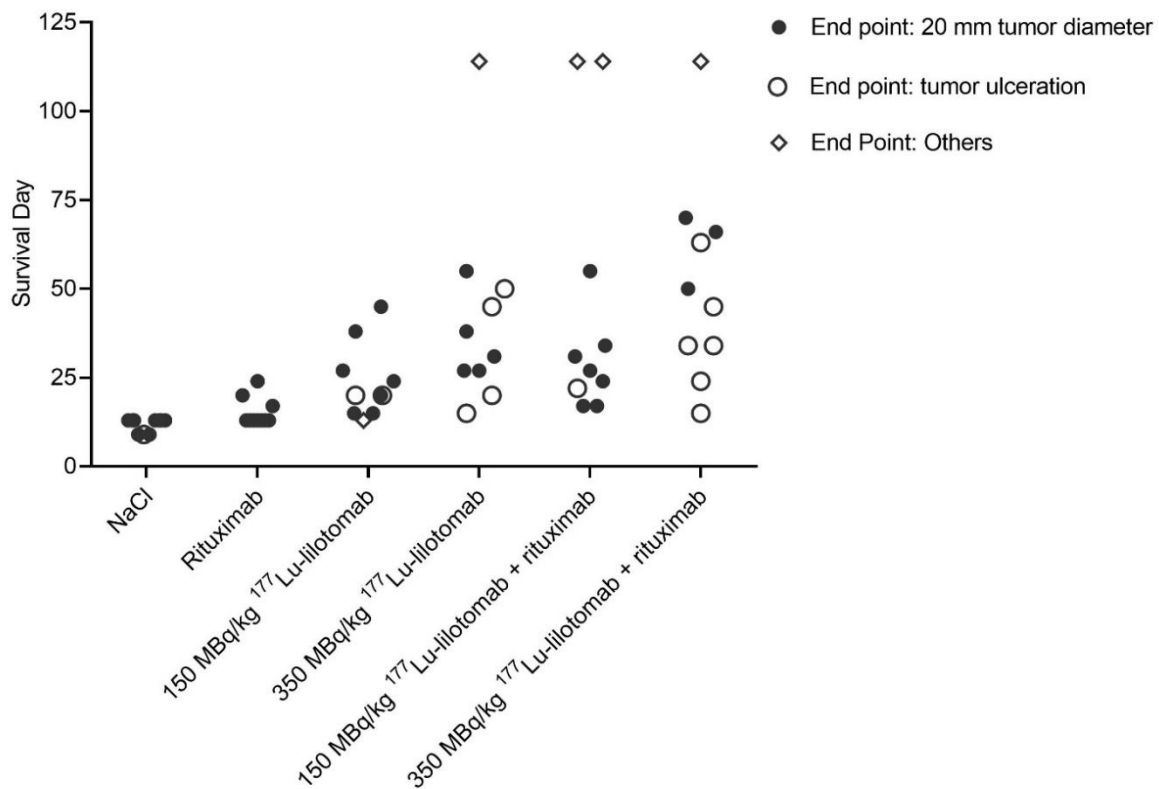*Fig. 5 Survival of Raji 2R-xenografted mice treated with saline, rituximab, 150 MBq/kg and 350 MBq/kg ¹⁷⁷Lu-lilotomab monotherapy or combination with rituximab. Full circles: mice euthanized due to tumor diameter=20mm. Open circles: mice euthanized due to tumor-ulceration. Diamonds: mice euthanized due to end of study (at 114 days) or due to symptoms of sickness or discomfort.*

TABLES

Table 1 Fold-change in average tumor volume from baseline of combination therapies vs corresponding monotherapies and Bliss synergy interaction values with 90% confidence intervals.

Study day	^{177}Lu-lilotomab (MBq/kg)	Fold-change from day 0		Interaction value (90% CI)
		-rituximab	+rituximab	
3	0	2.2	2.2	
	150	1.7	1.6	0.99 (0.41, 2.37)
	350	2.3	1.7	0.77 (0.32, 1.84)
7	0	6.1	5.5	
	150	3.3	2.4	0.80 (0.33, 1.91)
	350	2.7	1.6	0.66 (0.28, 1.57)
9	0	9.2	8.9	
	150	4.4	3.0	0.70 (0.29, 1.68)
	350	3.1	1.6†	0.53 (0.22, 1.23)
10	0	11.8	10.6	
	150	4.3	3.1	0.79 (0.33, 1.89)
	350	3.2	1.7	0.61 (0.26, 1.46)
13	0	20.4	16.6	
	150	5.0	3.2	0.79 (0.33, 1.89)
	350	3.1	1.3†	0.51 (0.22, 1.23)
15	0	36.2	28.8	
	150	5.7	3.3	0.74 (0.31, 1.77)
	350	3.3	1.3†	0.50 (0.21, 1.21)
17	0	57.8	42.6	
	150	7.7	3.5*	0.61 (0.25, 1.47)
	350	3.5	1.0†	0.39 (0.16, 0.94)‡
20	0	116.6	80.2	
	150	10.2	4.2*	0.60 (0.25, 1.43)
	350	4.1	1.0†	0.36 (0.15, 0.86)‡

*significant rituximab effect with 150 MBq/ kg ^{177}Lu-lilotomab (p<0.05)

†significant rituximab effect with 350 MBq/ kg ^{177}Lu-lilotomab (p<0.05)

‡significant synergism (p<0.05)

Table 2 Median survival time of mice treated with NaCl, rituximab, 150 and 350 MBq/kg ^{177}Lu-lilotomab and combination therapies with 20mm tumor diameter as endpoint.

Treatment Group	Median survival ±SE (days)
4×NaCl	13 ±0
4×10mg/kg rituximab	13 ±3
150 MBq/kg ^{177}Lu-lilotomab	24 ±4*,†
350 MBq/kg ^{177}Lu-lilotomab	38 ±11*,†
150 MBq/kg ^{177}Lu-lilotomab+rituximab	31 ±5*,†
350 MBq/kg ^{177}Lu-lilotomab+rituximab	70 ±8*,†
*Significantly different from NaCl ($p < 0.001$)	
†Significantly different from 4x10mg/kg rituximab ($p < 0.01$)	

Table 3 Bliss synergy interaction values calculated using the hazards found through Cox Proportional-Hazards model fitting to the mice survival (end point: tumor diameter larger than 20mm).

	Interaction Value (90% confidence interval)	p-value
150 MBq/kg ^{177}Lu-lilotomab+rituximab	0.88 (0.30-2.63)	0.85
350 MBq/kg ^{177}Lu-lilotomab+rituximab	0.83 (0.22-3.15)	0.82

Supplementary Data

Bliss independence analysis of tumor volume

Bliss analysis of tumor volume was performed using extrapolation of tumor volumes and was restricted to the first 20 days of the study. This was because there were no control animals beyond study day 13 and any analysis beyond day 20 would impose uncertainty. The tumor volumes were log transformed and data for mice withdrawn before study day 20 were extrapolated by linear regression. Beyond day 20 tumor sizes become infeasibly large. Difference from baseline was calculated on the log scale and all statistical analysis were performed on the log-transformed data. A mixed effects linear model was used including fixed effects of each of the treatments (referred to as between group factors) and the associated interaction between these factors. Additionally, study day was included as a within animal fixed effect. All the interactions between the group factors and study day were included. Animal within group and the side of the tumor were included as random effects in the model. An autoregressive correlation structure was assumed. The effects of treatment with and without rituximab were evaluated separately at each dose of ^{177}Lu-lilotomab (control, 150 MBq/kg and 350 MBq/kg), for each study day. The size of these effects was compared for 150 MBq/kg ^{177}Lu-lilotomab against the control and 350 MBq/kg ^{177}Lu-lilotomab against the control using the interaction test of the Bliss independence model using SAS 9.4 (SAS Institute, NC, USA). Interaction values less than 1 were considered synergistic and statistical significance defined by $p < 0.05$.

Survival and Bliss synergy analysis with endpoint criteria: >20 mm tumor diameter and tumor-ulceration

Treatment with ^{177}Lu-lilotomab alone and in combination with rituximab significantly prolonged survival compared to saline and rituximab treatment (Supplemental Fig.1,

Supplemental Table 1). However, treatment with ^{177}Lu-lilotomab in combination with rituximab did not significantly differ from treatment with rituximab alone.

Bliss independence analysis did not provide statistically significant results (Supplemental Table 2). However, with only 10 mice per group the hazard proportionality is an approximation. The lack of significance is because of the poor Proportional Hazards assumption in the Cox model (p = 0.07).
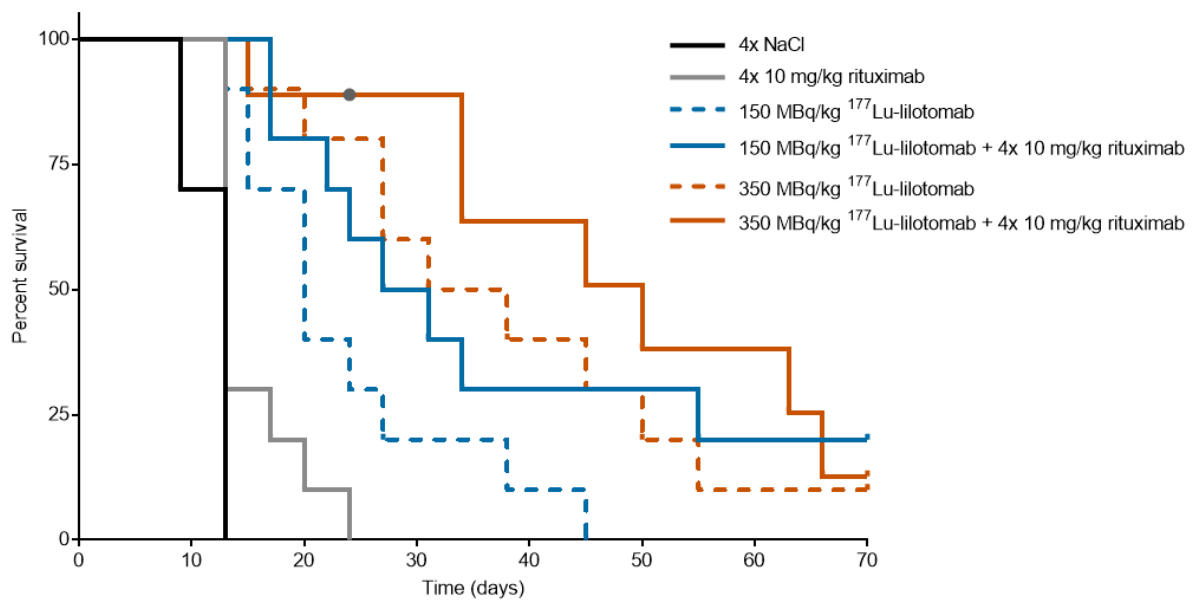
Supplemental Fig.1 Kaplan-Meier survival curves of Raji2R-xenografted mice treated with saline, rituximab, 150 MBq/kg and 350 MBq/kg ^{177}Lu-lilotomab monotherapy or combination with rituximab. N=10. Gray dots: censored animals.

Supplemental Table 1 Median survival time of mice treated with NaCl, rituximab, 150 and 350MBq/kg ^{177}Lu-lilotomab and combination therapies.

Treatment Group	Median survival ± SE (days)
4×NaCl	13±0
4×10mg/kg rituximab	13±3
150MBq/kg ^{177}Lu-lilotomab	20±3*,†
350MBq/kg ^{177}Lu-lilotomab	38±9*,†
150MBq/kg ^{177}Lu-lilotomab + rituximab	27±6*,†
350MBq/kg ^{177}Lu-lilotomab + rituximab	50±7*,†
*Significantly different from NaCl ($p<0.001$)	
†Significantly different from 4x10 mg/kg rituximab ($p<0.01$)	

Supplemental Table 2 Bliss synergy interaction values

	Interaction Value* (90% confidence interval)	p-value
150 MBq/kg ^{177}Lu-lilotomab + rituximab	0.7 (0.43-1.25)	0.54
350 MBq/kg ^{177}Lu-lilotomab + rituximab	1.58 (0.61-4.08)	0.43

*calculated using the hazards found through Cox Proportional Hazards model fitting to mouse survival.

Measurement of cell viability and apoptosis (Method)

At a concentration of $2.5×10^5$ cells/ml, Raji and Raji2R cells were incubated at 37°C with either 50µg/ml rituximab or PBS. At 1 hour and 3 days after start of incubation, the cells were

transferred to 96 well plates and incubated with RealTime-Glo™ MT Cell Viability Assay (Promega, USA) following the manufacturer's protocol. The luminescence, proportional to the number of viable cells, was measured at each timepoint on a Spark microplate reader (TECAN, Switzerland). The experiment was performed in duplicates and the results are presented as mean± standard deviation (SD).

On day 3, 2.0×10^6 cells were fixed using ice cold methanol in preparation for evaluation of apoptosis by flow cytometry analysis. A positive control was included in the study by incubating the unfixed control cells with a topoisomerase inhibitor; etoposide, for 18 hours prior to analysis. The fixed cells were then washed and incubated with Alexa conjugated anti-cleaved PARP antibody (BioNordika, Norway) diluted 1:100 in 5% non-fat milk for 1 hour. The cells were once again washed, and the fluorescent apoptosis signal determined by flow cytometry (Guava® easyCyte12HT, Millipore).

Effect of rituximab treatment on cell viability and apoptosis (Results)

Treatment with rituximab did not yield any significant effect on cell viability relative to the untreated cells after 1 hour and on day 3 for both Raji and Raji2R cells (Supplemental Fig. 2). In addition, treatment of Raji and Raji2R cells with rituximab had no significant effect on initiating apoptosis. The percentage of total number of apoptotic cells in rituximab treated Raji cells was similar to those in the untreated control cells at day 3 (Supplemental Fig.3). Raji 2R cells were overall resistant to rituximab treatment and no apoptosis was observed (Supplemental Fig. 3).
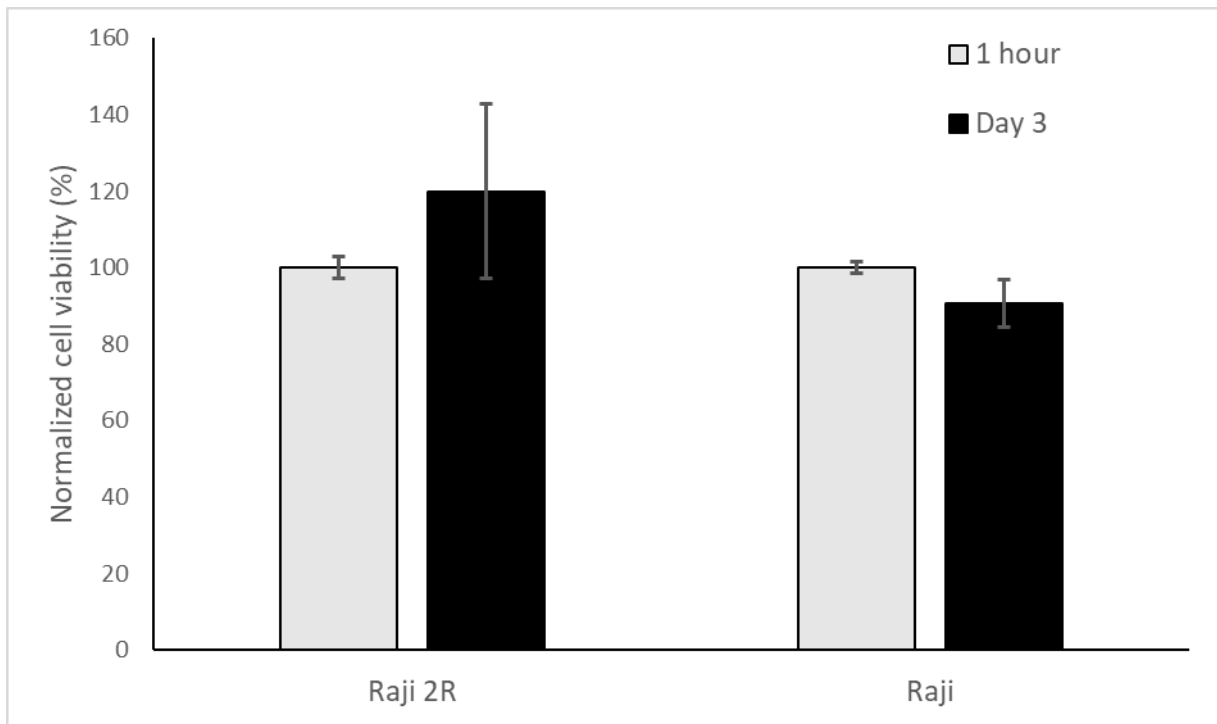
Supplemental Fig. 2 Effect of rituximab-treatment on viability in Raji and Raji2R cells. Mean

±SD, N=2
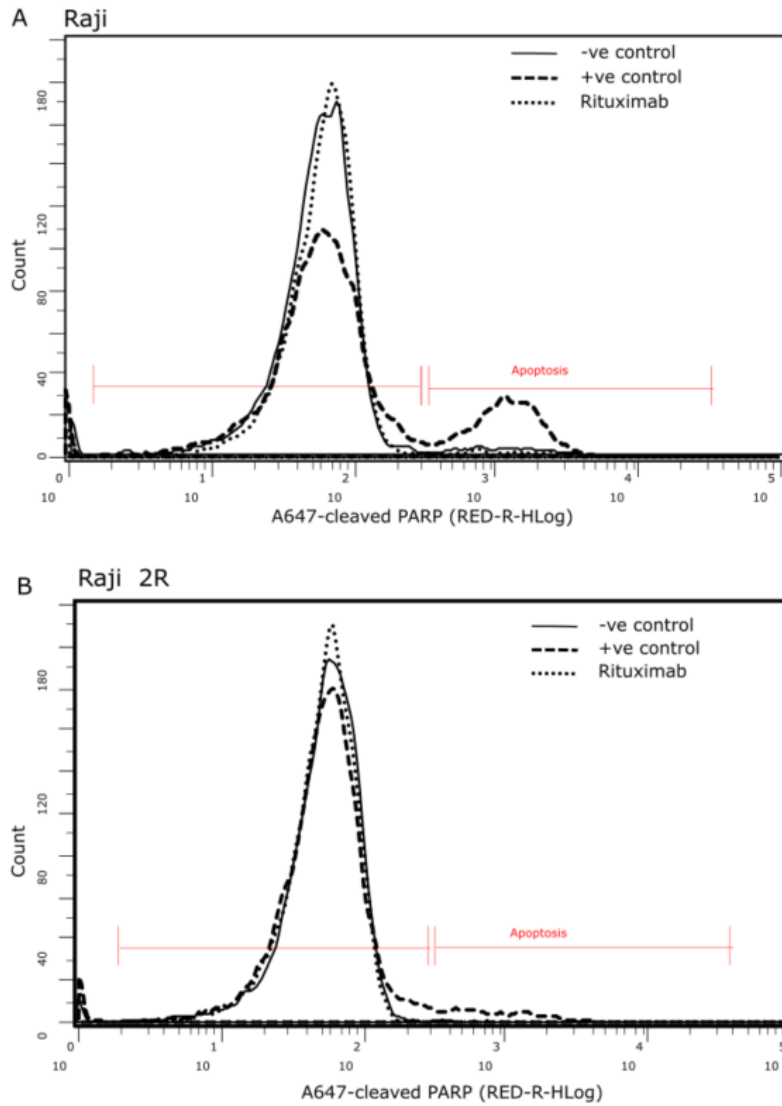
Supplemental Fig.3 Example histograms showing the change in induction of apoptosis after treatment of Raji and Raji 2R cells with PBS as a negative control, etoposide as a positive control denoted as -ve and +ve control respectively or 50μg/ml rituximab.

III

Anti-CD37 radioimmunotherapy with ^{177}Lu-NNV003 synergises with the PARP inhibitor olaparib in treatment of non-Hodgkin's lymphoma *in vitro*

Marion M. Malenge[1,2,3,*], Astri Fjelde Maaland[1,2,*], Brian Middleton[4], Sebastian Patzke[1,3], Arne Kolstad[5,6], Trond Stokke[3], Anne Hansen Ree[2,7], Helen Heyerdahl[1], Ada Repetto-Llamazares[1], Jostein Dahle[1]

[1]Nordic Nanovector ASA, Kjelsåsveien 168B, 0884 Oslo, Norway

[2] Institute of Clinical Medicine, University of Oslo, 0317 Oslo, Norway

[3] Department of Radiation Biology, Institute for Cancer Research, Norwegian Radium Hospital, Oslo University Hospital, Oslo, Norway

[4] Inferstats Consulting Ltd, Cheshire SK104TG, UK

[5]Department of Oncology, Norwegian Radium Hospital, Oslo University Hospital, Oslo, Norway

[6]KG Jebsen Center for Cancer Immunotherapy, Institute of Clinical Medicine, University of Oslo, Norway.

[7]Department of Oncology, Akershus University Hospital, 1478 Lørenskog, Norway

*These authors contributed equally to this work

Abstract

Background and purpose: PARP inhibitors have been shown to increase the efficacy of radiotherapy in preclinical models. Radioimmunotherapy results in selective radiation cytotoxicity of targeted tumour cells. Here we investigate the combined effect of anti-CD37 β-emitting ^{177}Lu-NNV003 radioimmunotherapy and the PARP inhibitor olaparib, and gene expression profiles in CD37 positive non-Hodgkin's lymphoma cell lines.

Materials and methods: The combined effect of ^{177}Lu-NNV003 and olaparib was studied in seven cell lines using a fixed-ratio ray design, and combination index was calculated for each combination concentration. mRNA was extracted before and after treatment with the combination of the two drugs. After RNA-sequencing, hierarchical clustering was performed on basal gene expression profiles and on differentially expressed genes after combination treatment from baseline. Functional gene annotation analysis of significant differentially expressed genes after combination treatment from baseline was performed to identify enriched biological processes.

Results: The combination of olaparib and ^{177}Lu-NNV003 was synergistic in four of seven cell lines, antagonistic in one and both synergistic and antagonistic in two, depending on the concentration ratio between olaparib and ^{177}Lu-NNV003. Cells treated with the combination significantly overexpressed genes in the TP53 signalling pathway. However, cluster analysis did not correlate with the sensitivity of cells to single agent or combination treatment.

Conclusion: The cytotoxic effect of the combination of the PARP inhibitor olaparib and the β-emitting radioimmunoconjugate ^{177}Lu-NNV003 was synergistic in the majority of tested lymphoma cell lines.

Introduction

Non-Hodgkin's Lymphoma (NHL) is the most common haematological malignancy and is classified into different histologic subtypes (1). Among the aggressive NHLs diffuse large B-cell lymphoma (DLBCL) can be subdivided into activated B-cell (ABC) and germinal centre (GCB) DLBCL based on either immunostaining or gene expression profiling (1). Mantle cell lymphoma (MCL) is a distinct and more uncommon NHL (1). NHL occurs as a consequence of genetic alterations occurring during the error prone process of B-cell differentiation and maturation. The resulting lymphomas often have deficiencies in DNA damage response (DDR) pathways linked to mutations in *ATM, PTEN* and *TP53* tumour suppressor genes (2-4). Malignant cells utilise compensatory DNA repair strategies to prevent catastrophic DNA damage. Targeting these complementary DNA repair pathways results in dysfunction of both DNA repair pathways, inducing synthetic lethality (5, 6).

Olaparib inhibits the DNA repair enzymes poly (ADP ribose) polymerase 1 and 2 (PARP1 and PARP2), which are activated in response to DNA single strand breaks (SSB) (7). Consequently, the PARPs are unable to recruit DNA repair proteins and are trapped at the SSB site causing stalling and collapse of the DNA replication fork which results in cytotoxic double strand breaks (DSB) (8). Olaparib has been approved by the FDA for *BRCA* mutated ovarian and breast cancer. The *BRCA* mutation causes impairment of DNA DSB repair, making the cells harbouring this mutation sensitive to olaparib. Olaparib has also been shown to be effective in preclinical models of MCL harbouring *ATM* mutation (9), which is present in 41-56% of MCL and 13-20% of DLBCL patients (10-12), and also impairs the DSB repair pathway. The PARP inhibitor veliparib has shown clinical activity in NHL in combination with the alkylating agent bendamustine and the anti-CD20 antibody rituximab (13).

Radiation induces cytotoxic DNA lesions in form of SSB or DSB, where the latter is more lethal. Combination of radiation with PARP inhibition results in the transformation of the induced SSBs to DSBs, increasing the cytotoxic effect of the treatments. Several preclinical studies have shown that PARP inhibitors sensitise tumour cells to radiation (14-24) and combine synergistically with antibody-drug conjugates (25). The combination of the anti-EGFR antibody cetuximab, olaparib and radiation has been studied in patients with head and neck squamous cell carcinoma (26) and there are currently several phase 1 studies ongoing

investigating olaparib in combination with radiotherapy in patients with glioblastoma, lung cancer, breast cancer and head and neck squamous cell carcinoma (27-29).

Radioimmunotherapy (RIT) delivers targeted radiation that induces DNA damage, priming malignant cells for apoptosis with limited toxicity to normal tissue. We have developed a next generation RIT, ^{177}Lu-NNV003, for treatment of B-cell malignancies. It consists of a chimeric mouse-human anti-CD37 antibody (NNV003), conjugated with p-SCN-Bn-DOTA (DOTA) that chelates the ß-emitting radionuclide lutetium-177 (30). The murine version of ^{177}Lu-NNV003; ^{177}Lu-lilotomab satetraxetan, is currently in clinical testing for treatment of relapsed/refractory follicular lymphoma (NCT01796171) and DLBCL (NCT02658968).

In the present study, we aimed to determine the *in vitro* cytotoxicity and phenotypic outcomes of combining ^{177}Lu-NNV003 with olaparib in DLBCL and MCL cell lines.

Materials and methods

Labelling and Quality Control of antibodies with [177]Lu

NNV003 (IgG$_1$, mouse variable regions, κ, and human constant region, κ) was conjugated with p-SCN-Bn-DOTA (Macrocyclics, USA) and labelled with ^{177}Lu as previously described (30). Briefly, the pH of DOTA-NNV003 was adjusted to 5.4 using 0.25 M ammonium acetate buffer and ^{177}Lu in 10 mM HCl (ITG, Germany) was added to obtain specific activity of approximately 550 MBq/mg. The sample was incubated for 30 min at 37˚C and then diluted in a solution of 0.3% Tween 20 (VWR, USA) and 20% Glycerol (Merck KGaA, Germany). Radiochemical purity above 95% was verified by instant thin layer chromatography (Tec-Control ITLC strips, Biodex Medical, USA) and the immunoreactivity was verified using a modified Lindmo model (31) using a standardised setup with one cell concentration of 75 x10^6 Ramos cells/ml.

Cell lines

The MCL cell lines REC-1 and GRANTA-519, the GCB-DLBCL cell lines DOHH-2, SU-DHL-4, and WSU-DLCL-2 and the ABC-DLBCL cell lines U-2932 and OCI-LY-10 were used in this study. REC-1, DOHH-2, SU-DHL-4, WSU-DLCL-2 and U-2932 were cultured in RPMI medium, GRANTA-519 was cultured in DMEM medium and OCI-LY-10 was cultured in IMDM medium. The media were supplemented with 15% (OCI-LY-10) or 10% (all others) heat inactivated foetal bovine serum and 1% penicillin/streptomycin (media and supplement

from Thermo Fisher Scientific, USA). All cell lines were provided by University Medical Center Groningen (Netherlands), except OCI-LY-10, which was kindly provided by Institute of Oncology Research (Switzerland).

Sensitivity to single agents

Olaparib (Selleck Chemicals USA) was dissolved in DMSO, aliquoted and stored at -20˚C. Cells were seeded in 96-deep-well plates at concentrations of 2 mill/ml for OCI-LY-10, GRANTA-519 and U-2932 and 8 mill/ml for REC-1, DOHH-2, SU-DHL-4 and WSU-DLCL-2. Using a digital drug dispenser (D300e, TECAN, Switzerland), 1.3 nM – 316 µM of olaparib or 0.09 ng/ml – 88.5 µg/ml of ^{177}Lu-NNV003 was randomly added to the wells. The cells were incubated for 20-24 h while shaking at 37°C and 5% CO_2. The cells were diluted 200x in cell culture medium to decrease the amount of unbound ^{177}Lu-NNV003 in the medium and the wells containing olaparib were refilled to maintain the initial drug concentration. The cells were transferred to 384-well-plates for further growth for 3 days, after which they were incubated with RealTime-Glo™ MT Cell Viability Assay (Promega, USA). Luminescence, proportional to the number of viable cells, was measured after 1 hour, 24 hours and 48 hours using a Spark microplate reader (TECAN, Switzerland). Relative viability was calculated by dividing the luminescence values from treated cells by luminescence from non-treated cells. The relative viability was plotted against drug concentration and sigmoidal curve fitting (four-parameter logistic curves) was performed in GraphPad Prism 8.00 (GraphPad Software, USA). IC_{50}, area under the curve (AUC) and point viabilities (32) were used to estimate sensitivity to the drugs. The point viabilities for olaparib were measured at 21.6 µM, corresponding to the maximum achievable clinical plasma concentration at recommended monotherapy dose (33). The point viabilities for ^{177}Lu-NNV003 were measured at 250 ng/ml, which is close to the average IC_{50} for the drug across the cell lines.

Combination study

A fixed-ratio ray design (34) was used to study the effect of combining ^{177}Lu-NNV003 with olaparib. Briefly, the two drugs were mixed together at a constant ratio (Z) following Equation 1. Each combination Z is defined by a fraction, f, between 0 and 1, where f equal to 0 or 1 corresponds to only olaparib or ^{177}Lu-NNV003, respectively. Three combinations were made using f = 0.25, 0.5 and 0.75. To obtain a dose response curve of the combinations, 9

concentrations of Z were used by multiplying Equation 1 with factors ranging between 0.003 and 150 depending on cell line. See Table S 1 for concentrations used in the experiment.

$$Z = f \times {}^{177}LuNNV003\,_{IC50} + (1 - f) \times olaparib_{IC50} \qquad 1$$

Analysis of Ray design

The relative cell survival was calculated by dividing the luminescence values of treated cells by the luminescence values of non-treated cells. 1 minus this ratio was taken to represent the proportion of killed cells. The bottom asymptote of the dose response curve was fixed to 0 and the top asymptote was set to be less than or equal to 1. Sigmoid curves (3-parameter logistic curves) were fitted for each ray, with the assumption that the variability about the fitted curve would be similar for all rays, allowing the use of a global model (34). The variance was dependent on the response, so to account for this effect the variance was modelled for each dose using Equation 2

$$var = c^2 \times response^p \qquad 2$$

where the response is the proportion of cells killed at that dose, and c and p are parameters from the global model. The curve fitting was done using SAS/STAT 14.1 software in SAS Version 9.4, in particular PROC NLMIXED. Combination indices (CInd) were calculated per concentration using a model based on different maximum effects of the drugs, and unequal Hill slopes of the dose response curves (35), derived by Grabovsky and Tallarida (36). CInd for concentrations leading to 0% cell death were regarded as not relevant and excluded from the analysis. A point was considered significantly synergistic or antagonistic if the 95% confidence interval of the CInd was below or above 1, respectively. If the CInd was below 0.85 or above 1.15 and the 95% confidence included 1, the point was considered non-significantly synergistic or antagonistic. Points were considered additive between 0.85 and 1.15, and if the 95% confidence interval was within this range, it was considered significant. Some dose response curves could not be well fitted and therefore the CInd could not be calculated and these points are presented as missing data.

Gene expression analysis

The cells were treated for 24 hours with the combination of the drugs at concentrations corresponding to their monotherapy (see Table S 1 for treatment concentrations). The cells including untreated controls were washed and total RNA isolated using RNeasy mini kit (Qiagen©, Germany) following the manufacturers' protocol.

RNA integrity was verified using 2100 Bioanalyzer (Agilent Technologies Inc., CA, USA) and adjusted to an acceptable concentration. Libraries were generated from the RNA using Illumina stranded mRNA kit (Illumina Inc., CA, USA) and sequenced on an Illumina NextSeq500 system (Illumina Inc., CA, USA) using 75 bp single reads. Obtained reads were aligned against the reference human genome (UCSC hg19) using STARalign v2.5.0.

Genes that were expressed at very low levels were excluded from the analysis by a cut-off of 10 normalised reads, applied to the sum of gene expression at baseline and in the respective treated samples. This reduced the gene list data from 23,269 genes to 6,054 genes (Figure S1). The resulting 6,054 genes were log2-transformed and genes with a standard deviation larger than 1 of the baseline expressions in the 7 cell lines were included for further analysis, which resulted in 559 genes that were then min-max normalised to scale the entire dataset to a 0 to 1 range.

Hierarchical cluster analysis on the baseline genes was performed on the scaled data using Morpheus software (broadinstitute.org). For this analysis, Euclidean distance and complete linkage were used to compute the distance between clusters. This analysis was used to visualise the correlation of clusters to cell line histology subtypes, drug sensitivity and drug combination outcome.

Differential gene expression between the untreated cell lines and the corresponding combination treated samples was analysed using Cufflinks and Cuffdiff v2.2.1. To identify genes that were significantly up- or down- regulated after treatment with the combination of ^{177}Lu-NNV003 and olaparib, a threshold was set on the log2 fold change (FC) >0.5 or <-0.5 and $p < 0.05$ compared to baseline (Figure S 1).

Functional and pathway enrichment analysis was done using the web-based functional annotation tool: DAVID 6.8 (david.ncifcrf.gov) (37). The *Homo sapiens* genome was selected as the background and the differentially expressed genes mapped against it. Gene Ontology (GO) biological process terms and Kyoto Encyclopedia of Genes and Genomes (KEGG) pathway with $p < 0.05$, count ≥ 2 and FDR < 1% were considered to be statistically significant.

The GO terms were matched against the outcome of drug combinations to identify their correlation and contribution towards the assigned synergy score.

Gene mutation analysis

To identify mutations in expressed genes related to DNA damage repair, mutation calling was done using Isaac Variant Caller version 2.3.13-31 c98c29-dirty and hg19 reference. Variant calls passing all quality requirements were annotated using VEP Ensembl GRCh37 release 98.

Results

Single-agent viability

To determine the sensitivity of the cell lines to ^{177}Lu-NNV003 and olaparib IC$_{50}$s, AUCs and individual viabilities were calculated (Figure 1 and Table S1). The three viability estimates were in accordance and showed that the cell lines had diverse response to the single-agent treatments. To better see a trend in the responses of cell lines, the data from the three measurements were normalised from most sensitive to least sensitive and plotted on a scale. The MCL cell line GRANTA-519 was the most sensitive cell line for both drugs, whereas the other MCL cell line REC-1 (Figure 1 C and D) was the least sensitive. For treatment with olaparib, only REC-1 was determined as resistant with around 50 % viability at the maximum plasma concentration of the drug. All the cell lines were classified as sensitive to ^{177}Lu-NNV003 because the IC$_{50}$s were below 8 µg/ml which has been reported in a previous study to be the concentration conferring resistance to ^{177}Lu-lilotomab, the murine version of ^{177}Lu-NNV003 (38).
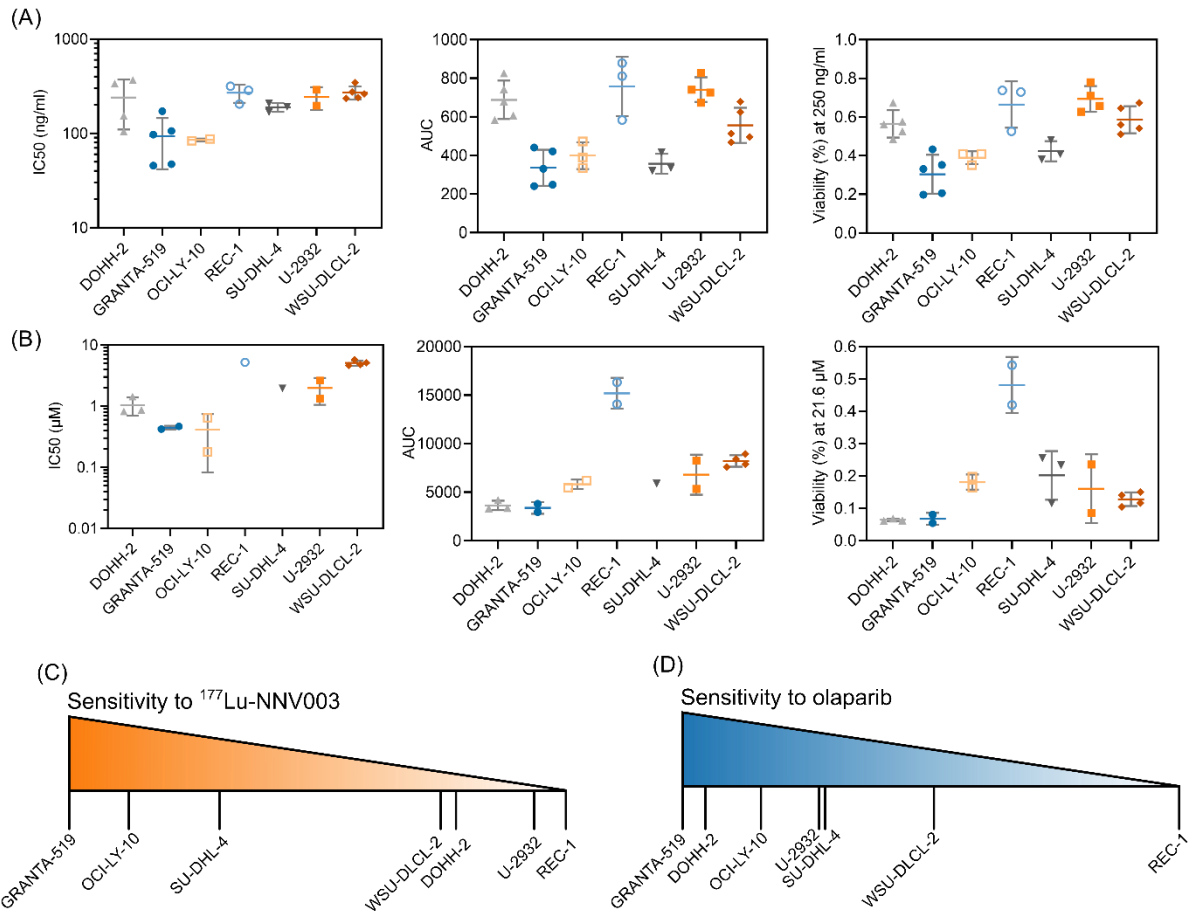
Figure 1) Sensitivity of seven cell lines to (A) ^{177}Lu-NNV003 and (B) olaparib at day 5. The plots in (A) and (B) show IC$_{50}$ to the left, AUC in the middle and the individual viabilities of one concentration to the right. Data point from independent experiments, lines show the mean and error bars the SD. The data from (A) and (B) were normalised from 1 (most sensitive) to 0 (least sensitive) and plotted on a scale in (C) and (D)

Combination of ^{177}Lu-NNV003 and olaparib

To estimate the effect of the combined treatment of ^{177}Lu-NNV003 and olaparib, CInd were calculated for three different ratios of the drugs (f= 0.25, 0.5, 0.75, Equation 1). The dose response curves of the rays in each cell line are presented in Figure S 2 and S 3. The CInd for the combination of olaparib with ^{177}Lu-NNV003 varied across cell lines, rays, days of measurement and concentrations of the combination. The trend for each cell line is summarised in Figure 2. The combined effect of olaparib and ^{177}Lu-NNV003 was synergistic in four out of the seven tested cell lines: GRANTA-519, OCI-LY-10, U-2932 and WSU-DLCL-2. In REC-1 and SU-DHL-4 the combination was both synergistic, at lower concentrations (REC-1) or for two of the rays (SU-DHL-4), and antagonistic, at higher concentrations (REC-1) or for one ray (SU-DHL-4). The average CInd for each day is presented in Figure 3, to classify the cell lines

to an overall combination outcome. The average CInd of the combination in REC-1 and SU-DHL-4 was close to 1 (Figure 3), and these combinations were neither synergistic nor antagonistic. They were however defined as conditionally synergistic for further studies. The two experiments performed with the cell line DOHH-2 gave varying results in CInd. The asymptote of the dose response curve of ^{177}Lu-NNV003 alone was not well defined in these experiments (Figure S 3), giving rise to a large error in the IC$_{50}$ estimates. However, there is a trend of antagonism at lower concentrations and when the relative fraction of olaparib is high. At day 5, the combination tends towards synergism and additivity at higher relative fractions of ^{177}Lu-NNV003. The combination treatment was therefore classified as antagonistic in this cell line (Figure 3).
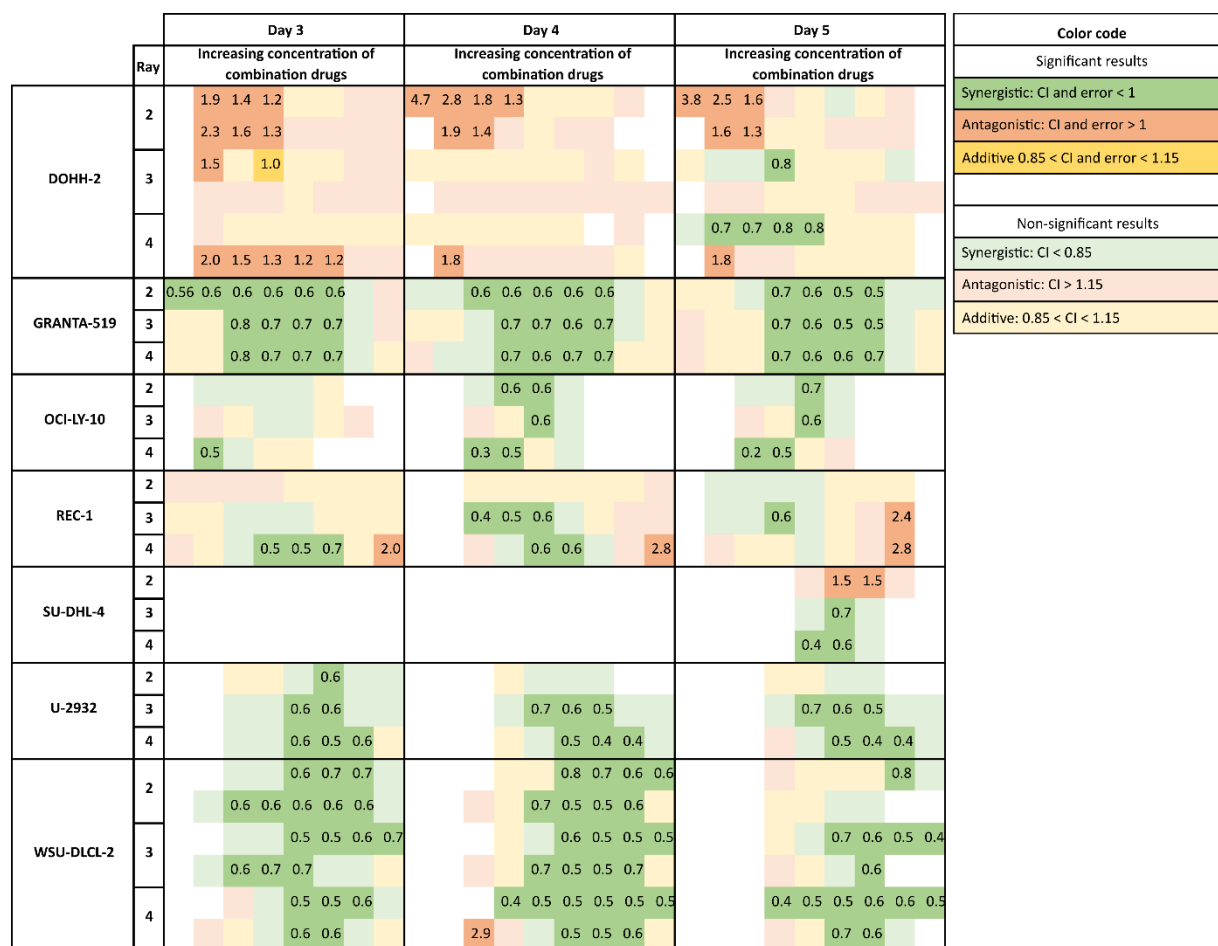

Figure 2) Heat map showing CInd of the combination treatments for olaparib and ^{177}Lu-NNV003 in all cell lines. White square = data missing or non-relevant. The numbers in the square indicate the calculated CInds.
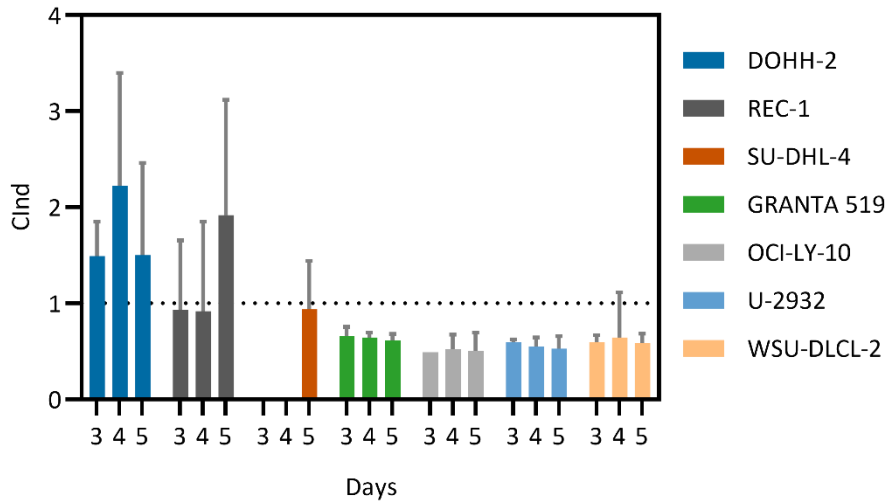
Figure 3) Average of statistically significant CInd of the combination treatments with olaparib and ^{177}Lu-NNV003 in all cell lines.

Correlation of baseline gene expression and histology, drug sensitivity and combination outcomes.

To investigate if the baseline gene expression of the seven cell lines correlated with the outcome of the combination treatment, we performed unsupervised hierarchical cluster analysis of the 559 genes that showed differential expression between the non-treated cell lines (Figure 4). The similar heights of the different nodes indicated that none of the cell lines were more closely related to any of the others. OCI-LY-10 and REC-1 cells showed the most similar expression patterns. The cluster groups did not reflect the NHL subtype histology of the cell lines, drug sensitivity or the combination outcome (Figure 4).

Differential gene expression after combination treatment

To identify the influence of gene expression on the outcome of the combination treatment, we compared baseline expression to gene expression after combination treatment to highlight the differentially expressed genes. The hypothesis was that these genes could provide further insight into the difference observed in the combination outcome of the different cell lines. In total, 397 genes across the cell lines were identified as differentially expressed genes 24 hours after combination treatment following the aforementioned criteria. Among them 188 genes were upregulated and 209 genes were downregulated (Table S 2). The majority of the differentially expressed genes in DOHH-2 and GRANTA-519 cells were upregulated, while the majority were downregulated in WSU-DLCL-2 and SU-DHL-4 (Table S 2). Cluster analysis

of the differentially expressed genes did not correlate with the sensitivity to single agent treatment or the combination outcomes (Figure 5).
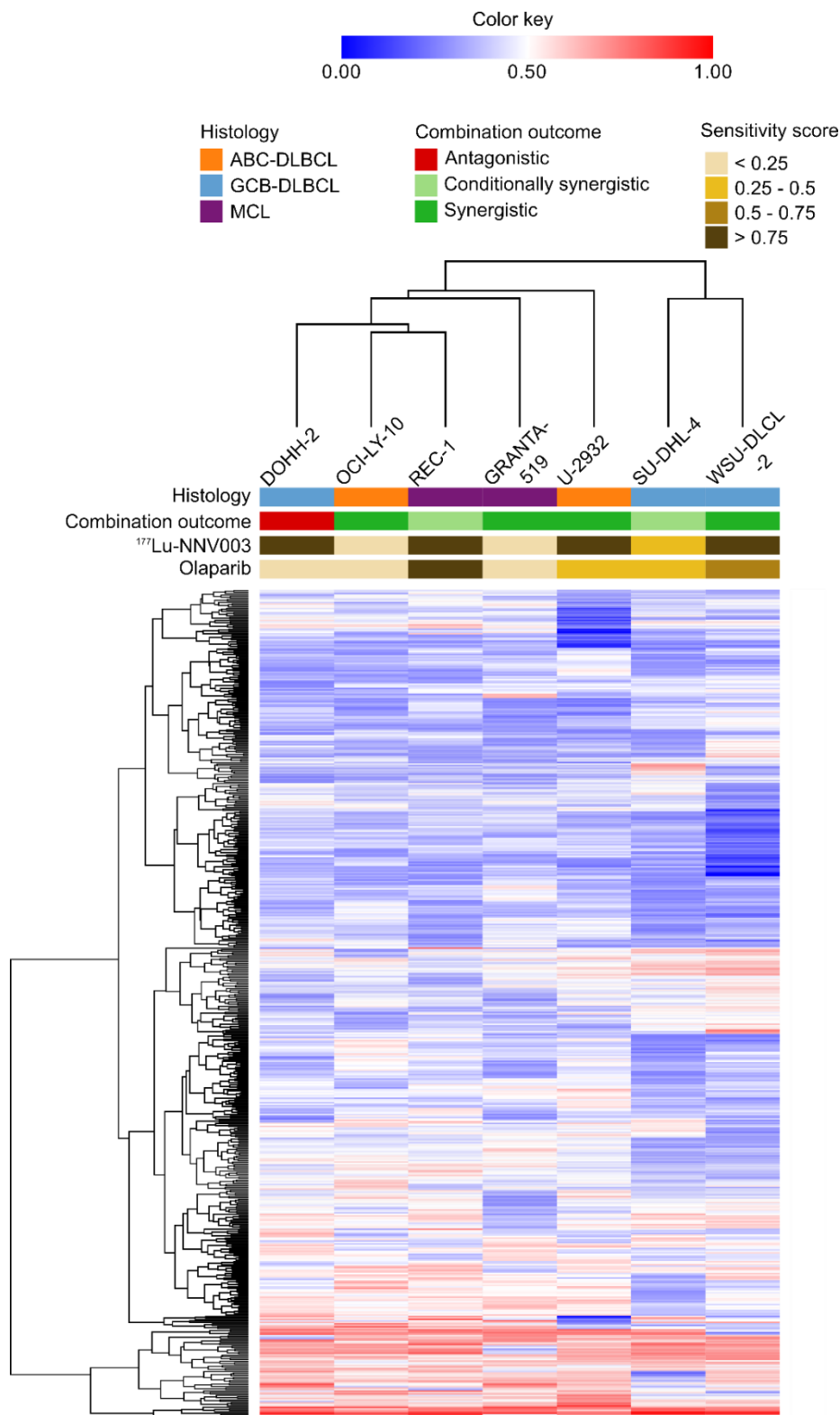

Figure 4) Hierarchical clustering of cell line baseline samples for the prediction of sample histology, sensitivity to single agent treatment and combination outcome of ^{177}Lu-NNV003 and olaparib treatment. Colour key indicates the intensity of normalised gene expression values.

Functional and pathway enrichment of differentially expressed genes after treatment with the combination

Although the unsupervised clustering of differentially expressed genes did not correlate with the combination outcome (Figure 5), we further investigated functional annotations of the differentially expressed genes to see if they could explain the observed outcomes of the combination treatment in the different cell lines. Functional gene annotation of the upregulated and downregulated genes identified genes that were predominantly associated with enriched GO biological processes and KEGG pathways for each cell line.

Upregulated genes in DOHH-2, GRANTA-519 and OCI-LY-10 cells were commonly associated with TP53 mediated DNA damage response and intrinsic apoptotic signalling, all significantly enriched in the TP53 signalling pathway (Table 1). The genes: *CDKN1A, DDB2* and *SESN1* had the highest log2 fold change of 1.5, 1.1 and 1.1 respectively (Table S 3) in GRANTA-519 cells while *MDM2* had the highest log2 fold change of 1.0 in DOHH-2 cells. Of the three cell lines, OCI-LY-10 had the lowest fold change in these genes. *CDKN1A* encodes a cyclin-dependent kinase inhibitor which functions as a regulator of cell cycle progression, mediating the TP53-dependent cell cycle G_1 phase arrest, apoptosis and DNA repair in response to DNA damage (39).

DDB2 encodes a damage specific DNA binding protein that participates in nucleotide excision repair of DNA (40). However, under distinct conditions, *DDB2* upregulation could increase the susceptibility of cells to detrimental genome stability (41). *MDM2* is a proto-oncogene commonly overexpressed in tumour cells. It inhibits TP53 mediated cell cycle arrest and apoptosis (42). *SESN1*, also highly differentially expressed in GRANTA-519, encodes a protein that mediates TP53 inhibition of cell growth by activating AMP-activated protein kinase on detection of radiation induced DNA damage and oxidative stress causing regeneration of antioxidant proteins (43).

Genes upregulated in U-2932 cells were shown to be involved in cytoskeleton organisation and enriched in the gap junction KEGG pathway (Table 2). Genes upregulated in REC-1, SU-DHL-4 and WSU-DLCL-2 cells were not significantly enriched in any GO terms or KEGG pathway.

Downregulated genes in DOHH-2 and SU-DHL-4 cells were commonly associated with the cell division process and the cell cycle pathway, while those in WSU-DLCL-2 cells were enriched in the canonical glycolysis process and the central carbon metabolism in cancer KEGG

pathway (Table 3). Genes downregulated in GRANTA-519, OCI-LY-10, REC-1 and U-2932 cells were not significantly enriched in any GO terms or KEGG pathway.

Downregulated genes: *PSRC1, PLK1, KIF20A, CDC20, HILPDA* and *FAM83D,* were significantly enriched in the KEGG pathway 'cell cycle' and were expressed in DOHH-2, SU-DHL-4 and WSU-DLCL-2 cells. These genes are involved in mitotic cell cycle progression by mediating amongst other microtubule bundle formation (44-46).
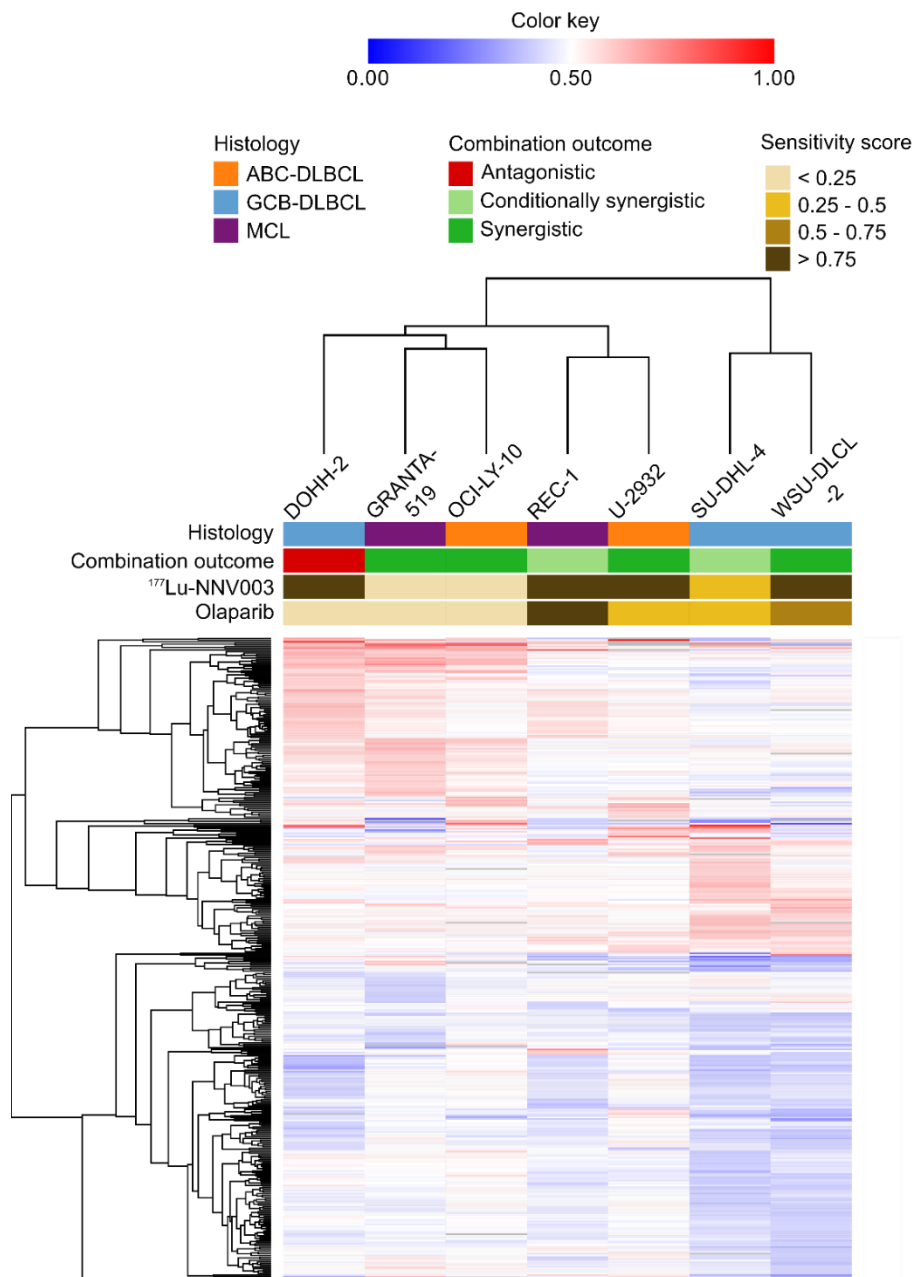

Figure 5) Hierarchical clustering of normalised differentially expressed genes in cell lines treated with the combination of ^{177}Lu-NNV003 and olaparib to visualise the correlation of changes in gene expression to the combination outcome.

Table 1) Top 5 GO and KEGG pathways significantly enriched in upregulated genes for each cell line after treatment with the combination of ^{177}Lu-NNV003 and olaparib.

Cell line	Term	Biological process	Up-regulated 'hit' genes	p value
DOHH-2	GO:0006977	DNA damage response, signal transduction by p53 class mediator resulting in cell cycle arrest	CDKN1A, E2F7, MDM2, ZNF385A, ATM	0.00006
	GO:0006974	Cellular response to DNA damage stimulus	CDKN1A, ZMAT3, ATM RPS27L, HERC2, ZNF385A	0.00069
	GO:0002040	Sprouting angiogenesis	NOTCH1, E2F7, RNF213	0.00323
	GO:0043065	Positive regulation of apoptotic process	ARHGEF3, NOTCH1, ATM ZMAT3, PRKDC, PHLDA3	0.00345
	GO:0042771	Intrinsic apoptotic signalling pathway in response to DNA damage by p53 class mediator	CDKN1A, RPS27L, PHLDA3	0.00494
	hsa04115	p53 signalling pathway	CDKN1A, ZMAT3, DDB2, MDM2, SESN1, ATM	0.000003
GRANTA-519	GO:0006977	DNA damage response, signal transduction by p53 class mediator resulting in cell cycle arrest	TRIAP1, CDKN1A, BTG2, E2F7, BAX, MDM2, GADD45A	0.00000
	GO:0042771	Intrinsic apoptotic signalling pathway in response to DNA damage by p53 class mediator	CDKN1A, AEN, RPS27L, PHLDA3	0.00013
	GO:0043065	Positive regulation of apoptotic process	ARHGEF3, NOTCH1, ZMAT3, BAX, ID3, GADD45A, PHLDA3	0.00039
	hsa04115	p53 signalling pathway	PPM1D, CDKN1A, BBC3, ZMAT3, BAX, DDB2, MDM2, SESN1, GADD45A	0.00000
OCI-LY-10	GO:0006977	DNA damage response, signal transduction by p53 class mediator resulting in cell cycle arrest	CDKN1A, BAX, MDM2, ZNF385A	0.000038
	GO:0006974	Cellular response to DNA damage stimulus	CDKN1A, BBC3, ZMAT3, RPS27L, ZNF385A	0.000061
	GO:0072332	Intrinsic apoptotic signalling pathway by p53 class mediator	ZMAT3, BAX, EDA2R	0.000375
	GO:0097193	Intrinsic apoptotic signalling pathway	CDKN1A, BBC3, BAX	0.000464
	hsa04115	p53 signalling pathway	CDKN1A, BBC3, ZMAT3, BAX, DDB2, MDM2, SESN1	0.00000
U-2932	GO:0007010	Cytoskeleton organisation	TUBB2B, TUBB2A, TUBA1A, TUBB4A	0.00075
	hsa04540	Gap junction	TUBB2B, TUBB2A, TUBA1A, TUBB4A	0.00041

Table 2) Top 5 GO and KEGG pathways significantly enriched in downregulated genes for each cell line after treatment with the combination of ^{177}Lu-NNV003 and olaparib.

Cell line	Term	Biological process	Down-regulated 'hit' genes	p value
DOHH-2	GO:0051301	Cell division	CCNB1, FAM83D, CDCA8, CCNB2, NEK2, PSRC1, BUB1, TPX2, CDCA2, AURKA, CDC20, PTTG1, UBE2C, CDCA3	0.0000
	GO:0007067	Mitotic nuclear division	FAM83D, CCNB2, PLK1, NEK2, BUB1, TPX2, CDCA2, AURKA, CDC20, PTTG1, CDCA3	0.0000
	GO:0000086	G2/M transition of mitotic cell cycle	CCNB1, CCNB2, PLK1, NEK2, TPX2, AURKA, HMMR	0.0000
	GO:0031145	Anaphase-promoting complex-dependent catabolic process	CCNB1, PLK1, AURKA, CDC20, PTTG1, UBE2C	0.0000
	GO:0042787	Protein ubiquitination involved in ubiquitin-dependent protein catabolic process	CCNB1, PLK1, AURKA, CDC20, PTTG1, UBE2C	0.0000
	hsa04114	Oocyte meiosis	CCNB1, CCNB2, PLK1, BUB1, AURKA, CDC20, PTTG1	0.0000
	hsa04110	Cell cycle	CCNB1, CCNB2, PLK1, BUB1, CDC20, PTTG1	0.0000
	hsa04914	Progesterone-mediated oocyte maturation	CCNB1, CCNB2, PLK1, BUB1	0.0002
SU-DHL-4	GO:1904668	Positive regulation of ubiquitin protein ligase activity	PLK1, CDC20, UBE2C, UBE2S	0.0000
	GO:0051301	Cell division	CCNB1, FAM83D, PSRC1, KIF18B, CDC20, UBE2C, UBE2S, REEP4, CDCA3	0.0000
	GO:0051439	Regulation of ubiquitin-protein ligase activity involved in mitotic cell cycle	CCNB1, PLK1, CDC20, UBE2C	0.0001
	GO:0000281	Mitotic cytokinesis	KIF23, CENPA, PLK1, KIF20A	0.0001
	GO:0031145	Anaphase-promoting complex-dependent catabolic process	CCNB1, PLK1, CDC20, UBE2C, UBE2S	0.0001
WSU-DLCL-2	GO:0061621	Canonical glycolysis	PFKFB4, PFKFB3, ALDOC, HK2	0.0003
	hsa05230	Central carbon metabolism in cancer	SLC16A3, PDK1, SLC2A1, HK2, MYC	0.0008

Mutation of genes related to DNA damage repair

Mutations in genes related to DNA damage repair might explain the difference in single agent sensitivity and the combination outcomes observed. The mRNA sequencing data was used to check for mutations in relevant genes (Table S 4) (47-49). *TP53* was mutated in two cell lines; in REC-1, a nonsense mutation at position p.Q317* that created a stop codon (COSM1709728) and a G>A change in p.G245 that caused a glycine to aspartic acid change. In U-2932, a cysteine was changed with a tyrosine in position p.C176Y in *TP53*. In GRANTA-519, a mutation in position p.R2832C of *ATM* (COSM1351027) caused an arginine to cysteine change. *RAD51C* was mutated in DOHH-2, where the amino acid proline was replaced by a glutamine in position p.P127Q, which is expected to affect the protein function or structure. See Table S 5 for summary.

Discussion

The combination of targeted RIT, which damages lymphoma cells while sparing surrounding healthy tissue, with a DNA repair inhibitor may increase the therapeutic effect and overcome radio-resistance. In this study, we have shown that the combination of the β emitter ^{177}Lu-NNV003 and the PARP inhibitor olaparib was robustly synergistic in four of seven NHL cell lines, conditionally synergistic in two and antagonistic in one. The outcome of the combination was dependent on the ratio of the two drugs, the concentration of the mixture, and the time of measurement. Synergism did not correlate with unsupervised clustering analysis of gene expression nor did it correlate with single-agent activity.

The dependence of combination outcome on time of measurement demonstrates the importance of optimising the schedule for combination treatments. Our study suggest that it is paramount to attain a suitable drug combination ratio and dose so as to obtain a synergistic combination outcome. The combination outcome did, however, not seem to depend on the sequence of treatment with the two drugs. We tested if adding olaparib four hours before, 24 hours after or simultaneously as ^{177}Lu-NNV003 had any effect on the combination outcome. Although negligible differences in scheduling were observed, there was a tendency towards better effect by adding olaparib at the same time or prior to ^{177}Lu-NNV003 (data not shown). Studies have shown that olaparib can sensitise cells to radiation therapy (14, 22, 24). Indeed, ongoing phase 1 clinical trials on the combination of olaparib and radiotherapy have different drug scheduling protocols where olaparib treatment is started some days or weeks before, or the same day as the radiotherapy treatment (26-29). This would have to be tested in clinical settings with RIT,

however, particularly because of the lower dose-rate of RIT than of radiotherapy. The aforementioned clinical trials have the same dose regimen; the radiotherapy dose is kept constant while the olaparib dose is escalated to obtain the maximum tolerated dose (26-29). Our cell line findings indicate that the optimal combination outcome is not always at the highest drug concentrations. Hence, it might be that drug doses lower than the maximum tolerated dose should be investigated in an early clinical trial setting.

CDKN1A, DDB2 and *SESN1* had the highest log2 fold change of 1.5, 1.1 and 1.1 respectively (Table S 3) in GRANTA-519 cells while *MDM2* had the highest log2 fold change of 1.0 in DOHH-2 cells. Of the three cell lines, OCI-LY-10 had the lowest fold change in these genes. *CDKN1A* encodes a cyclin-dependent kinase inhibitor which functions as a regulator of cell cycle progression, mediating the TP53-dependent cell cycle G_1 phase arrest, apoptosis and DNA repair in response to DNA dam

Changes in gene expression in response to drug combination were different in the 7 cell lines which might explain the difference in the combination outcome.

The induction in *MDM2* expression in DOHH-2 possibly overcame the effects of the other co-upregulated genes, *CDKN1A, DDB2* and *SESN1*, making the cells continuously proliferate and thereby possibly explaining the antagonistic outcome of the combination in this cell line. Additionally, *ATM* was upregulated in this cell line that might have provided these cells with an alternative DDR strategy. However, ATM activation was not evaluated.

Pronounced upregulation of *CDKN1A* in the cell lines that responded synergistically to the drug combination could be as a consequence of its role as a tumour suppressor gene, increasing DNA damage induced apoptosis in these cells. Upregulation of the same gene in DOHH-2 cells can be explained by the reports on the conflicting role played by *CDKN1A*, as an oncogene, protecting cells against DNA damage-induced cell death. Either role is primarily dependent on the TP53 status of the cells but also dependent on the cytotoxic stimuli and cell type (39, 50, 51).

Downregulated genes as a consequence of combination treatment were enriched in processes that inhibit cell division and proliferation while inducing apoptosis. This could elaborate the synergism observed in SU-DHL-4 and WSU-DLCL-2 cells but is not in accordance with the antagonism observed in DOHH-2.

We did not detect an accurate correlation pattern of subtype histology, single agent sensitivity or the combination outcome through unsupervised cluster analysis of filtered baseline gene

expression. This could be a result of limited number of cell lines and little diversity in the tested samples.

REC-1 has a nonsense mutation p.Q317* and a missense mutation p.G245D in *TP53*. The latter mutation is located in the highly conserved part of the protein and would probably affect the function (52). The mutations in *TP53* might explain the low sensitivity to radiation and PARP inhibition, because of a compensating effect. U-2932 also has a mutation in *TP53*, p.C176Y, in the DNA binding domain, which could affect the protein structure and has been shown to inhibit apoptosis (53, 54). The p.R2832C mutation found in *ATM* in GRANTA-519 is situated in the PI-3 kinase domain which might impact ATM activity (55, 56). In our study there was no difference in mRNA expression of *ATM* in the cell lines (data not shown), however, ATM activity was not measured. There are conflicting evidence whether this mutation affects *ATM* expression and kinase activity (57, 58). However, GRANTA-519 has been shown to have non-functional ATM (59), which might be due to this mutation. The lack of ATM functionality is in accordance with the high measured sensitivity to ^{177}Lu-NNV003 and olaparib. Cells deficient of RAD51 are sensitive to PARP inhibition treatment (47) so the mutation in *RAD51C*, p.P127Q, found in DOHH-2 could explain the high sensitivity it has for olaparib treatment. These mutations could possibly explain the sensitivity of the mutated cells to the single drugs, but no clear association with the combination outcome was found.

In conclusion, the combined effect of ^{177}Lu-NNV003 and olaparib was synergistic in four NHL cell lines, partially synergistic in two and antagonistic in one. The effect of the two drugs were dependent on the ratio of the two drugs, as well as the concentration of the mixture, showing the importance of optimising the parameters for further studies. The anti-tumour effect of the combination of RIT and PARP inhibition should be tested in an *in vivo* setting to confirm the results observed *in vitro*.

Acknowledgement

References

1.   Swerdlow SH, Campo E, Pileri SA, Harris NL, Stein H, Siebert R, et al. The 2016 revision of the World Health Organization classification of lymphoid neoplasms. Blood. 2016;127(20):2375-90.

2.   Choi M, Kipps T, Kurzrock R. ATM Mutations in Cancer: Therapeutic Implications. Mol Cancer Ther. 2016;15(8):1781-91.

3.   Wang X, Huang H, Young KH. The PTEN tumor suppressor gene and its role in lymphoma pathogenesis. Aging. 2015;7(12):1032-49.

4.   Xu-Monette ZY, Medeiros LJ, Li Y, Orlowski RZ, Andreeff M, Bueso-Ramos CE, et al. Dysfunction of the TP53 tumor suppressor gene in lymphoid malignancies. Blood. 2012;119(16):3668-83.

5.   Fece de la Cruz F, Gapp BV, Nijman SM. Synthetic lethal vulnerabilities of cancer. Annual review of pharmacology and toxicology. 2015;55:513-31.

6.   Parvin S, Ramirez-Labrada A, Aumann S, Lu X, Weich N, Santiago G, et al. LMO2 Confers Synthetic Lethality to PARP Inhibition in DLBCL. Cancer Cell. 2019;36(3):237-49 e6.

7.   Bochum S, Berger S, Martens UM. Olaparib. Recent results in cancer research Fortschritte der Krebsforschung Progres dans les recherches sur le cancer. 2018;211:217-33.

8.   Livraghi L, Garber JE. PARP inhibitors in the management of breast cancer: current data and future prospects. BMC Med. 2015;13:188.

9.   Williamson CT, Muzik H, Turhan AG, Zamo A, O'Connor MJ, Bebb DG, et al. ATM Deficiency Sensitizes Mantle Cell Lymphoma Cells to Poly(ADP-Ribose) Polymerase-1 Inhibitors. Molecular Cancer Therapeutics. 2010;9(2):347-57.

10.   Ahmed M, Li L, Pinnix C, Dabaja B, Nomie K, Lam L, et al. ATM mutation and radiosensitivity: An opportunity in the therapy of mantle cell lymphoma. Crit Rev Oncol Hematol. 2016;107:14-9.

11.   Fang NY, Greiner TC, Weisenburger DD, Chan WC, Vose JM, Smith LM, et al. Oligonucleotide microarrays demonstrate the highest frequency of ATM mutations in the mantle cell subtype of lymphoma. Proc Natl Acad Sci U S A. 2003;100(9):5372-7.

12.   Grønbæk K, Worm J, Ralfkiaer E, Ahrenkiel V, Hokland P, Guldberg P. ATM mutations are associated with inactivation of theARF-TP53 tumor suppressor pathway in diffuse large B-cell lymphoma. Blood. 2002;100(4):1430-7.

13.   Soumerai JD, Zelenetz AD, Moskowitz CH, Palomba ML, Hamlin PA, Jr., Noy A, et al. The PARP Inhibitor Veliparib Can Be Safely Added to Bendamustine and Rituximab and Has Preliminary Evidence of Activity in B-Cell Lymphoma. Clin Cancer Res. 2017;23(15):4119-26.

14.   Senra JM, Telfer BA, Cherry KE, McCrudden CM, Hirst DG, O'Connor MJ, et al. Inhibition of PARP-1 by Olaparib (AZD2281) Increases the Radiosensitivity of a Lung Tumor Xenograft. Molecular Cancer Therapeutics. 2011;10(10):1949-58.

15.   van Vuurden DG, Hulleman E, Meijer OLM, Wedekind LE, Kool M, Witt H, et al. PARP inhibition sensitizes childhood high grade glioma, medulloblastoma and ependymoma to radiation. Oncotarget. 2011;2(12):984-96.

16.   Chow JPH, Man WY, Mao M, Chen H, Cheung F, Nicholls J, et al. PARP1 Is Overexpressed in Nasopharyngeal Carcinoma and Its Inhibition Enhances Radiotherapy. Molecular Cancer Therapeutics. 2013;12(11):2517-28.

17.   Gani C, Coackley C, Kumareswaran R, Schutze C, Krause M, Zafarana G, et al. In vivo studies of the PARP inhibitor, AZD-2281, in combination with fractionated radiotherapy: An exploration of the therapeutic ratio. Radiother Oncol. 2015;116(3):486-94.

18.   Verhagen CVM, de Haan R, Hageman F, Oostendorp TPD, Carli ALE, O'Connor MJ, et al. Extent of radiosensitization by the PARP inhibitor olaparib depends on its dose, the radiation dose and the integrity of the homologous recombination pathway of tumor cells. Radiotherapy and Oncology. 2015;116(3):358-65.

19.   Mangoni M, Sottili M, Salvatore G, Meattini I, Desideri I, Greto D, et al. Enhancement of Soft Tissue Sarcoma Cell Radiosensitivity by Poly(ADP-ribose) Polymerase-1 Inhibitors. Radiation Research. 2018;190(5):464-72.

20.   Mao YZ, Huang X, Shuang ZY, Lin GH, Wang J, Duan FT, et al. PARP inhibitor olaparib sensitizes cholangiocarcinoma cells to radiation. Cancer Medicine. 2018;7(4):1285-96.

21.   Parsels LA, Karnak D, Parsels JD, Zhang Q, Velez-Padilla J, Reichert ZR, et al. PARP1 Trapping and DNA Replication Stress Enhance Radiosensitization with Combined WEE1 and PARP Inhibitors. Molecular Cancer Research. 2018;16(2):222-32.

22.   Nile DL, Rae C, Hyndman IJ, Gaze MN, Mairs RJ. An evaluation in vitro of PARP-1 inhibitors, rucaparib and olaparib, as radiosensitisers for the treatment of neuroblastoma. Bmc Cancer. 2016;16.

23.   Tesson M, Rae C, Nixon C, Babich JW, Mairs RJ. Preliminary evaluation of prostate-targeted radiotherapy using I-131-MIP-1095 in combination with radiosensitising chemotherapeutic drugs. Journal of Pharmacy and Pharmacology. 2016;68(7):912-21.

24.   Schaefer NG, James E, Wahl RL. Poly(ADP-ribose) polymerase inhibitors combined with external beam and radioimmunotherapy to treat aggressive lymphoma. Nucl Med Commun. 2011;32(11):1046-51.

25.   Portwood SM, Cantella MC, Cronin TL, Wang ES. Addition of the PARP Inhibitor, Talazoparib, to Gemtuzumab Ozogamicin Significantly Enhances Anti-Leukemic Activity in Human CD33+ Acute Myeloid Leukemia. Blood. 2019;134(Supplement_1):1371-.

26.   Karam SD, Reddy K, Blatchford PJ, Waxweiler T, DeLouize AM, Oweida A, et al. Final Report of a Phase I Trial of Olaparib with Cetuximab and Radiation for Heavy Smoker Patients with Locally Advanced Head and Neck Cancer. Clinical Cancer Research. 2018.

27.   Fulton B, Short SC, James A, Nowicki S, McBain C, Jefferies S, et al. PARADIGM-2: Two parallel phase I studies of olaparib and radiotherapy or olaparib and radiotherapy plus temozolomide in patients with newly diagnosed glioblastoma, with treatment stratified by MGMT status. Clin Transl Radiat Oncol. 2018;8:12-6.

28.   de Haan R, van Werkhoven E, van den Heuvel MM, Peulen HMU, Sonke GS, Elkhuizen P, et al. Study protocols of three parallel phase 1 trials combining radical radiotherapy with the PARP inhibitor olaparib. BMC Cancer. 2019;19(1):901.

29.   Lesueur P, Lequesne J, Grellard JM, Dugue A, Coquan E, Brachet PE, et al. Phase I/IIa study of concomitant radiotherapy with olaparib and temozolomide in unresectable or partially resectable glioblastoma: OLA-TMZ-RTE-01 trial protocol. BMC Cancer. 2019;19(1):198.

30.   Maaland AF, Heyerdahl H, O'Shea A, Eiriksdottir B, Pascal V, Andersen JT, et al. Targeting B-cell malignancies with the beta-emitting anti-CD37 radioimmunoconjugate 177Lu-NNV003. European Journal of Nuclear Medicine and Molecular Imaging. 2019;46(11):2311-21.

31.   Lindmo T, Boven E, Cuttitta F, Fedorko J, Bunn PA, Jr. Determination of the immunoreactive fraction of radiolabeled monoclonal antibodies by linear extrapolation to binding at infinite antigen excess. J Immunol Methods. 1984;72(1):77-89.

32.   Tomska K, Kurilov R, Lee KS, Hullein J, Lukas M, Sellner L, et al. Drug-based perturbation screen uncovers synergistic drug combinations in Burkitt lymphoma. Sci Rep. 2018;8(1):12046.

33.	Mateo J, Moreno V, Gupta A, Kaye SB, Dean E, Middleton MR, et al. An Adaptive Study to Determine the Optimal Dose of the Tablet Formulation of the PARP Inhibitor Olaparib. Target Oncol. 2016;11(3):401-15.

34.	Straetemans R, O'Brien T, Wouters L, Van Dun J, Janicot M, Bijnens L, et al. Design and Analysis of Drug Combination Experiments. Biometrical Journal. 2005;47(3):299-308.

35.	Foucquier J, Guedj M. Analysis of drug combinations: current methodological landscape. Pharmacology research & perspectives. 2015;3(3):e00149.

36.	Grabovsky Y, Tallarida RJ. Isobolographic analysis for combinations of a full and partial agonist: curved isoboles. J Pharmacol Exp Ther. 2004;310(3):981-6.

37.	Huang DW, Sherman BT, Tan Q, Collins JR, Alvord WG, Roayaei J, et al. The DAVID Gene Functional Classification Tool: a novel biological module-centric algorithm to functionally analyze large gene lists. Genome biology. 2007;8(9):R183.

38.	Rodland GE, Melhus K, Generalov R, Gilani S, Bertoni F, Dahle J, et al. The Dual Cell Cycle Kinase Inhibitor JNJ-7706621 Reverses Resistance to CD37-Targeted Radioimmunotherapy in Activated B Cell Like Diffuse Large B Cell Lymphoma Cell Lines. Front Oncol. 2019;9:1301.

39.	Al Bitar S, Gali-Muhtasib H. The Role of the Cyclin Dependent Kinase Inhibitor p21(cip1/waf1) in Targeting Cancer: Molecular Mechanisms and Novel Therapeutics. Cancers. 2019;11(10).

40.	Stoyanova T, Roy N, Kopanja D, Bagchi S, Raychaudhuri P. DDB2 decides cell fate following DNA damage. Proceedings of the National Academy of Sciences of the United States of America. 2009;106(26):10690-5.

41.	Puumalainen MR, Lessel D, Ruthemann P, Kaczmarek N, Bachmann K, Ramadan K, et al. Chromatin retention of DNA damage sensors DDB2 and XPC through loss of p97 segregase causes genotoxicity. Nature communications. 2014;5:3695.

42.	Giono LE, Resnick-Silverman L, Carvajal LA, St Clair S, Manfredi JJ. Mdm2 promotes Cdc25C protein degradation and delays cell cycle progression through the G2/M phase. Oncogene. 2017;36(49):6762-73.

43.	Budanov AV, Lee JH, Karin M. Stressin' Sestrins take an aging fight. EMBO Mol Med. 2010;2(10):388-400.

44.	Hsieh WJ, Hsieh SC, Chen CC, Wang FF. Human DDA3 is an oncoprotein down-regulated by p53 and DNA damage. Biochemical and biophysical research communications. 2008;369(2):567-72.

45.   Kumar S, Sharma AR, Sharma G, Chakraborty C, Kim J. PLK-1: Angel or devil for cell cycle progression. Biochimica et biophysica acta. 2016;1865(2):190-203.

46.   Wu WD, Yu KW, Zhong N, Xiao Y, She ZY. Roles and mechanisms of Kinesin-6 KIF20A in spindle organization during cell division. European journal of cell biology. 2019;98(2-4):74-80.

47.   McCabe N, Turner NC, Lord CJ, Kluzek K, Bialkowska A, Swift S, et al. Deficiency in the repair of DNA damage by homologous recombination and sensitivity to poly(ADP-ribose) polymerase inhibition. Cancer Res. 2006;66(16):8109-15.

48.   Lord CJ, Ashworth A. BRCAness revisited. Nat Rev Cancer. 2016;16(2):110-20.

49.   Zimmermann M, Murina O, Reijns MAM, Agathanggelou A, Challis R, Tarnauskaite Z, et al. CRISPR screens identify genomic ribonucleotides as a source of PARP-trapping lesions. Nature. 2018;559(7713):285-9.

50.   Wang Y, Blandino G, Givol D. Induced p21waf expression in H1299 cell line promotes cell senescence and protects against cytotoxic effect of radiation and doxorubicin. Oncogene. 1999;18(16):2643-9.

51.   Barboza JA, Liu G, Ju Z, El-Naggar AK, Lozano G. p21 delays tumor onset by preservation of chromosomal stability. Proceedings of the National Academy of Sciences of the United States of America. 2006;103(52):19842-7.

52.   Srivastava S, Zou Z, Pirollo K, Blattner W, Chang EH. Germ-line transmission of a mutated p53 gene in a cancer-prone family with Li–Fraumeni syndrome. Nature. 1990;348(6303):747-9.

53.   Bergamaschi D, Gasco M, Hiller L, Sullivan A, Syed N, Trigiante G, et al. p53 polymorphism influences response in cancer chemotherapy via modulation of p73-dependent apoptosis. Cancer Cell. 2003;3(4):387-402.

54.   Mullany LK, Wong KK, Marciano DC, Katsonis P, King-Crane ER, Ren YA, et al. Specific TP53 Mutants Overrepresented in Ovarian Cancer Impact CNV, TP53 Activity, Responses to Nutlin-3a, and Cell Survival. Neoplasia. 2015;17(10):789-803.

55.   Vořechovský I, Luo L, Dyer MJS, Catovsky D, Amlot PL, Yaxley JC, et al. Clustering of missense mutations in the ataxia-telanglectasia gene in a sporadic T-cell leukaemia. Nature Genetics. 1997;17(1):96-9.

56.   Becker-Catania SG, Chen G, Hwang MJ, Wang Z, Sun X, Sanal O, et al. Ataxia-telangiectasia: phenotype/genotype studies of ATM protein expression, mutations, and radiosensitivity. Mol Genet Metab. 2000;70(2):122-33.

57.   Barone G, Groom A, Reiman A, Srinivasan V, Byrd PJ, Taylor AM. Modeling ATM mutant proteins from missense changes confirms retained kinase activity. Hum Mutat. 2009;30(8):1222-30.

58.   Mitui M, Nahas SA, Du LT, Yang Z, Lai CH, Nakamura K, et al. Functional and computational assessment of missense variants in the ataxia-telangiectasia mutated (ATM) gene: mutations with increased cancer risk. Hum Mutat. 2009;30(1):12-21.

59.   Williamson CT, Kubota E, Hamill JD, Klimowicz A, Ye R, Muzik H, et al. Enhanced cytotoxicity of PARP inhibition in mantle cell lymphoma harbouring mutations in both ATM and p53. EMBO Mol Med. 2012;4(6):515-27.

Supplementary data

Table S 1) Concentrations of olaparib and ^{177}Lu-NNV003 used to treat cells for fixed-ratio ray design and mRNA sequencing study, corresponding to IC$_{50}$ for each cell line

Cell line	IC$_{50}$	
	Olaparib (µM)	**^{177}Lu-NNV003 (ng/ml)**
DOHH-2	1.31	138
GRANTA-519	0.86	189
OCI-LY-10	0.89	41
REC-1	12.66	287
SU-DHL-4	2.36	177
U-2932	1.31	111
WSU-DLCL-2	5.66	234

Table S 2) Number of significantly up-regulated and down-regulated genes after combination treatment in each cell line. Some genes were common across the cell lines.

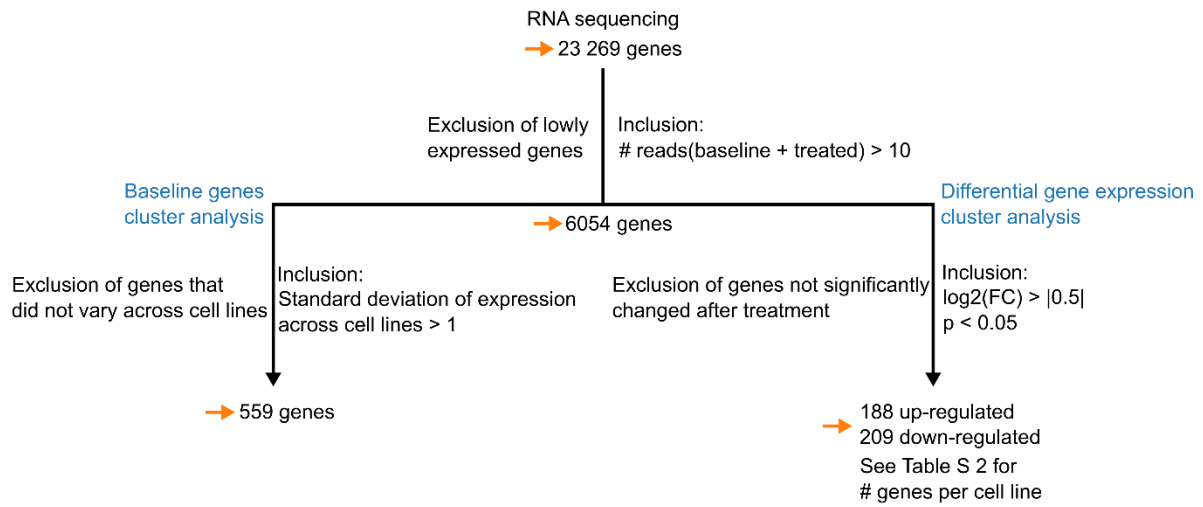| Cell line	Number of genes	
	Up-regulated	**Down-regulated**
DOHH-2	68	29
GRANTA-519	59	22
OCI-LY-10	20	2
REC-1	11	21
SU-DHL-4	28	73
U-2932	22	7
WSU-DLCL-2	18	109
Total	188	209

Figure S 1) Flow chart of filtering methods for gene expression analysis

Table S 3) Fold change of differentially expressed genes commonly annotated in combination treated cells

Hit genes	Log2 fold-change				
	DOHH-2	GRANTA-519	OCI-LY-10	SU-DHL-4	WSU-DLCL-2
CDKN1A	1.0	1.5	0.8	--	--
DDB2	0.7	1.1	0.8	--	--
SESN1	0.8	1.1	0.6	--	--
MDM2	1.0	0.8	0.7	--	--
PSRC1	-1.1	--	--	-0.7	-0.6
PLK1	-0.7	--	--	-0.7	-0.5
KIF20A	-1.0	--	--	-0.9	-0.8
CDC20	-0.8	--	--	-0.6	-0.6
HILPDA	-0.6	--	--	-0.6	-0.8
FAM83D	-0.8	--	--	-0.7	-0.6

Table S 4) Genes related to DNA damage repair

Gene list for mutation analysis		
ATM	*DDB1*	*TONSL*
ATR	*XAB2*	*XRCC2*
CHK1	*XRCC1*	*XRCC3*
CHK2	*BARD1*	*COMMD1*
DSS1	*BRCA1*	*FAAP24*
FANCA	*EMSY*	*FANCD2*
FANCC	*PALB2*	*FANCE*
NBS1	*PSMC3IP*	*FANCM*
RAD51	*RAD51B*	*UBE2T*
RAD54	*RAD51C*	*EME1*
RPA1	*RAD51D*	*HUS1*
BRCA2	*RBBP8*	*MUS81*

Table S 5) Mutations in genes related to DNA damage repair

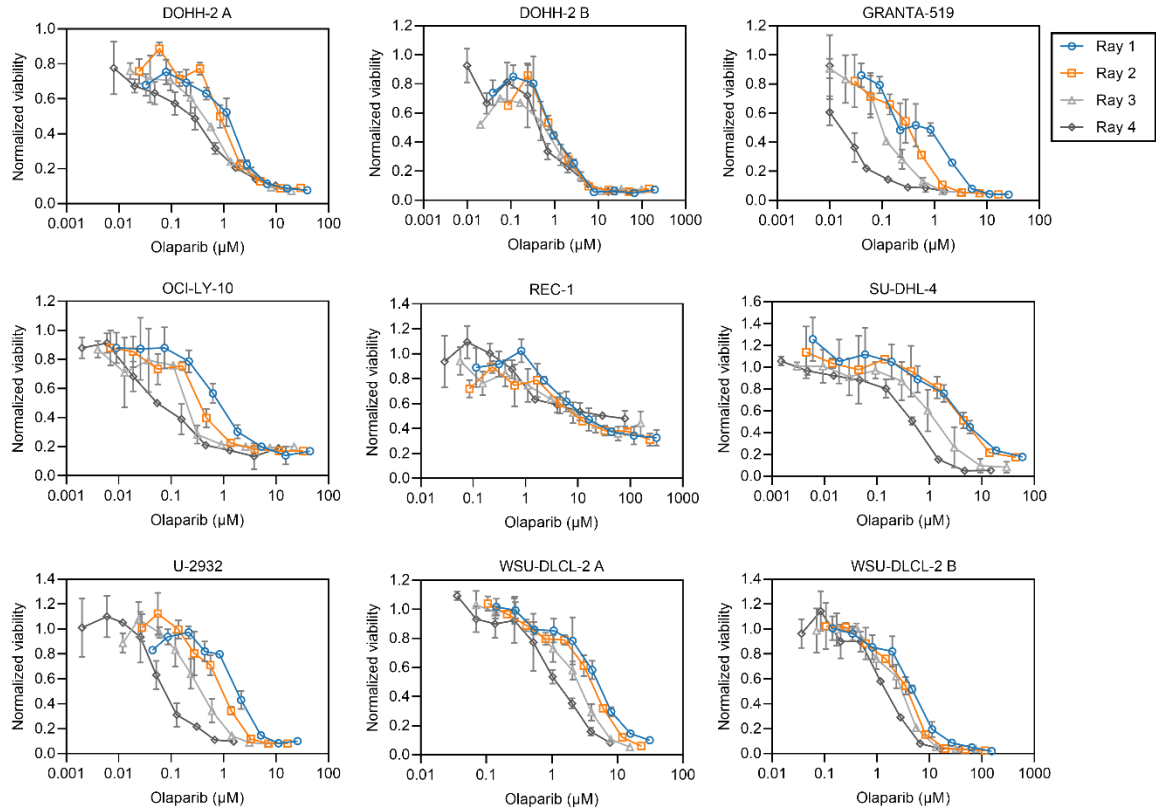| Cell line	Gene	Amino acid change	dbSNP or COSMIC identification number
DOHH-2	*RAD51C*	p.P127Q	NA
GRANTA-519	*ATM*	p.R2832C	rs587779872/COSM1351027
REC-1	*TP53*	p.Q317*	COSM1709728
	TP53	p.G245D	rs121912656
U-2932	*TP53*	p.C176Y	rs786202962

Figure S 2) Dose response curves of seven cell lines treated with olaparib in combination with ^{177}Lu-NNV003; Ray 1, Ray 2, Ray 3 and Ray 4 as a function of olaparib concentration. Data points shown as average and error bars= SD. The experiments in DOHH-2 and WSU-DLCL-2 cells were performed twice (marked A and B)

Figure S 3) Dose response curves of seven cell lines treated with olaparib in combination with ^{177}Lu-NNV003; Ray 2, Ray 3, Ray 4 and Ray 5 as a function of ^{177}Lu-NNV003 concentration. Data points shown as average and error bars= SD. The experiments in DOHH-2 and WSU-DLCL-2 cells were performed twice (marked A and B)
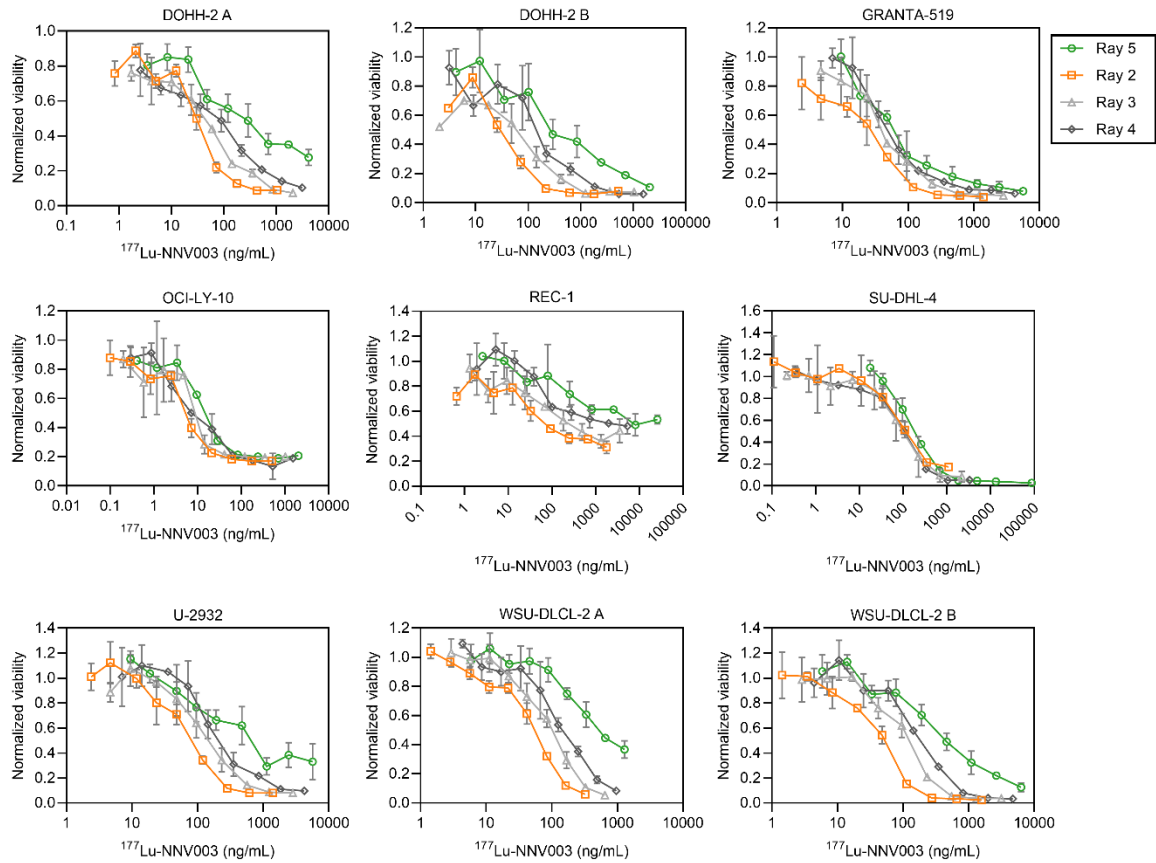
Errata from submitted version vs. printed version of thesis

Abbreviations for the types of corrections:

CoL – correction of spelling and language

Page	Line	Original text	Type of correction	Corrected text
VIII	8	Subcutaenous	CoL	Subcutaneous
10	13	… antigen-specific as requires…	CoL	… antigen-specific as it requires…
11	1	Activation	CoL	Activated
13	15	… a variety of cancers types…	CoL	… a variety of cancer types…
14	16-17	…the first humanised approved for therapy of metastatic breast cancer (84)The…	CoL	…the first humanised mAb approved for therapy of metastatic breast cancer (84). The…
15	12	… and obinutuzumab example…	CoL	… and obinutuzumab are example…
15	25	… an adaptive immune responses against…	CoL	… an adaptive immune response against…
17	22	… mAbs have been also developed…	CoL	… mAbs have also been developed…
22	27	This cells are…	CoL	These cells are…
31	13	… the *in vitro* the studies,…	CoL	… the *in vitro* studies,…
35	12	This studies make…	CoL	These studies make…
37	3-4	In paper II, Raji and Raji 2R cells were treated with either PBS, lilotomab or Betalutin, and in these cells 3 and 6 days after treatment.	CoL	In paper II, Raji and Raji 2R cells were treated with either PBS, lilotomab or Betalutin, and CD20/rituximab binding was evaluated in these cells 3 and 6 days after treatment.
46	8	… the tumour weight showed…	CoL	… the tumour height showed…